INFLUENCE OF GRAIN SIZE AND NIOBIUM CONTENT ON THE CREEP RESISTANCE OF FERRITIC STAINLESS STEELS

A thesis submitted to the Faculty of Engineering and the Built Environment of the University of Cape Town in fulfilment of the requirements for the degree of Master of Science in Engineering

Centre for Materials Engineering
Department of Mechanical Engineering
University of Cape Town
March 2008

Prepared by:

Victoria Cain

Supervised by:

Professor Rob Knutsen

Acknowledgements

Firstly I would like to thank my supervisor, Prof Rob Knutsen for his guidance and support throughout the undertaking of this project.

A thank-you goes to the staff and students at the Centre for Materials Engineering, for providing such a pleasant working environment. In particular I am grateful to Penny Park-Ross for always offering her assistance in the laboratories and to Sarah George for being a loyal friend.

Thank-you also to the Department of Mechanical Engineering workshop staff, I am particularly indebted to Glen Newins for always being so helpful and kind.

I am also grateful to Miranda Waldron from the Electron Microscope Unit for her endless patience.

A very special thank-you goes to my parents for their never-ending support and encouragement.

Finally, I am especially thankful to my best friend and partner, Thomas for always standing by me.

Abstract

Type 441 ferritic stainless steel is used for the production of catalytic converter housings. As the housing is subjected to high temperatures it is necessary that the material offers creep resistance. Type 441 is dual stabilised with Ti and Nb to provide improved weldability; however, Nb addition also enhances the hot strength and creep resistance by means of precipitation and solid solution strengthening. Notwithstanding the Nb strengthening effect, the strong dependence of creep resistance on grain size also means that the relationship between creep resistance and Nb content may be complicated by grain growth inhibition that arises from aspects of solute drag and grain boundary pinning. Thus it may not be simple to predict the relative creep resistance of standard production heats on the basis of Nb level alone and other factors affecting solid solution and grain size also need to be taken into account. Consequently, it is pertinent to evaluate more closely the sensitivity of these parameters in influencing creep resistance by choosing two alloy heats with different Nb contents and subjecting them to a range in heat treatments that will modify solute level and grain size. This thesis reports on the examination of the dependence of creep resistance on Nb level by eliminating the influence of grain size. The latter was achieved by manipulating the post-cold roll recrystallisation temperature in such a way that equivalent grain sizes were produced in two alloy heats with Nb levels of 0.46 and 0.74 wt.% respectively.

Although the grain size was essentially stabilised by recrystallisation between 1050-1100°C for 30 minutes, the solution treatment prior to creep testing was varied for each heat to evaluate not only the influence of bulk Nb level on creep resistance, but also to consider the influence of the distribution of Nb in the microstructure. Consequently, the total heat treatment cycle prior to constant load creep testing at 850°C involved recrystallisation, ageing at 700°C, and final solution treatment at 950, 1000 or 1050°C for 200 seconds. The microstructure after the different heat treatments was investigated using light microscopy, scanning electron microscopy (SEM) and electron backscattered diffraction (EBSD). The latter was particularly useful in accurately measuring grain size. The microstructural evolution of both alloys during creep testing was also monitored. This was done in order to examine the microstructural changes that occur during the prolonged creep testing period. Not surprisingly, the creep tests at initial stresses of 5, 10 and 15 MPa all revealed greater creep resistance for the higher Nb-containing alloy heat. However, the correlation with solution treatment practice was much less obvious, particularly for the alloy with

the lower Nb content. Detailed analysis of the precipitate distribution after the various heat treatments is presented to illustrate the difference in microstructure that can arise and consequently consideration is given to the influence of precipitation on creep behaviour.

Table of contents

1. Chapter 1: Introduction

1.1. Project background

Ferritic stainless steel is used for the production of catalytic converter housings, which form part of the exhaust system of a motorcar. Stainless steel is popular in this application owing to its attractive properties such as high temperature strength, exceptional fabrication properties and oxidation resistance. For this particular application the creep resistance (i.e. hot strength) of this material is of utmost importance as catalytic converters can be exposed to temperatures in excess of 800 °C[1] in service and are in operation for prolonged periods of time. The average life span of a catalytic converter varies between 5 to 7 years, practically the average period an initial owner keeps a vehicle[2].

Type 441 (DIN 1.4509) ferritic stainless steel, is produced for use in automotive components, particularly for the front end of an exhaust system. This is largely due to its superior mechanical strength at elevated temperatures[3]. It is this particular property which makes it preferable for the fabrication of catalytic converter housings. Although the austenitic grades of stainless steels generally have a superior creep and oxidation resistance to the ferritic grades, the ferritics are the more economical choice, therefore generally the preferred choice. The austenitic grades are more costly due to their Ni content, whereas the ferritics do not contain Ni as an intentional alloying element.

Owing to the fact that there are certain requirements that manufacturers of catalytic converters need to adhere to with regards to degradation of the material under service conditions i.e. exposure to high temperatures, thermal shock, etc, it is necessary that the type 441 produced renders maximum reliability and performance. Creep resistance is an important property that the material should possess due to the high temperatures that the material is exposed to during service. In order to improve the creep resistance of this grade of stainless steel it is necessary to understand the effect the thermo-mechanical processes have on the steel and whether or not these processes can in fact be enhanced to guarantee the ultimate in results and promote a level of consistency with regards to quality. Prior research has indicated that in order to promote

optimum creep resistance for type 441, an increase in Nb content, an enlarged grain size and a high final annealing temperature is advantageous[4].

The present project includes investigating the findings of creep test results on two alloys of type 441, where the creep test results are used as a measure of the hot strength. Throughout this report the two alloys are referred to as alloy A and alloy B. The fundamental difference between the two is that the one alloy (alloy B) has a higher Nb content than the other (alloy A). This percentage weight difference is of great importance to the study as it allows an analysis into the differences in creep resistance as a result of Nb content and the effect this difference has on other microstructural aspects such as grain size and precipitate behaviour.

In a previous study, it was established that alloy A showed superior creep resistance to alloy B[5]. This is, however, contradictory to the literature, which states that, due to the higher Nb content a higher creep resistance of the material should result[6]. Whilst, alloy B has the higher Nb content, alloy A on this occasion had a larger grain size than that of alloy B (after a predetermined heat treatment, which is performed to promote recrystallisation). This study showed that the effect of Nb in solution appeared to be inferior to the effect that grain size had on the creep resistance in relation to these two alloys.

Owing to the fact that alloy A was more creep resistant than alloy B, explained by the final larger grain size, it was questioned as to whether it would be feasible to increase the grain size of alloy B to match that of alloy A at its optimum grain size (and creep resistance) and then repeat the various creep tests. This would therefore omit the influence of the grain size on the creep resistance of the alloys (as the grain sizes would be the same) and conclude how the Nb content was in fact affecting the creep resistance.

This research will also include examination of the microstructure of the material post heat treatment to determine the grain size and level of precipitate (which would include identifying precipitates) that could be influencing the creep resistance. Microstructural analysis will also be performed on aged (soaked) samples to monitor the effect of prolonged time at temperature on the precipitate activity and the effect this may have on grain size variance. Therefore an

analysis of the creep curves in relation to the microstructural features would assist in determining the principal factors that influence the creep resistance of the material.

1.2. Project aims

Broadly the aims of the project can be noted as follows:

- To optimise the creep resistance of type 441 stainless steel
- To determine the influence of bulk Nb content on the creep resistance of type 441
- To determine the influence of microstructural effects, including solute level of Nb, precipitate population and grain size on the creep resistance of type 441

1.3. Project constraints

The majority of creep tests were run until fracture of the specimen occurred. In some cases depending on the alloy used, prior heat treatment and creep load, the test time could endure over 1000 hours. The longer test periods clearly presented a hindrance with regards to time constraints. These long test times also became particularly problematic due to unannounced power failures that became prevalent in the Western Cape from February 2006. Power failures remained a concern throughout the testing phase.

2. Chapter 2: Literature Review

2.1. Introduction to stainless steel

Stainless steels are well-known for having a high resistance to corrosion; this is largely due to the Cr content of the steel. Broadly speaking the corrosion resistance of stainless steels improves as the Cr content increases. When Cr combines with O it results in a Cr containing oxide that forms a passive protective thin film on the surface of the steel, it is this film that prevents the Fe in the steel from oxidising. This film is self-healing so if the surface of the steel becomes damaged, more oxide quickly forms and protects the exposed surface. Nevertheless and contrary to popular belief, stainless steels are not indestructible. The passive film can weaken under certain conditions which can result in corrosion. It is therefore crucial to select the correct type and grade of stainless steel for a certain application. Whilst choosing a type and grade it is also necessary to consider the mechanical and physical properties that it has, as the manner in which it performs in service is mainly due to the composition and prior thermal processing of the steel.

There are many different types of alloys that can be clustered into the stainless steel group, with new grades still being developed today. These new grades are produced by alloying the basic composition of stainless steel (Fe, C and Cr) with other elements such as Ni, Mo, Ti, Nb, Si, Ta, W, V, Al, Mn, Co and Cu. The addition of these elements allows certain material properties to be produced and or enhanced.

Stainless steels are the ideal choice of material in a wide variety of industries due to their numerous favourable properties, which include the following[7, 8].

- Long Term Value: When the total life cycle costs are considered, stainless steel is often the least expensive option in a life cycle cost comparison.
- Low Maintenance Costs: Stainless steel is fairly easily maintained and normally only requires a periodic clean using a dilute solution of household detergent and water.

- Ease of Fabrication: Modern steel manipulation techniques mean that the majority of stainless steels can be cut, welded, formed and fabricated as readily as traditional steels and other materials.
- Corrosion Resistance: Lower alloy grades resist corrosion in normal atmospheric and water environments, while the more highly alloyed grades can resist corrosion in many acids and alkaline solutions, and some chloride bearing environments.
- Extreme temperature resistance: Some grades will maintain high strength at very high temperatures, while resisting scaling, although others show exceptional toughness at cryogenic temperatures.
- High Strength: The mechanical properties of stainless steels allow thinner sections to be used than with other materials, thus reducing weight without compromising strength. This in turn not only reduces weight, but also cost.
- Hygienic properties: Stainless steel is internationally known as the most hygienic surface for the preparation of foods, due to its non toxicity. The unique surface of stainless steel has no pores or cracks to amass dirt and or bacteria. This 'cleansability' trait far exceeds other surfaces and makes it the first choice for strict hygienic environments, such as hospitals, commercial kitchens, abattoirs and other food and beverage processing plants.
- Aesthetic appeal: The shiny, easily maintained surface of stainless steel provides a stylish appearance.
- Recyclable: Stainless steel is fully recyclable.

2.2. Stainless steel types

The crystal structure of a metal relies on its chemical composition, these crystal structures are known by specific names. The crystal structures of the main types of stainless steels are martensite, ferrite and austenite. The names of these crystal structures are used to classify the three types of stainless steels, namely austenitic, ferritic and martensitic.

The American Iron and Steel Institute (AISI) use three numbers to categorise the standard grades of stainless steel. Austentic grades are designated by numbers in the 200 and 300

series, whereas ferritic and martensitic grades are designated by numbers in the 400 series. The following paragraphs discuss each of the three key types of stainless steels.

2.2.1. Austenitic stainless steels

This grade is the most recognized of the stainless steel family and accounts for more than 70 % of production. These non-magnetic alloys contain a maximum of 0.15 % C, a minimum of 16 % Cr and adequate Ni and/or Mn to maintain an austenitic structure at all temperatures from the cryogenic point up to the melting point of the alloy. They are, however, by and large more expensive than the other grades because of their Ni content. The Ni content is responsible for their superior corrosion resistance as compared to the other grades.

Austenitics are used in diverse applications, which range from cutlery to medical equipment to food and beverage processing to marine hardware. In particular their resistance to attack by acids, alkalis and other chemicals has led to their extensive use in the chemical and process plant industries[7].

2.2.2. Martensitic stainless steels

Martensitic stainless steels were the first stainless steels that were commercially developed. The basic composition of this magnetic alloy is typically between 12 % and 18 % Cr with a higher C content than the ferritic grades. Some of the grades include additional alloying elements in small quantities. They are, however, not as corrosion resistant as the ferritic and austenitic types, but are extremely strong and highly machineable, and can be hardened by heat treatment.

Applications for this grade range from cutlery to surgical instruments to springs and fasteners[7].

2.2.3. Ferritic stainless steels

Ferritic stainless steels are plain Cr stainless steels, which typically have a low C content. They contain between 10.5 % and 30 % Cr and very little Ni (generally less than 0.35 %) or no Ni at all. It is their lack of Ni content that allows this grade of stainless steel to be more cost effective. Due to this reason this grade is known as the economical stainless steel and is

usually used in more mildly corrosive environments, often being used for less severe applications. Compositions of this grade generally include alloying of various elements such as Mo, Ti and Nb.

Ferritic stainless steels are magnetic and have moderate ductility and formability and resistance to corrosion and oxidation. Although corrosion resistant, they are less corrosion resistant than the austenitic grades, but have superior corrosion resistance to martensitic stainless steels.

A key benefit of the material is its resistance to stress corrosion cracking in chloride environments. However, with regards to welding the material there are limitations. These limitations restrict their use to thinner gauges (up to a thickness of 2,5 mm)[9].

Within the range of ferritic stainless steels, four distinctive compositions can be broadly classified, based on their Cr percentages. They are as follows[10]:

- The 'minimum' steel which contains 11 to 12 % Cr.
- The 17 % Cr grade; type 430 is the most common of this composition.
- The stabilised 17 % Cr steels, which contain additions of elements such as Ti, Nb or Zr.
- The high Cr ferritic grades, which have Cr levels within the vicinity of 24 % to 28 %.

They can then be further classified following typical applications for the different grades (400 Series—ferritic and martensitic alloys classification) as defined by the AISI and include:

- Type 408: Heat-resistant, although poor corrosion resistance.
- Type 409: Used extensively in the automotive industry particularly for automobile exhaust tubing and trim.
- Type 410: Martensitic grade, has high-strength.
- Type 420: Known as the "Cutlery Grade" (martensitic).
- Type 430: Used generally for decorative purposes, often for automotive trim; cutlery and catering equipment.
- Type 444: Used for hot water tanks.

- 3CR12: Unlike other ferritic stainless steels this grade can be welded in thicknesses of up to 30mm. It is used in the mining, materials handling and sugar industries due to its high resistance to atmospheric corrosion and wet abrasive corrosion.
- Type 441 (also known as DIN 1.4509): Various alloys have been developed over the years for specific applications, still it became increasingly important to develop a stainless steel that could endure higher temperatures. Nb was therefore added to the 18 % Cr, ferritic alloy; the grade then became branded as type 441. Its advanced mechanical strength at high temperatures (see table 3) made it the ideal material for the front end of an exhaust system[9]. The high temperature strength of this type exceeds that of type 409 and 439[11]. It also shows a noticeable increase in corrosion and oxidation resistance to type 409, this is probably due to its higher percentage Cr content; 409 has an 11 % Cr content. It has been observed that the proof strength of Nb added stainless steels is higher than that of type 409 and 410 particularly in the temperature range of 600-900 °C, a temperature range which is of particular importance to this study[12]. Properties and temperature conditions that type 441 can be exposed to are seen in table 1, 2 and 3.

Table 1: Mechanical Properties of stainless steel type 441[9]

Property	Nominal
Tensile Strength	430 MPa (min)
0,2 % Proof Stress	250 MPa (min)
Elongation	18 % (min)
Brinell Hardness	180 (max)

Note: The above table is for the product as cold rolled strip and the elongation is over a gauge length of 50 mm.

Table 2: Short time elevated temperature strength of type 441[9]

Temperature (°C)	100	300	500	700
Tensile Strength (MPa)	460	400	350	200

Table 3: Maximum recommended service temperature (in oxidising conditions) of type 441[9]

Operating conditions	Temperature (°C)
Continuous	850
Intermittent	950

2.2.3.1. Stabilisation of ferritic stainless steels

The corrosion resistance of stainless steels can be unfavourably affected by sensitisation (intergranular corrosion after welding). Sensitisation and weld decay of stainless steel is due to the precipitation of unfavourable Cr carbides therefore if the amount of stabiliser is adequate, Cr carbide precipitation is inhibited, particularly in the heat affected zones of welds. The primary effect therefore of stabilisers such as Nb, Ti, Zn, Ta, Hf and V is to tie up C and N in the form of nitrides and carbides, which effectively remove C. The elements found to be the most useful as far as sensitisation is concerned are Ti and Nb[13].

Traditionally ferritic stainless steels have previously been stabilised with Ti only, which resulted in a single stabilised steel. Yet, the ensuing properties rendered the material inadequate for use in exhaust systems. Research has shown that by dual stabilising the stainless steel with Ti and Nb the steels exhibit superior service performance when compared with single-stabilised steels. These benefits include; improved surface quality, improved formability and weldability, improved creep resistance, enhanced thermal fatigue resistance and better high temperature oxidation resistance[14]. Type 441 is dual stabilised with Ti and Nb, in general the Ti is viewed as being responsible for reducing sensitisation and the Nb renders strength at elevated temperatures.

Stabilised stainless steels were developed mainly for high temperature applications such as superheater tubes; this was primarily because of their good oxidation resistance. In time, however, it became evident that they also have good high temperature creep resistance, in this case the use of Nb as an alloying element has been essential to the development of many creep resisting steels[15].

For a ferritic stainless steel to be described as stabilised it must remain ferritic at all temperatures.

2.2.3.2. Effect of Nb on high temperature properties of ferritic stainless steels

Generally ferritic stainless steels are preferred for high temperature applications; this is largely due to them being more cost effective as compared to the austenitic alloys. But, austenitic stainless steels do exhibit better thermal fatigue resistance and mechanical properties at higher temperatures than the ferritic grades. In fact ferritic stainless steels are inherently not strong at elevated temperatures, although with the addition of Nb as an alloying element and appropriate heat treatments they can be strong even at elevated temperatures.

The chemical element Niobium (Nb) is also often referred to as Columbium (Cb). Nb is added to ferritic stainless steels to promote numerous benefits that include the following[16]:

- Intergranular corrosion resistance (stabilisation)
- Creep resistance
- Roping and ridging resistance
- Improved surface quality

The methods used to increase the creep resistance in stainless steels are usually either by solid solution strengthening or by promoting the formation of precipitates either prior to or during service. Here Nb is mostly useful as an alloying element as it can fulfil both of these roles i.e. as a solid solution strengthener and then as a precipitate (in the form of Nb carbonitrides and also in the form of the intermetallic Laves phase). With reference to an alloy, some Nb combines with N and some with C, the amount of Nb added although is usually higher than is stoichiometrically required. This uncombined Nb is then available to function as an alloying element in the form of precipitates.

In fact previous studies have shown that small amounts of Nb in solid solution affect the high temperature strength of ferritic stainless steels considerably [6, 15, 17]. Figure 1 illustrates the superiority of Nb as an alloying element in stainless steels as compared to other elements regarding heightened proof strength.

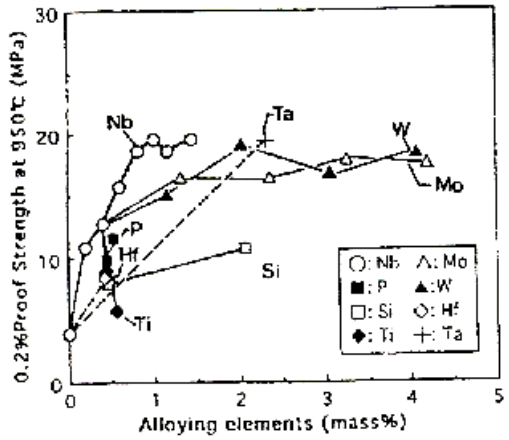

Figure 1: Effect of alloying elements on 0.2 % proof strength at 950 °C for 0.02 (C+N)-19Cr steels[6]

The most common high temperature applications of ferritic stainless steels include automobile exhaust systems; for this application materials should have high yield strength at high temperatures and low coefficient of thermal expansion. Ferritic stainless steels are evidently particularly useful for this application, which is also due to their excellent heat resistant properties, especially thermal fatigue resistance. In fact the material is generally the preferred choice for the hot end of exhaust systems; this is largely due to the precipitation of intermetallic precipitates of Nb (prior to service and during service) which promotes a higher creep resistance[18].

Other high temperature applications include steam turbine rotors, boiler tubing, heater elements and components for nuclear reactors and petroleum refineries.

2.3. Stainless steel and automotive exhaust components

Stainless steel is preferred to mild steel for the manufacture of exhaust components for obvious reasons such as higher oxidation and creep resistance, which will result in a longer service life. Automotive components that are often manufactured from stainless steel range from mufflers, to manifolds, to resonators, to housings of catalytic converters, to heat shields, brackets and pipes[14].

For the manufacture of automotive exhaust components materials that are easily weldable, have good formability, resistance to degradation (up to 950 ºC), creep, thermal oxidation, cracking from thermal shock and resistance to high oscillating stresses (due to vibration) are necessary. Corrosion resistance to chloride solutions is also required because of the use of ice-melting salts on the roads in cold conditions. Yet due to the fact that the automotive industry is subject to strong competition, materials used in this application need to be economically competitive.

For these reasons many parts of exhaust systems have in the past been manufactured from ferritic stainless steel type 409[19], which is a more cost effective Ti stabilised lower percentage Cr stainless steel. Nevertheless, metal temperatures of some of the components within the exhaust system are expected to exceed 815 °C, which is the useful temperature limit of type 409[20]. This material therefore lacked the essential oxidation resistance and hot strength capability, predominantly for some engines with higher than average exhaust temperatures. In order to handle the oxidation encountered at the higher temperatures and enhance the resistance to surface rust staining which type 409 was prone to, type 439 was made use of instead. This raised the Cr content to 18 %. Yet as temperatures got even higher for exhaust gases (which can be in excess of 900 °C) it became necessary to increase the material's hot strength (creep resistance and thermal fatigue strength) capabilities; to do this Nb was added to the 18 % Cr alloy, thus creating type 441[21]. This steel has adequate heat resistance in the temperature range of 815-982 °C and also allows the progressive oxidation scaling resistance to be raised to the 900-980 ºC range[20, 21].

2.4. Stainless steel and the catalytic converter

The catalytic converter was developed in the 1970's to help to decrease the emissions from car exhausts and since the 1980's the use of these devices has been necessitated due to legislation in many countries. In fact in the European Union since January 1993, all new petrol driven cars sold have been fitted with a catalytic converter[22], this is similar to the United States were in 2005 100 % of new cars sold were fitted with one. This is in order to comply with provisions of the Federal Clean Air Act, which is United States federal legislation relating to

the reduction of smog and air pollution. On a worldscale over 90 % of new cars sold had a catalytic converter fitted[23].

South Africa produces an estimated 14 % of the world's automotive catalytic converters[24], with Port Elizabeth being touted as the 'catalytic converter capital of the world[25]. Annual production of catalytic converters in South Africa has increased markedly from 1993, where the amount of converters produced was below two million, to 2005 which was in excess of fourteen million[26].

Catalytic converters are the largest of the automotive component groupings being exported from South Africa, which presently amounts to about $500 million per year in revenue. This makes this industry one of the biggest stainless steel users in South Africa, consuming about 43000 tonnes per annum[27].

A catalytic converter usually consists of a ceramic honeycomb structure known as a monolith; the catalyst is coated onto this structure. The monolith is housed in a stainless steel housing or casing. On assembly, the housing is welded together and then secured to the exhaust pipe. The device is installed in the exhaust line, generally between the exhaust manifold and the muffler. As exhaust gasses pass through the catalyst (which is in the form of Pt, Rh and or Pd) a chemical reaction occurs which converts harmful compounds that occur in cars exhaust fumes into harmless compounds.

High temperature application of ferritic Cr steels are usually restricted to conditions with low stresses, therefore its use as the housing of catalytic converters is supported. The majority of the stress exerted on the housing would be due to its own weight and the weight of the monolith that is held inside the housing.

2.5. Introduction to material deformation behaviour

To understand how materials deform under various conditions (such as elevated temperature) it is firstly necessary to understand how the mechanical behaviour and properties of materials

can be affected by deformation and defects. The following paragraphs will therefore deal with these concepts.

When a material is exposed to an applied stress it reacts either in an elastic or plastic manner. Elastic behaviour is the strain of a material that is not permanent, meaning that the material can return to its original geometry when the applied stress is taken away. Plastic behaviour, on the other hand, describes a material that has been strained and that does not return to its original geometry even after the stress has been removed. The instance where a material's behaviour changes from elastic to plastic is called the yield stress. For some materials, this point is difficult to isolate on a stress strain curve and in such cases it is preferential to quote the proof stress rather. Proof stress can then be defined by the stress which produces permanent strain equal to a specified percentage of the specimen length. A broad-spectrum proof stress is one that is equivalent to 1 % strain.

When a ductile material is deformed in tension, it first behaves nearly linearly. Upon further applied stress, past a material's ultimate tensile strength (UTS), the material's cross-sectional area decreases, which can result in the necking of the specimen. Necking is a decrease in a restricted region (usually the gauge length) of a tensile/creep specimen instead of over its entire length. During necking voids begin to form which weaken the material and increase the local stress which eventually pulls the material apart. While the cross-sectional area decreases, the amount of stress within the area of necking will continue to increase, since stress is given by:

$$\sigma = \frac{F}{A}$$

Where: σ = stress; F = the force being applied and A = the instantaneous cross-sectional area. The decreasing cross-sectional area causes the stress to increase, although the force being applied remains the same.

Necking usually occurs due to either defects that are caused by stress or by pre-existing defects. The usual order for failure by necking is:

- Neck formation

- Cavity void formation
- Void coalescence to form cracks caused by dislocation movement
- Crack propagation through the neck
- Failure

For engineering materials there are two potential modes of fracture, namely ductile and brittle. Typically the main difference between a brittle and a ductile fracture is the amount of plastic deformation that the material undergoes before fracture actually occurs. Ductile materials exhibit large amounts of plastic deformation whereas brittle materials show little or no plastic deformation before fracture. Figure 2 shows these differences on a macroscopic level.

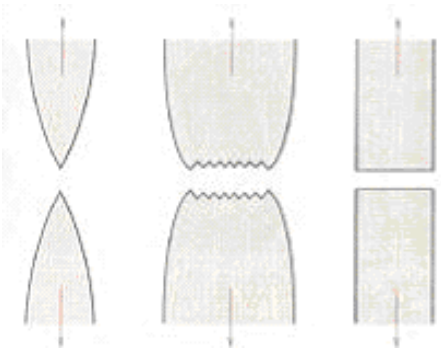

(a) (b) (c)

Figure 2: Three examples of fracture, showing: (a) a highly ductile fracture in which the specimen necks down to a point, (b) a moderate ductile fracture after some necking and (c) a brittle fracture without any plastic deformation[28].

So for fracture to occur it is necessary for a crack to commence and then propagate throughout a section. The behavior through which the crack propagates through the material can indicate the mode of fracture. For a ductile fracture, the crack moves slowly with a large amount of plastic deformation. Contrary to this for a brittle fracture, cracks spread quickly with little or no plastic deformation. A crack that passes through the grains within the material is undergoing transgranular fracture. However, a crack that propagates along the grain boundaries is known as an intergranular fracture. The two sides of a fracture point can be matched up after the material has failed[28].

2.5.1. Defects

Metals are made up of crystalline grains that are detached by grain boundaries. Nevertheless, within grains crystals are not perfect and contain defects, which can have an effect on the mechanical properties of a material. There are three types of defects, namely:

2.5.1.1. Point defects

A point defect involves a single atom change to a normal crystal.

The three major types of point defects are as follows[29]:

- Substitutional impurities: Is an atom that occupies a normal lattice site, but is of a different element than the bulk material.
- Interstitial impurities: Is an atom occupying a position between normal lattice sites (such as C, O and N). A self interstitial is when the interstitial is of the same type as the bulk material.
- Vacancies: Where there is a vacant lattice site in the crystal lattice, resulting in a hole.

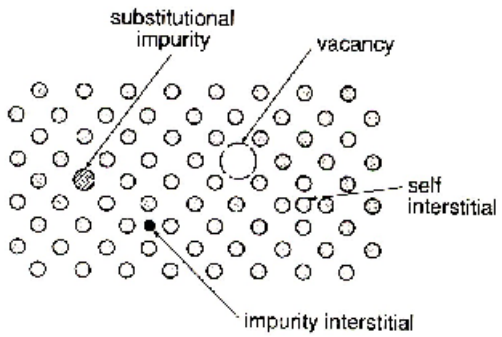

Figure 3: Different types of point defects within a crystal[29].

2.5.1.2. Line defects

- Line defects: Are linear bands of lattice imperfections.
- Dislocations: A linear band of atoms that joins an area in a crystal that has slipped relative to the rest of the crystal i.e. a line discontinuity. There are two basic types: edge and screw dislocations.

2.5.1.3. Planar/surface defects

- Grain boundaries: The majority of metals are polycrystalline, which means that their microstructure is made up of small grains, each of which is an individual crystal[30]. These grains are separated by grain boundaries, which are in themselves planar defects, as they can act as the agents of intergranular deformation. Grain boundaries can move in their plane (sliding) or normal to it (migration).

- Microcracks: These cracks can also be regarded as planar defects. Failures of components can begin from these tiny cracks. Although it does require permanent deformation for a metal to fail in fatigue, the failure may start at these tiny cracks, particularly in an area of stress concentration.

Another type of defect which can be referred to as a three-dimensional defect would be a precipitate.

2.5.2. Diffusion

The dominant diffusion mechanism in most metals and alloys is vacancy movement; consequently diffusion occurs due to the presence of vacancies within the crystal lattice[32]. Due to the process being thermally activated an atom can only move to the site of an adjacent vacancy, if there is enough thermal energy to allow it to move from its original site. However, even if an atom has sufficient energy to move from its original site it can only move if a vacancy exists on the adjacent site to allow the move to take place. The process of diffusion becomes significant in metals at high temperatures, which is usually greater than 0.4 times the melting temperature of that metal.

At high temperatures there is enough thermal energy for diffusion to move through the bulk of the lattice; this is known as bulk or volume diffusion. But, at lower temperatures diffusion occurs along paths that offer less resistance such as grain boundaries, this process is known as grain boundary diffusion[30].

2.5.3. Dislocation motion

A material deforms under an applied stress due to the movement of dislocations gliding through the crystal lattice, the motion of these dislocations is preferred in particular crystallographically controlled directions.

There are two types of dislocations: edge dislocations and screw dislocations. An edge dislocation is formed in a metal when an extra row of atoms has been inserted or removed in the crystal structure. This is demonstrated in figure 4 where an edge dislocation can be seen to be moving through a crystal. The one side of the crystal slips a distance relative to the other side of the crystal; thereby introducing an extra half plane of atoms into the crystal lattice. The direction and magnitude of the amount of slip is known as the Burgers vector, b[30].

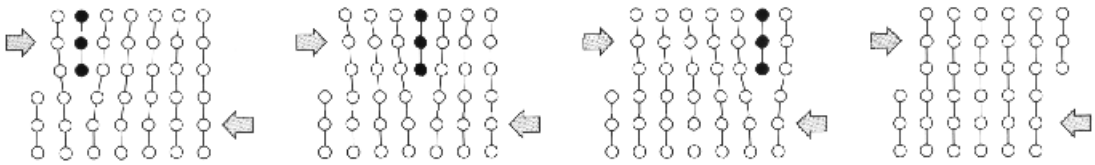

Figure 4: Glide of an edge dislocation through a crystal lattice[30]

A distinction between the motion of a screw dislocation and an edge dislocation is that the screw dislocation is symmetrical about its axis like a helical type of structure as illustrated in figure 5. Also an edge dislocation is restricted to a single glide plane whereas a screw dislocation is not and can cross slip into another glide plane.

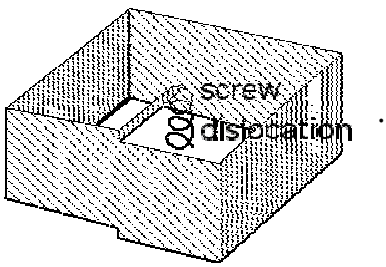

Figure 5: Screw dislocation[31]

Dislocations in solids generally have a combined edge and screw nature and form curves and loops. This combination of types of dislocations is often referred to as mixed dislocations.

Where many of these mixed dislocations are present intricate tangles of dislocation lines may form.

The plane in which a dislocation moves through the lattice is called the slip plane or the glide plane and the direction in which it moves is called the slip direction. The combination of the two is referred to as a slip system.

The Critical Resolved Shear Stress (CRSS), or the Peierls stress, is the stress needed to initiate the dislocation motion. Even so, once the CRSS has been reached, dislocation movement may still be impeded by obstacles within the crystal lattice, such as precipitates. Nevertheless it is possible for the dislocations to prevail over these obstacles by various methods. In crystalline materials plastic deformation is generally denoted to dislocation movements through various rate controlling processes such as glide, cross-slip or climb. In the case of an edge dislocation, dislocations climb over the obstacles, whereas in the case of screw dislocations they cross slip over the obstacles.

A fundamental difference between slip and climb is the temperature dependence. Since the mobility of atoms increases with high temperature, diffusion controlled processes become more noticeable at higher temperatures. In particular climb occurs much more rapidly at high temperatures than at low temperatures due to an increase in vacancy motion. Slip, although has only a small dependence on temperature.

In real terms dislocations also contain kinks and jogs. Kinks and jogs are normally formed during glide when dislocations interact. A kink is a step in the dislocation line in the slip plane, while a jog is a step in the dislocation line onto a different slip plane.

Dislocations can also further dissociate into one or more partial dislocations. This dissociation may result in the atoms between them being no longer stacked in the correct sequence, which results in a stacking fault, these faults then carry certain stacking fault energy.

2.6. High temperature creep in metallic materials

Creep is the term used to explain the time-dependant plastic deformation of materials under conditions of constant load or stress (below its yield stress) at elevated temperatures (with respect to the materials melting temperature)[32]. Creep rate increases with increasing temperature and stress and involves dislocation motion and diffusion of vacancies. The defects start to move through the material when there is enough thermal energy provided, which is provided by high temperatures. Creep damage accumulates in the form of internal voids, which appear on grain boundaries normal to the tensile stress. This deformation of a material is a result of defects moving through the crystal lattice of the material, although as diffusion occurs most rapidly at grain boundaries, creep deformation is often concentrated here. Over a period of time the voids that have accumulated grow bigger until they eventually link together which results in creep fracture.

From this it can be seen that for creep to occur there are three basic parameters that need to be considered, namely[32]:

- stress (σ)
- temperature (T)
- time (t)

These parameters are then expressed by the following formula:

$$\dot{\varepsilon} = \text{f, } (\sigma, \text{T, t})$$

Where $\dot{\varepsilon}$ is the creep strain rate

The strength of most materials is effected by the temperature to which the material is exposed to, in other words if a material is exposed to a temperature above a certain range, the strength of this material will inherently decrease. The temperature above which this slow deformation occurs does differ depending on the selected material. It is due to this factor that during a design process, the temperature of service to which the component may be exposed to, must be considered. Operating temperatures are often limited by the high temperature performance of available engineering materials, owing to this efforts have been made and are being made to develop and or improve the high temperature properties of engineering materials. The

temperature at which creep becomes an issue is related to the melting point of the alloy concerned. Creep specifically becomes a limiting factor when a material is operating at a high homologous temperature (the ratio of a material's absolute temperature, T to its melting temperature, Tm). For metals, it is generally accepted that creep becomes a limiting factor in the region of 0.4 Tm, this region is then known as the regime of high-temperature creep.

It is obvious then that creep is undesirable as it can result in the change of geometry of components, which could ultimately end in fracture or failure. Therefore in order to render the best probable creep resistance there are a number of processes that can be used to develop the creep resistance of materials. These processes range from solid solution strengthening (for example alloying with Nb), precipitation strengthening (in order to act as obstacles in the way of dislocations moving through the lattice), and the promoting of a large grain size. These processes will be discussed in more detail at the end of the chapter. To promote creep resistance it would also be beneficial to use a material that has a high melting point, predominantly when designing components that have long-term exposure to high temperatures. Creep resistance is also greater in a matrix of low stacking fault energy. This is because the dislocations are dissociated, so it is more difficult for them to cross-slip and climb in their efforts to avoid obstacles.

It should be noted that service lives in creep situations may be limited by excess deformation rather than by failure, where creep is not just a measure to failure, but instead a measure to ensure that creep does not cause unacceptable dimensional changes.

For the various grades of stainless steels the areas of application involving creep range quite substantially. Martensitics are used under high stresses, but at temperature that do not exceed 550 °C. Austenitics are used at lower stresses, but at temperatures that may reach up to 1150 °C. Ferritics are generally only used in low stresses applications and are used mainly for their resistance to oxidation[10].

When plotting creep data a characteristic creep curve (as seen in figure 6) often results. Take note this graph shows strain plotted against time. Strain is often substituted for extension (mm).

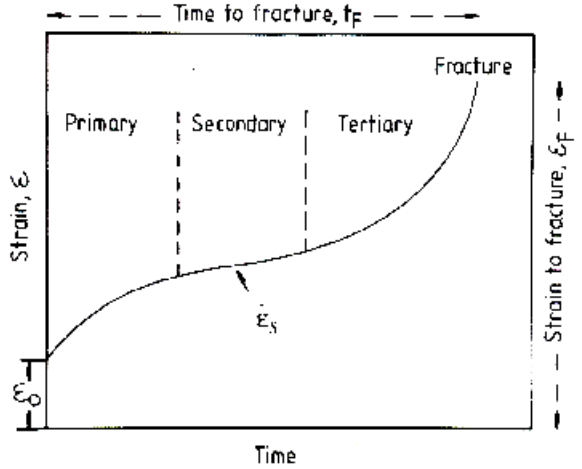

Figure 6: Characteristic creep curve, showing the different stages of creep[32]

With reference to figure 6 it is clear that there are three distinctive regions of creep:

- Primary (transient)
- Secondary (steady-state)
- Tertiary

Each one of these regions can be investigated to determine the strain/creep rate pertaining to that particular stage. The creep curve in figure 6, demonstrates on application of load a decreasing creep rate with time, in the primary region. As the creep rate stabilises a state is reached which is known as the secondary creep region (steady state creep). This stage indicates a minimum creep rate, and is usually the longest stage showing little change over a significant range of strain and time. In contrast with the first stage, steady state creep increases markedly with temperature and stress. Once the material develops voids and or cracks tertiary creep becomes predominant, which results in the material having a sharpened increase in creep rate. Tertiary creep can and often does end in fracture. This point of fracture is termed creep rupture. Tertiary creep is not taken into account for design purposes since excessive elongation usually occurs prior to tertiary creep. The various types of creep damage

leading to tertiary creep can be recognized as necking, void formation, microstructural evolution and environmental degradation. The microstucture that arises during creep is influenced by these processes, although it can be said that creep properties are dependant on the initial microstructure of the metal, which is controlled by heat treatments.

Generally the most significant part of a creep curve, particularly to designers and engineers, is the steady state section. This is because steady state creep usually takes up most of the time of a creep test and components ideally spend most of their service life in this section. Steady state creep rate is given by the slope of the straight line (when the slope is constant). By establishing the creep rate or the strain rate designers and engineers can approximate how much time it takes for a component to reach a definite amount of deformation[32]. This region represents a section in which there is a balance between work hardening and recovery processes which result in the minimum constant creep rate.

Creep curves, on the other hand, do not always resemble the characteristic creep curve as seen in figure 6. Material properties and also the temperature and applied stress to which the material is exposed to during the creep test can influence the curves appearance quite substantially. Actual creep curves that have been produced from metals and alloys could predominantly exhibit either the primary or tertiary stages. For example a specific form of creep curve that has been extensively reported in precipitation strengthened nickel-based superalloys exhibits a short primary stage followed by an extended tertiary creep stage, an example of which is seen in figure 7. Similar creep curves were observed by Borneman and likewise Cain in their work on creep testing of ferritic stainless steel[5, 33].

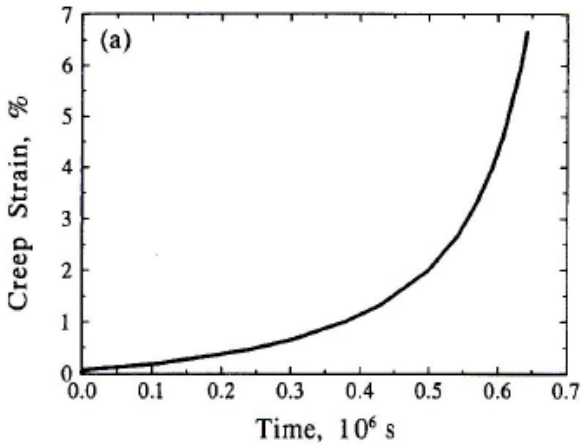

Figure 7: Creep curve of a precipitation strengthened Ni-based superalloy[34]

2.7. Creep testing: General concepts

A creep test measures the deformation of a material under predetermined conditions of temperature and stress/load over a definite period of time (or until fracture/failure). Tensile testing is the universally accepted method to conduct creep testing, although the technique used for creep testing is more complex than the standard tensile test. The reason for this is that a creep test includes the prolonged application of a constant load to the specimen, the application and monitoring of the temperature of the specimen during the test and the measurement of the deformation of the specimen at specific intervals over a certain time period. The monitoring of this deformation is often complex as it must be done in such a way as to not disturb the test itself.

Creep testing is typically a lengthy practice; in fact test time periods can range from 100 hours to 10000 hours or even longer. Depending on the type of information required from a creep test it is frequently important to run tests for prolonged periods as it is necessary to replicate lifetimes of components and service conditions. In order to shorten long term tests a particular value of creep strain is often noted, such as the time taken to reach 1 % or 2 % strain, this value could then be considered to represent failure. Also for theoretical studies, such as evaluating how a change in microstructure can affect the creep behaviour of a material, short-term test programmes are often employed[35].

Due to the fact that small changes of stress and temperature can result in large changes of strain, tolerances on the variables have to be small in order to produce accurate results. Creep testing therefore can often prove to be quite tedious, as purpose built rigs often prove to be complicated to operate and accurate measurement of temperatures and deformation is often complex.

There are various types of creep testing, with each test being able to measure different aspects relating to creep, such as tests that measure creep, stress-rupture and stress relaxation. The most common form of creep tests are constant load creep tests, in these tests the load is kept constant for the duration of a test. Hence, as the specimen elongates and the cross sectional area decreases the stress increases, even so, when reporting creep test results the initial applied stress that was applied to the specimen is the stress that is documented.

Creep tests can also be performed under constant stress conditions. This type of testing, although is more intricate than constant load creep testing as it requires a method wherein the applied load can be adjusted as the specimen elongates. This configuration is necessary in order to maintain a constant stress on the specimen itself.

Two types of creep tests can typically be run on similar rigs, depending on what information is needed. The stress rupture test lets the specimen deform until fracture happens; this type of test is run under a constant stress and temperature. In this type of testing it is not necessary to monitor the displacement of the specimen just the time taken for the specimen to fail is noted. The stress-relaxation test is in contrast, a test that has the load continually decreasing at specific intervals instead of remaining constant; this is done in order to sustain a constant strain on the specimen.

It is crucial that precise test procedures be in place to establish the creep rates of various materials to promote standardisation and accuracy. This is why a series of international standards have been created for creep testing.

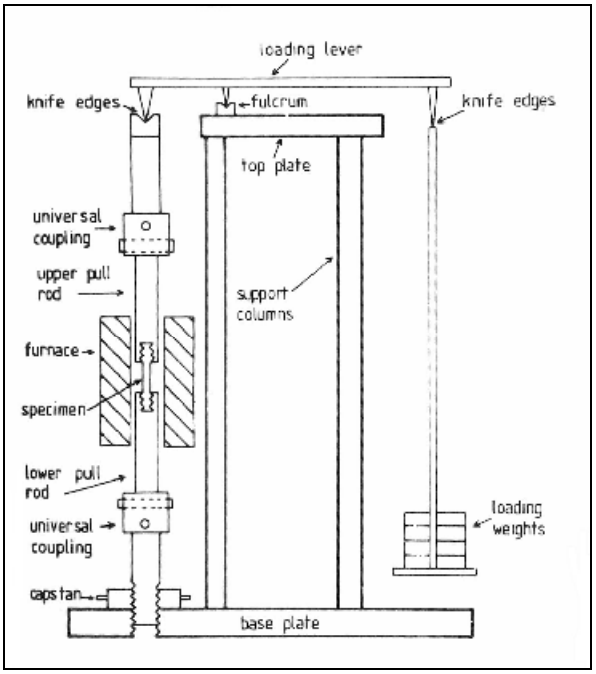

Figure 8: Schematic of constant load creep rig[32]

Apart from using creep test rigs to monitor the hot strength of materials another method that is often used is the sag test which was developed as a more cost effective system; this is because creep rigs are often costly to purchase and also trained personnel are needed to operate them. Sag testing is usually used to compare alloys creep resistances against one another. The most common method that is used is referred to as the two-point beam arrangement[2]. A typical example of such is shown in figure 9. In simple terms the specimens are placed onto the rig longitudinally, across the two supports. The rig (including the specimens) is then placed into a furnace for a specific time at a specific temperature and the specimens are allowed to sag under their own weight for this specified time. The amount by which the specimen has sagged is then determined by monitoring how much the specimen has deflected, from a reference position before the test, in comparison to that after the test.

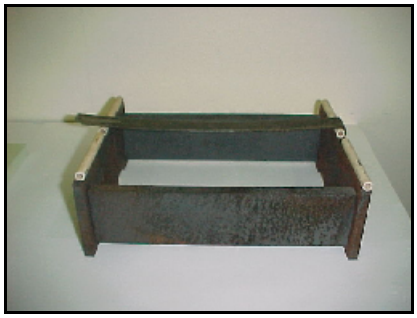

Figure 9: Typical two point beam sag test rig (with specimen lying across the supports)[5]

Although simplistic, this method is a convenient and economical means of comparing the hot strength of different materials and is often used as a form of quality control.

2.8. Creep mechanisms

The primary categories of creep that occur can be divided into two main categories, these are diffusional and dislocation creep. In order to identify which mechanism is operative, the temperature and the applied stress to which the material is exposed to is considered. It is by and large accepted that diffusional creep is prevalent at high temperatures and low stresses while dislocation creep is prevalent at lower temperatures and higher stresses. It must also be noted that the microstructure of the material also generally plays a role in the mechanism of creep that is operative. To this end these two primary mechanisms of creep can further be classified. A broad explanation of each one of these mechanisms and information pertaining to them is presented in the following paragraphs.

2.8.1. Diffusional creep mechanisms

Diffusional creep is accepted as the movement of vacancies through a crystal lattice[36]. There are various types of diffusional creep, such as:

2.8.1.1. Nabarro-Herring creep

At high temperatures vacancies and atoms diffuse through the bulk of the material leading to Nabarro Herring creep. Due to the vacancies and atoms diffusing across the bulk of the material the grains become elongated in the direction of the tensile axis[37].

2.8.1.2. Coble creep

The Nabarro-Herring mechanism of creep, however, neglects diffusion along the grain boundaries. Due to the fact that diffusion is usually easier along grain boundaries, this is because vacancies are more common in the grain boundary than in the bulk of the lattice, Coble proposed that grain boundary diffusion could be controlling the creep rate[38]. This theory then became known as Coble creep. Coble creep though should be more prominent at lower temperatures where grain boundaries provide an easier path for diffusion to take place[37].

2.8.1.3. Grain boundary sliding

To maintain continuity during creep grains must rearrange themselves, this they do by sliding past one and other along a common boundary. During diffusion creep, each grain becomes elongated along the tensile axis; it is consequently necessary that the grains slide over each other with the sliding occurring as a rearrangement process, this process is known as Lifshitz sliding[39]. In Lifshitz sliding the grains maintain their relative positions in the matrix and there is no increase in the number of grains lying along the tensile axis. In contrast to this, a situation can occur where grains slide past one another with no grain elongation, this then results in an increased number of grains along the tensile axis of the material, this process is known as Rachinger sliding[39].

In order to prevent grain boundary sliding grain boundaries should be rich in precipitation, as the precipitation acts as a blockage to the sliding process.

2.8.2. Dislocation creep mechanisms

Dislocation creep is caused by the climb and glide of dislocations in a crystal lattice. This mechanism of creep is described broadly in the following section.

As a dislocation moves on its slip plane it may come into contact with an obstacle within the lattice, this obstacle can block the movement of the dislocation. Therefore in order to move away from this obstacle the dislocation will climb until it reaches a new slip plane, the climb of this dislocation is enabled by thermal energy (when the influence of diffusion becomes significant) and a high enough stress. Once the dislocation reaches the new slip plane it is

then able to glide again within the new slip plane until it once again may come across another obstacle and become blocked. This cycle of climb and glide may continue at this point. The rate of creep can consequently be determined by the rate at which the dislocations move through the crystal lattice.

2.8.3. Harper-Dorn creep

It is generally accepted that the mechanism of Harper-Dorn creep is the climb of edge dislocations that occurs at high temperatures and very low stresses[40]. This was concluded by Harper and Dorn, who in 1957 researched the mechanism of creep on a high purity Al (99.99% purity) at very low stresses (0.1 MPa)[41]. It has been proved that this mechanism is independent of grain size[42].

2.9. The effects of material microstructure on creep

The continuous plastic flow of a material during creep can result in large deformations and significant modifications to the microstructure of a material. The creep rate can, nonetheless, be influenced by certain microstructural parameters such as crystal structure, grain size (and grain size distribution), precipitate percentage and morphology and the level of solid solution. In general terms to ensure adequate creep resistance it is accepted that grains should be a certain maximum size and a certain degree of precipitation should be present within the microstructure. Another effective method of improving creep resistance is by producing a complex solid solution and then distributing through this fine particles of another phase. This is done by either dispersion or precipitation hardening techniques. Precipitation hardening is produced by heat treatments, in which a high temperature solution treatment is followed by a lower temperature precipitation stage. These microstructural parameters are discussed in more detail in the following paragraphs.

2.9.1. Crystal structure

A densely packed face-centred cubic metal has superior creep resistance to a body-centred cubic metal of a similar melting point. This is associated with the lower rates of atomic diffusion in the close packed structures, a factor which is responsible for the superior creep

resistance of face-centred cubic austenitic steels as compared with the body-centred cubic ferritic steels[43].

2.9.2. Grain size

In pure metals and single phase solid solutions creep resistance increases with grain size[43]; this is particularly apparent in high temperature applications. In fact at low temperatures grain boundaries act as a source of strength, this leads to a fine grain size amounting to improvements in resistance to deformation. On the other hand, at high temperatures the opposite is usually true as grain boundaries act as sources of high temperature weakness, therefore resulting in a fine grain size offering reduced creep strength; this shows that a minimum grain boundary volume is beneficial for creep resistance[44]. This is achieved by the fact that increasing the grain size of the material decreases the diffusion pathways; therefore there is less grain boundary per unit volume. An example of where this is apparent is in the case of a single crystal, precipitation hardened nickel based alloy that is used for turbine blades in jet engines.

In ferritic stainless steels the beneficial effect of an enlarged grain size on heightened creep resistance is quite significant[4, 5]. In fact Johnson found that in general for materials with low uncombined contents of Nb, one of the effects of annealing was an increase in grain size, thereby showing that grain size can be controlled by final annealing time and temperature[4].

In order to encourage creep resistance, grain growth can be promoted either during service or can be deliberately induced by a prior heat treatment such as the annealing treatment discussed above. This method of promoting heightened creep resistance can, however, lead to grain coarsening which can result in embrittlement. In fact for type 441 extended holding times over 1000 °C should be avoided as excessive grain growth may occur, which can detrimentally affect the ductility of the material[9].

2.9.3. Precipitates

A precipitate consists of a substance that has a different solid phase of composition than the rest of the lattice.

Precipitates can be introduced into a solid solution by carefully controlled heat treatments, supporting the fact that precipitation is a thermally activated process. By manipulating the time and temperature of a heat treatment the morphology and distribution of precipitates that are formed can be controlled. The heat treatment procedure often involves a high temperature solution treatment followed by a lower temperature precipitation stage. Although this needs to be carefully monitored as too short a time i.e. under aging and the particles will be too small to impede dislocations effectively; on the other hand, too long a time i.e. over aging, and they will be too few and far between to interact with the majority of dislocations.

The precipitates that are formed can greatly affect the mechanical properties of the material, particularly the strength of the material which is substantiated by precipitates collecting on grain boundaries or within grains. This is largely due to the pinning effect of precipitates as these particles strengthen the metal by preventing diffusion and impeding the movement of dislocations through the crystal lattice. Different types, shapes, sizes, the distance between the precipitates and their level of coherency can considerably affect the degree of strengthening. In general terms optimum creep strength of heat resistant steels can be obtained by a dispersion of fine and thermally stable precipitate particles combined with adequate solid solution strengthening. For long term efficiency precipitates must be stable at service temperatures to maintain the effect of precipitation strengthening for as long as possible. Many commercial creep resistant alloys obtain their strength from a uniform dispersion of precipitates, as they act to strengthen the matrix when precipitated as fine particles within the grains[45].

The type of precipitate formed depends on the levels of C and N present and the levels of other alloy additions. Ti forms stable Ti nitride precipitates when in the presence of N, and Ti carbides in the presence of C. While in the presence of both C and N, titanium carbonitrides Ti (C,N) form owing to the mutual solubility of TiC and TiN[46].

Similarly when Nb is in solid solution it not only improves the high temperature strength and the resistance to thermal fatigue of ferritic steels, it also has a strong affinity for combining with C and N to form carbides and nitrides or carbonitrides, in the presence of N and C[47].

NbC and NbN are similar compounds and the two have complete solid solubility, meaning that they form carbonitride[16]. The element Nb forms small, sphere-shaped precipitates; these micron-sized precipitates of NbC are virtually insoluble in steels at all processing temperatures and their location at grain boundaries hinders excessive grain growth due to the possibility of the pinning effect of the Nb precipitates[48]. Cubic carbides such as NbC and TiC are highly effective in promoting creep resistance as the deformation of the matrix is affected by its interaction with carbide particles[49]. However, the composition, morphology and crystal structure of these carbides have a tendency to change slowly at elevated temperatures and over time, this change can result in a decrease in creep resistance, which is clearly detrimental, although Ti additions should retard coarse precipitation[47]. In fact particle coarsening is one of the most noted degradation processes for creep resistant steels[50].

Recently the utilisation of more complex precipitation involving the intermetallic Laves phase has drawn much interest for the development of creep strength, as it is expected that ferritic steels strengthened by Laves phase will show excellent high temperature strength[51]. Therefore the promotion of the development of stable intermetallic compounds[45], such as Laves phase has became an alternative method used to enhance the high temperature creep strength. In particular for ferritic stainless steels precipitation strengthening by a dispersion of particles such as carbides, nitrides and/or Laves phase (Fe_2Nb) and their morphology formed during and before testing (or during service) can add to the improvement of their high temperature strength[6].

2.9.4. Intermetallic phases

Intermetallic compounds are not soluble in an alloy, and will precipitate, forming small particles. These compounds contain two or more metallic elements, whose structure is distinct from that of any of the constituents. The phase can be identified through x-ray diffraction techniques.

Additions of carbonitride forming elements such as Cr, Ti, Nb and Mo encourage the precipitation of intermetallic compounds in ferritic stainless steels. These intermetallic

compounds can also affect the mechanical properties of the material, in particular increasing the strength and decreasing the elongation of the steel[50].

An example of one of these intermetallic compounds is the Laves phase (Fe_2Nb), which is a common compound that forms in both ferritic and austenitic stainless steels, although this phase of closely packed hexagonal structure usually only forms in steels that have a higher Nb content[15]. For optimum strengthening the Nb must previously be taken into solution by a high temperature treatment after cold rolling. Ideally then the required intergranular precipitation of intermetallic phases will then occur during exposure at high temperatures. But, only the Nb that is not tied up in carbides and nitrides will be available for this purpose.

The Laves phase forms in heat resisting ferritic stainless steels and affects their creep strength quite substantially[52]. The phase also affects the ductility of the steel; this is because precipitation of the Laves phase in a fine dispersion leads to a considerable increase in hardness[53], showing that a correlation exists between the changes in hardness and the amount of precipitate that is present.

It is generally accepted that the Laves phase formed in ferritic stainless steels is considered to contribute to their precipitation strengthening at high temperatures[6]. This is possibly due to the dislocations being pinned by the Laves phase precipitate. On the other hand, the phase can induce embrittlement at low temperatures[54] and due to the brittleness of the phase may lower the toughness[51].

Laves phase forms at grain boundaries and dislocations and throughout the matrix in that order of preference[53]. This is beneficial for creep resistance as grain boundary precipitation is advantageous in reducing grain boundary sliding.

Laves phase generally forms as a consequence of ageing[55]. Although seen to be beneficial for increased creep resistance, this topic is subject to debate as the formation of precipitates could also lead to a decline in high temperature strength during service (ageing) in the case of these precipitates coarsening[47]. Miyakazi et al reported that Nb added ferritic stainless steels

showed a particularly high proof strength at 700 °C; this was attributed to the precipitation of Nb as a fine Laves phase (Fe_2Nb) that formed during testing[12]. Contrary to this Sim et al found that with an increased ageing time at 700 °C a noticeable reduction in the high temperature proof strength occurred[48]. This appeared to be related to the coarsening of the Laves phase particles[48]. This also confers with research done by Morris et al who observed that rapid coarsening of the Laves phase precipitate particles at high temperatures lead to high temperature strength loss[56].

Figure 10 illustrates the effect of ageing time on the yield strength of Nb bearing steels, this effect can be directly linked to figure 11, which shows the average diameter of the Nb precipitates at specific aging times. This shows that for Nb containing ferritic stainless steels the yield strength at 700 °C decreased as the ageing time increased, which appears to be related to the coarsening of the Laves phase particles. This outcome could also be linked to the loss of solid solution effect.

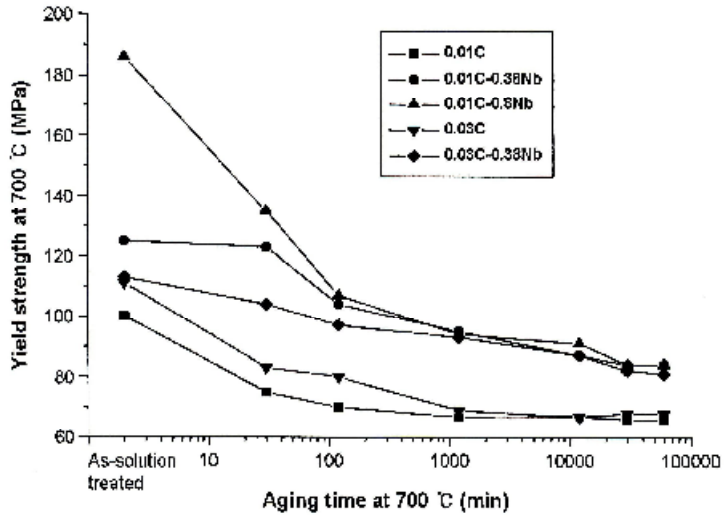

Figure 10: Change in yield strength at 700 °C with ageing time of Nb containing steels[48]

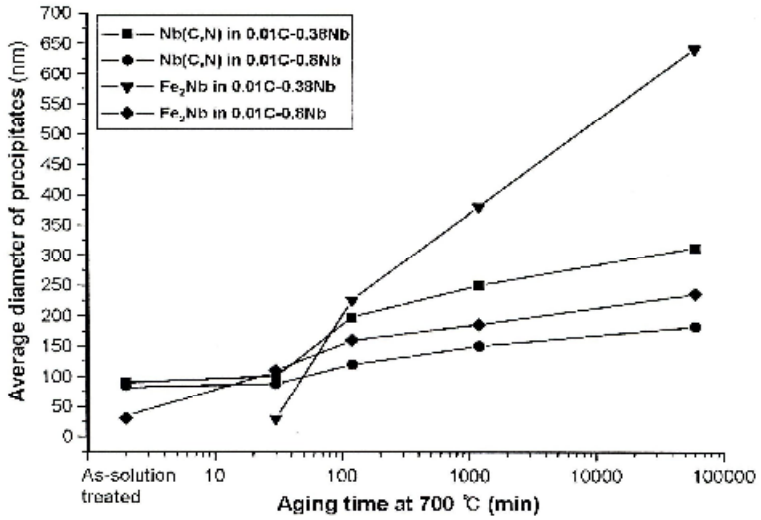

Figure 11: Average diameter of precipitates with ageing time in Nb containing steels[48]

Sim et al also noted that the Nb (C,N) did not coarsen as fast as the Fe_2Nb particles did[48].

2.9.5. Solid solution strengthening

Solid solution strengthening is a strengthening mechanism where one type of element (solute) dissolves into the crystal lattice of the host element (solvent). The strain caused by the mismatch in atomic size causes strain to build up in the surround thereby making it more difficult for slip to occur. Solid solutions in general are expected to have higher creep strength than pure metals. Research has shown that Mo is a powerful element in enhancing creep resistance, although Ti and Nb are more efficient, while in the presence of C these elements are mostly removed from solid solution due to the formation of carbides[49]. In fact Nb is readily precipitated out as carbonitride when the steel is used at high temperature around 900 °C for a long time[48]. Barteri and Mecozzi found that the precipitation of the Laves phase at about 800 °C could also decrease the effective Nb content in solid solution[57].

When Nb is in solid solution it contributes to the improvement of the initial high temperature strength of ferritic stainless steels effectively[47]. Actually one of the most effective methods for improving the high temperature strength of ferritic stainless steel is to increase the initial solid solution of Nb as much as possible[6].

For Nb bearing ferritic stainless steels it has been found that when the Nb content is less than 0.2 % mass, Nb is not in solid solution, but is in the form of precipitates. On the other hand, when the Nb addition exceeds 0.2 % mass the amount of Nb in solid solution increases as the Nb addition content increases[47].

2.10. High temperature creep behaviour of Nb bearing ferritic stainless steels

Figure 12 illustrates the effect of an increasing Nb content on the creep resistance of Nb bearing ferritic stainless steels. It is clear that as the Nb content is increased so is the creep resistance.

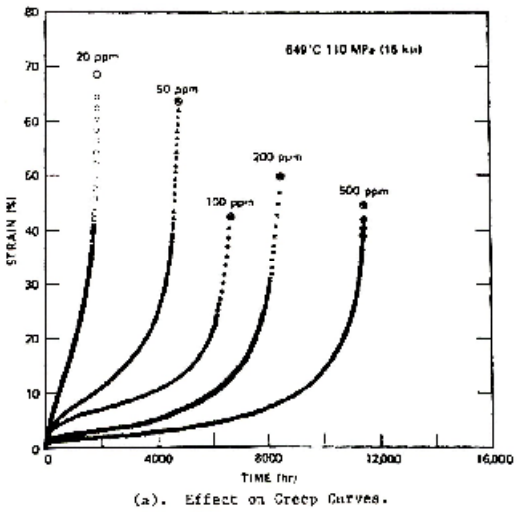

Figure 12: Effect of increasing Nb content on creep curves[15]

Although an increase in Nb content increases the high temperature strength, this is up to a threshold value. Therefore the high temperature strength reaches a saturation value at a high Nb content[57]. This is evident in the work of Borneman who monitored the effect of annealing temperature and Nb content on the creep resistance of a dual stabilised (with Ti and Nb) ferritic stainless steel[33]. Table 4 shows that once the Nb content is over 1% weight the creep resistance generally starts to decrease (although the annealing temperature also affects this).

		Annealing temperature (°C)							
		1010		**1038**		**1066**		**1093**	
Alloy	**Nb (wt %)**	**1%**	**2%**	**1%**	**2%**	**1%**	**2%**	**1%**	**2%**
O	0.42	33	43	42	60	60	80	13	25
P	0.61	148	195	155	208	130	172	65	89
Q	0.80	107	123	222	274	130	153	158	231
R	1.00	113	140	230	279	240	298	272	325
S	1.20	51	69	69	77	56	75	56	78
T	1.40	23	33	21	29	28	40	36	42

Table 4: Time (in hours) taken to reach a percentage creep elongation of varying Nb content[33]

Note: Table 4 shows results of the time taken to a 1% and 2% creep elongation and not to fracture. Ti contents are in the range of 0.30-0.36 % and Cr contents within the range of 16 %. Creep tests were run at a temperature of 871 °C and a stress level of 8.274 MPa.

Table 4 also shows how creep resistance of a Nb bearing ferritic stainless steel can be affected by a change in annealing temperature.

Barteri et al used sag testing to compare the hot strength of various grades of stainless steels[58], which included 441. The bar chart in figure 13 illustrates the differences between the hot strength of austentic stainless steel and ferritic stainless steel, showing the austenitics to be superior, although 441 is certainly comparable to them. Grade 409 is clearly the least creep resistant of all the alloys reviewed.

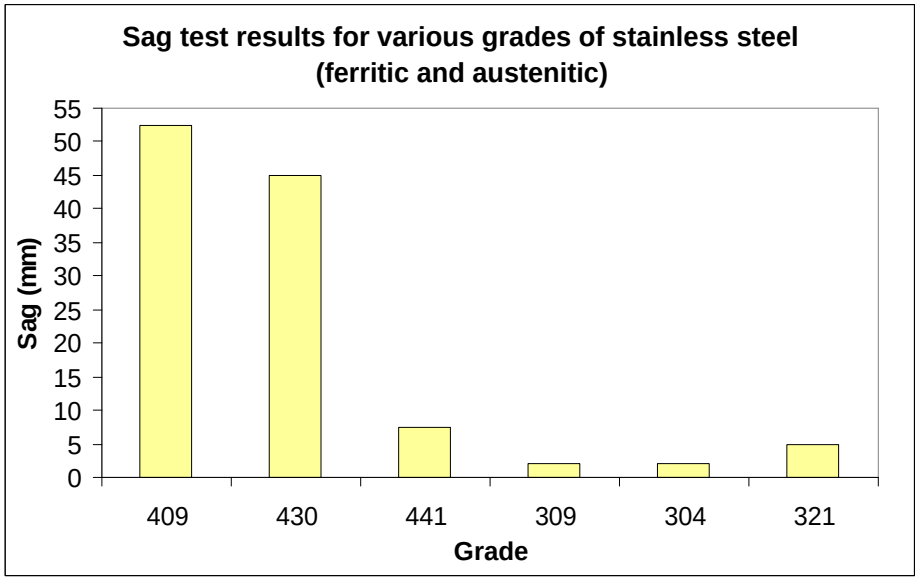

Figure 13: Bar chart showing differences in sag values between grades of stainless steel[58].

Note: The 400 series represent ferritic, whereas the 300 series represent the austenitic grades.

Barteri determined that the average value of sag deflection obtained for 441 at a temperature of 900 ºC over a period of 100 hours was 7.5 mm. It is, however, unclear as to the prior thermo-processing route that these specimens endured.

Similar work done more recently by Dollman[59] produced values of sag ranging from approximately 1.3 mm to 8.7 mm for 441. The respective final annealing temperatures of these specimens were 950 °C, 1000 °C and 1050 °C. Using a notion similar to Borneman this work was done in order to compare the creep resistance of two alloys of 441 with a different Nb content. Both of these alloys had a Nb content of less than 1 % weight. This work revealed that the alloy with the lower Nb content was the most creep/sag resistant, which was an unexpected result.

2.10.1. Effect of Nb percentage on the creep strength of type 441[5]

The effect of Nb percentage on type 441 can be seen in figure 14, this graph also shows the effect a change in annealing temperature can have on the creep resistance of the alloy.

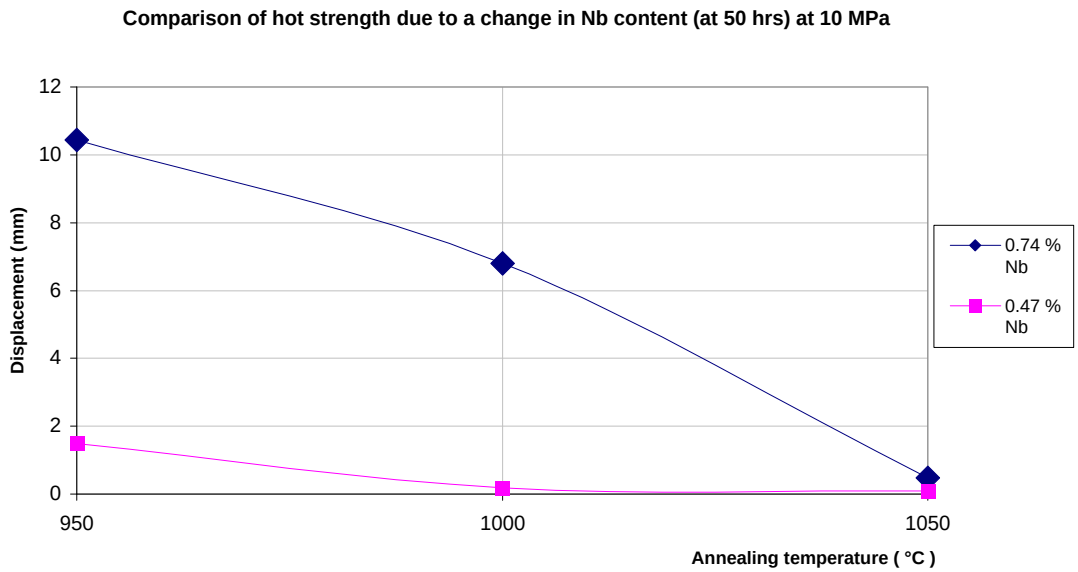

Figure 14: Change in creep strength for type 441 ferritic stainless steel for a varying Nb content and different annealing temperature. Note: Both alloys were received in the cold rolled condition and were subsequently annealed.

The increased creep resistance of both alloys was explained by an increase in grain size that was brought about by an increase in annealing temperature. In figure 14 it is clear that the alloy with the least Nb content (0.47 %) had the superior creep resistance. This phenomenon was explained by the fact that this alloy had a consistently larger grain size to that of the other alloy across the three different annealing temperatures. This showed that the effect of Nb level appeared to be inferior to the effect that grain size had on the creep resistance, in relation to these two alloys.

However, at an annealing temperature of 1050 °C even though the alloy with the higher Nb content has the smaller grain size its creep resistance is comparable to the alloy with the lower Nb content, this was explained by the higher level of Nb in this alloy.

3. Chapter 3: Experimental methods

3.1. Material

Both alloys of type 441 were supplied as sheet, in the cold rolled condition with an approximate gauge thickness of 1.5 mm.

The fundamental difference between the two alloys is that one has a higher Nb content than the other. For reference purposes these alloys will be referred to as alloy A and alloy B, where alloy B has 0.74 wt % Nb and alloy A has 0.47 wt % Nb. Table 1 shows the chemical composition percentages for both alloys.

Table 1: Alloy chemical compositions

Element	**Alloy A**	**Alloy B**
	(wt %)	**(wt %)**
C	0.02	0.01
Mn	0.56	0.47
Co	0.04	0.03
Cr	**17.96**	**17.63**
B	0.001	0.002
H	7.43	3.42
V	0.14	0.13
Pb	0	0
S	0.0004	0.004
Si	0.50	0.54
Ti	**0.20**	**0.18**
Ni	0.19	0.33
N	0.02	0.02
Al	0.006	0.005
P	0.03	0.02
Cu	0.07	0.17
Mo	0.02	0.01
Nb	**0.47**	**0.74**
O	0.01	0.01
Sn	0.01	0.01

3.2. Microstructural studies

Microscopy was performed in order to monitor the effect that any changes in the microstructure, which were effected by a variety of heat treatment procedures, would have on the creep resistance of both alloys. In particular any grain size changes and precipitate presence (volume fraction) and morphology was pertinent to the study.

Optical microscopy and scanning electron microscopy were used to examine the microstructure, each method having various advantages over the other.

In order to monitor the hot strength of the two alloys, creep testing was performed. The creep testing for the present study formed a continuation of testing based on previous testing as discussed in 2.10.1. Whereas the previous study involved testing that was to establish the role of Nb and grain size on the creep resistance of type 441[5], the continuation study was necessary in order to better understand what role Nb in solution and volume fraction of precipitation has had in aiding the material's creep resistance. It also became obvious during experimentation that it was necessary to determine the composition of precipitate phases, with particular emphasis on the identification of the Nb rich Laves phase (Fe_2Nb). The presence of this phase is an effective method of promoting creep resistance.

Due to the fact that results from the previous study[5] indicated that the alloy with the larger grain size, but the least Nb content (alloy A) was the more creep resistant, it was necessary to investigate further why the Nb content was not the dominant factor in the heightened creep resistance and also if it was feasible to expect the creep resistance of alloy B to improve if its grain size was larger.

Focus was therefore on increasing the grain size of alloy B to match that of the grain size of alloy A. This was done in order to eliminate the grain size factor as a variable, influencing the creep resistance. Alloy A produced a maximum creep resistance at a heat treatment temperature of 1050 ºC (as discussed in 2.10.1). The grain size of alloy A at this stage was in the region of 55 µm and it was therefore deemed necessary to determine what heat treatment temperature would produce the same grain size for alloy B. The focus then of the creep test

matrix was on tests that were performed once the grain size of alloy A and alloy B were equalised.

3.2.1. Heat treatments

Creep properties are dependent on the initial microstructure of the material. Therefore in order to render maximum creep resistance it is necessary to determine the optimum heat treatment, which can be varied by controlling the prior heat treatment procedure[60]. The optimum heat treatment should then ideally provide the material with the optimum microstructure for improved creep resistance.

To this end both alloys underwent a series of heat treatments, which consisted of three steps. These heat treatment steps were performed in order to promote various microstructural changes. The first treatment was to match the grain size of both alloys as discussed already. The second treatment was an ageing treatment that was performed in order to remove as much Nb from solution as possible by precipitate formation. The third and final treatment prior to creep testing was a solution treatment that was aimed at controlling the level of Nb in solid solution by progressively dissolving Nb rich precipitates that were formed during the prior ageing step.

After each subsequent heat treatment (after each step) samples were oil quenched in Isodur 220.

To promote accuracy during the treatments a separate temperature monitoring thermocouple (attached to a Testo 925 hand held thermometer) was used in order to confirm the temperature reading of the furnace.

Each heat treatment procedure is discussed in more detail in the following three paragraphs.

3.2.1.1. Step 1: To promote equivalent average grain size in the two alloys

Cold rolled sheets of Nb bearing ferritic stainless steels are typically heat treated with a final solution treatment temperature of 900 °C or more in order to promote recrystallisation. Since

larger grain sizes promote better creep resistance, temperatures were explored in the range of 950 °C-1150 °C in order to achieve equivalent grain sizes in the two alloys.

In order to equalise the grain sizes it was decided to match the grain size achieved after heat treating alloy A at 1050 ºC for 30 minutes. Consequently alloy B was subjected to a range of heat treatments as indicated in table 2. The heat treatments were performed in a Gallenkamp box furnace (maximum temperature = 1200 °C).

Table 2: Heat treatment practice to monitor the grain growth of alloy B

Temperature (°C)	Time (min)
950 °C	30
1000 °C	30
1050 °C	30
1080 °C	30
1100 °C	30
1150 °C	30

3.2.1.2. Step 2: Reduction in Nb solid solution

This treatment took the form of an ageing process. This was done for a period of 2 hours according to similar work done by Miyakazi et al[12]. Working with a ferritic stainless steel Miyakazi found that the precipitation of Nb would have reached saturation after ageing at a temperature of 700 °C for 2 hours. A number of samples of alloy A were also aged for a period of 20 hours to monitor the effect of a longer ageing time on the creep resistance of this alloy.

A Naber box furnace (maximum temperature = 1000 °C) was used to reduce the Nb level in solid solution.

3.2.1.3. Step 3: Controlled solution treatment

The final heat treatment procedure prior to creep testing was a high temperature solution treatment, which was necessary in order to control the level of Nb in solution of the specimens at the start of the creep test. The solution treatment was intended to produce different

morphology and distribution of the precipitates to monitor the effect this had on the creep resistance.

Three different solution temperatures were investigated; this was to monitor the effect of placing more or less Nb back into solution. The temperatures that were chosen were 950 ºC, 1000 ºC and 1050 ºC. Each of these treatments lasted for 200 seconds. In certain instances the solution treatment of 1000 ºC was not investigated as it was expected that the results for this treatment would fall between the results from the solution treatments of 950 °C and 1050 °C.

A salt bath furnace that was designed and manufactured by a local company, Kiln Contracts was used in order to affect rapid heating to temperature. The crucible is manufactured from Inconel in order to withstand high temperatures and is tolerant up to a temperature of 1050 ºC. The annealing salt that is used within the bath is GS 750, which is supplied by Houghton Durferrit. This salts main ingredient is Barium Chloride[61]; it has a working range of 900-1100 °C and melts at 750 ºC.

Decarburisation is prevented by avoiding a reaction between the salt bath furnace and the sample being heat treated. This is achieved by adding an inertor to the salt, which is designated R2 by the manufacturer (Houghton Durferrit).

Figure 1: Salt bath furnace

Figure 2: Salt bath in operation

Samples were also investigated to determine the effect of omitting the solution treatment. In this case the ageing treatment at 700 °C for 2 hours and 20 hours respectively was performed with no further solution treatment.

3.2.2. Sample preparation

In order to monitor grain size changes and volume fraction and morphology of precipitates it was necessary to study the microstructure of various samples at particular heat treatment stages (prior to creep testing). To do this a section of material is investigated so as to reveal an accurate replica of the microstructure. For this purpose samples are sectioned using a Struers type 02TRE cut-off wheel on an Imptech abrasive cutter. These samples are then set into a transparent acrylic resin using a Struers LaboPress 3 Hot Mounting apparatus. In order to render the surface smooth and scratch free the sample is then ground and polished using a Struers RotoPol-22 Automatic polisher (with the samples fitted into a single sample holder). The grinding and polishing method used is based on Method C of the Struers Metalog Guide as shown in table 6 [62]; slight adaptations were, however, made to this guide such as using longer periods of time or lower forces to be more effective. This method utilizes firstly a series of abrasive and polishing pads with a diamond suspension lubricant ending in a suspension of colloidal silica to produce the best possible surface for analysis.

Table 6: Polishing guide for alloy A and alloy B (type 441)

Step	**Grit/cloth**	**Revs/min**	**Force (Newtons)**	**Lubricant**	**Time (mins)**
Grinding	220 SiC grit	300	20	Water	Until plane
Fine grinding	MD-Largo	150	20	9 µm	5
Diamond polishing (DP)	MD-Dac	150	20	3 µm	5
Oxide polishing (OP)	MD-Nap	150	10	Collodial Silica	10
Oxide polishing (OP)	MD-Nap	150	10	Water	2

The water polish (final stage) is necessary as often the Collodial Silica can 'stain' a surface.

Samples that are prepared for optical microscopy are chemically etched in order to clearly reveal the grain structure and grain boundaries. For this purpose samples were placed into the etchant in the ultrasonic bath to promote a flow of etchant over the surface; this was done for between one and two minutes, using a solution of the following:

10 ml Nitric acid (HNO_3)
20 ml Hydrochloric acid (HCl)
30 ml water (H_2O)

Samples that are prepared for studying in the scanning electron microscope (and for electron backscatter diffraction) are, however, not etched and are examined in the polished state only (after the 10 minute polishing using the Collodial Silica).

3.2.3. Grain size investigation

This section of the work was vital in order to distinguish the differences in grain sizes between both alloys after particular heat treatments. Optical microscopy and electron backscatter diffraction (EBSD) was used to determine grain size values; both methods are discussed in more detail in the following paragraphs.

3.2.3.1. Matching grain sizes: Optical microscopy

Samples were studied using optical microscopy in order to monitor grain size changes after heat treatments.

For the optical microscopy a Reichart MeF3 optical microscope was used, that is fitted with a Leica DCF 320 camera. This was in turn connected to a computer that ran the Leica acquisition software that is necessary to capture the images of the surface of the sample.

Micrographs that were produced were analysed and grain size was measured from the etched samples, using the mean linear intercept method according to ASTM standard E112-88 [63].

The magnification in the light microscope was set such that grain boundaries could clearly be observed, at the same time as maintaining adequate sized fields of view to capture the overall grain size distribution. In accordance with the standard, four different fields of view were studied and an average grain size was then determined, which included a standard deviation value.

3.2.3.2. Matching grain sizes: Electron backscatter diffraction (EBSD)

Although using the mean linear intercept method is a widely accepted method to determine grain size, it was decided that due to the fact that it was imperative that the grain sizes were the same, these grain size values would be confirmed using EBSD. EBSD was therefore used as a confirmation evaluation for grain size measurement.

The advantages of EBSD over optical microscopy are varied. They include[64]

- Improved spatial resolution
- More accurate measurements of grain and subgrain size
- More complete microstructural characterisation

EBSD is a technique used for obtaining crystallographic information from samples in the scanning electron microscope. The data required for quantitative microstructural analysis using EBSD is typically obtained in the form of a crystal orientation map, while line scans may also be used, depending on the type and quantity of information that is required.

In order to set up an EBSD map once the acquisition programme (Flamenco) is opened, a stage job, new mapping is chosen. Initially for this investigation the map sizes were 2000 x 3000 µm and the step size of the beam was set at 10 µm, according to the enlarged grain size (as deduced from the lineal analysis method). The sample rate is approximately 2,6 seconds per sample point, therefore each map will take 43 hours and 20 minutes to complete. The end result of this process is a crystal orientation map that is representative of an area of the sample. An example of a map can be seen in figure 3. In this map the position of all the grains and grain boundaries are clearly visible, where, the grains represented by colours and points with

similar crystal orientations are shown in similar colours and black and white lines around these coloured regions represent grain boundaries.

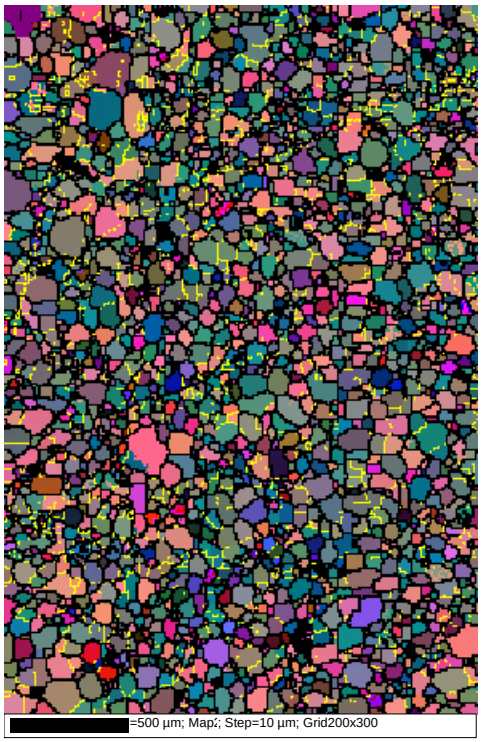

Figure 3: Example of a crystal orientation map (using a stage scan)

During processing of the map a quantitative definition of a high (above 15 °) or low (between 2 and 15 °) angle grain boundary is chosen. By doing this EBSD provides more accurate data than conventional imaging in which the grain boundaries to be counted depend on the technique used. Therefore the ability of EBSD to precisely define the boundaries constitutes a considerable advantage over methods such as optical microscopy. Consequently different grain boundary types can be identified and indicated[65].

Once the map is completed the average grain size can be calculated. Using a method similar to the mean linear intercept method, these results are then imported into Excel and an average value of grain size can be determined, along with a grain size distribution. The important difference between this approach and the light microscopy technique is that EBSD can accurately detect the presence of high angle grain boundaries.

A problem, however, that may occur is that non-indexed points may arise; this could be due to a poor pattern quality which is in turn related to a poor quality surface of the sample. If the number of these non-indexed points is large it may be difficult to acquire accurate microstructural data, but if the number of non-indexed points is small then the data may be 'repaired'. This repair is done after acquisition by assigning the orientation of a neighbouring point to the non-indexed point. Caution should be exercised though when using this function, as a map with many non-indexed points could be due to a problem with the sample itself. With this in mind it is clear that in order to be assured of a good quality EBSD map/line scan, the majority of points should be indexed (typically 70-80 % indexing rate).

It was deduced that a map may produce more information than is necessary for this work, not to mention the lengthy time period required to produce each map. As a result of this it was decided to also make use of line scans. Therefore when setting up an EBSD run once the acquisition programme (Flamenco) is in view, a stage job, new line scan is chosen. The line scan settings are chosen as displayed in table 3. Sampling was approximately 2,6 seconds per sample point and consequently each line scan took 4 hours and 30 minutes to complete. The line scan choice of method provided a much more effective and time saving way to measure grain size using EBSD.

Table 3: Line scan settings[66]

Line raster	
Line direction	Y
Number of lines	4
Number of points per line	1500
Step size (µm)	2
Distance between lines (µm)	45

The step size has been reduced in order to promote accuracy, since there is less chance of missing a grain at higher resolution.

Similarly once the line scan is completed the average grain size (including the number of grains that have been covered) can be determined. Using a method similar to the mean linear intercept method these results are then imported into Excel and an average value of grain size can be determined, along with a grain size distribution.

In order to reliably measure grain sizes, 2 maps and three line scans were performed per sample (in a different area). From this data, grain size distribution bar charts were produced to monitor any grain size distribution differences between the two alloys after heat treatment.

3.2.4. Precipitation studies

Scanning electron microscopy (SEM) was used to characterize the precipitates and the overall microstructure prior to creep testing. This choice of equipment was particularly useful in order to determine the effect the percentage volume fraction of precipitation has on creep resistance as precipitation was clearly visible at the high magnification produced by SEM. In particular it was necessary to identify and characterise the possibility of the Laves phase being present in certain samples to determine the effect this phase has on the creep resistance of the material. To study the precipitation the Leica 440 SEM at the Electron Microscope Unit at UCT was utilised.

SEM can be used for a broad range of applications due to its capability to produce high resolution images of a sample surface. Specific detectors are used to collect the secondary or backscattered electrons; the choice of the detector is dependent on what needs to be imaged. Although the more common SEM images are formed with secondary electrons, backscattered electrons also yield valuable information about a sample's topography and composition. Backscattered electrons may be used to detect differences in areas with different chemical compositions, especially when the average atomic number of the various regions is different. A brighter area (higher BSE yield) indicates an area of high atomic number and in contrast a darker area indicates a lower atomic number. Using this detector therefore not only produces visual information, but also relative elemental compositions can be gauged.

For this analysis the probe current used was in the region of 500 pA-1,2 nA with an accelerating voltage of between 20 kV and 30 kV. The choice of accelerating voltage was dependant on whether the bulk of the sample was being investigated or the precipitation itself. A balance between brightness and contrast was carefully controlled during usage.

3.2.4.1. Volume fraction of precipitation

To determine the effect of the volume fraction of precipitation on the creep resistance of samples it was necessary to firstly determine whether or not precipitation was present in samples. Secondly for those samples that did have precipitate presence it was necessary to then determine the percentage presence or volume fraction of the precipitation.

To determine the volume fraction of precipitation a simple procedure which entails surveying the microstructure and estimating the area fraction of the particles was used. This estimation is guided by the use of comparing the microstructure to a standard chart that shows different percentages of a specific structure[67]. The charts are presented in two different forms; percent by area of light constituent and percent by area of dark constituent. This chart can be seen in figure 4.

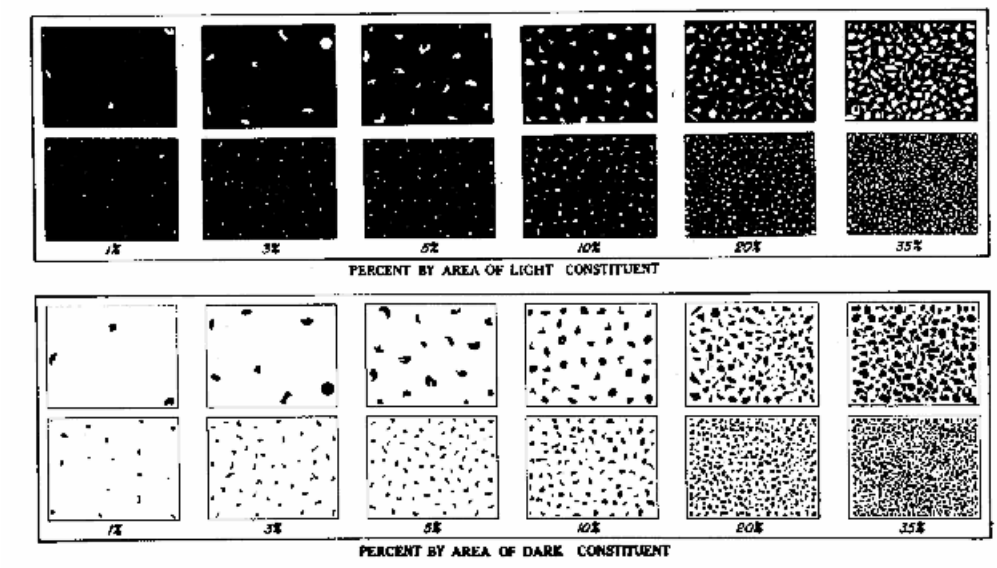

Figure 4: Chart for estimating volume fraction [67]

3.2.4.2. Energy dispersive spectroscopy (EDS) analysis

SEM's are often equipped with a spectrometer able to detect X-rays emitted by the sample during electron beam excitation. These X-rays hold a typical energy and wavelength which when measured will divulge the elemental composition of an area. A common type of X-ray analysis used in combination with SEM'S is EDS.

EDS was utilised in order to analyse the composition of the various precipitates found at grain boundaries and within grains of particular samples. This was to monitor the effect of the composition of the precipitation on the creep resistance of the material. The EDS on the Leica 440 SEM was deployed for this purpose.

3.3. Constant load creep testing

Constant load creep testing was performed on specimens as a measure of their hot strength. In particular, creep testing was performed in order to:

- Determine the influence of Nb content on the creep resistance of type 441 ferritic stainless steel using two heats with different Nb levels.
- Determine the influence of Nb solute level on the creep resistance of the respective alloys A and B.
- Determine the influence of precipitate population on the creep resistance of the respective alloys A and B.

3.3.1. Constant load creep test rig

Creep tests were performed using two lever-arm type, constant load creep test rigs at the Centre for Materials Engineering, UCT.

The creep test rigs have the following components:

- Load frame
- Base plates (between which the load is applied)
- Adjustable lever arm (through which the load is applied to the specimen). The lever ratio available on these rigs is: 1:3, 1:5 and 1:10. This allows loads of between 10 kg and 1000 kg to be applied to the specimen.

- A weight pan in which to place the required load.
- A screw jack to allow vertical positioning of the lower pull rod to enable various lengths of specimens to be tested.
- A vertical electric tube furnace that has a maximum operating temperature of 1200 °C. The furnace has three heat zones; the temperature inside of the furnace is maintained at a constant level by three temperature controllers (RKC SA 200).
- Load cell used to monitor the load on the specimen.
- Extensometer system, which is made up of four rods that extend into the furnace and attach directly onto the notches of the specimen gauge length.
- LVDT (linear variable differential transducer) to continually monitor the elongation of the specimen.
- 2 type K thermocouples to monitor the temperature of the specimen (one at the top and one at the bottom of the gauge length). These thermocouples are attached directly onto the specimen.
- Data acquisition system. The control unit's purpose is for logging the information from the sensors to a suitable data acquisition system. Voltage outputs from sensors are transmitted to the control unit, where these readings are adjusted to give values of load, extension and temperature. Values are transmitted to the computer via an analogue to digital card (Eagle Technologies PCI 703S) where they may be logged. The software logs data at user defined intervals. Each rig has 4 available channels: one for load, one for the LVDT and the remaining two, for the thermocouples. Data from the data acquisition programme can then be exported to a suitable spreadsheet programme such as Excel, where the data can be analysed.
- Cooling system for load cells. This feature allows cooling water (necessary for the load cells) to be re-circulated preventing water wastage.

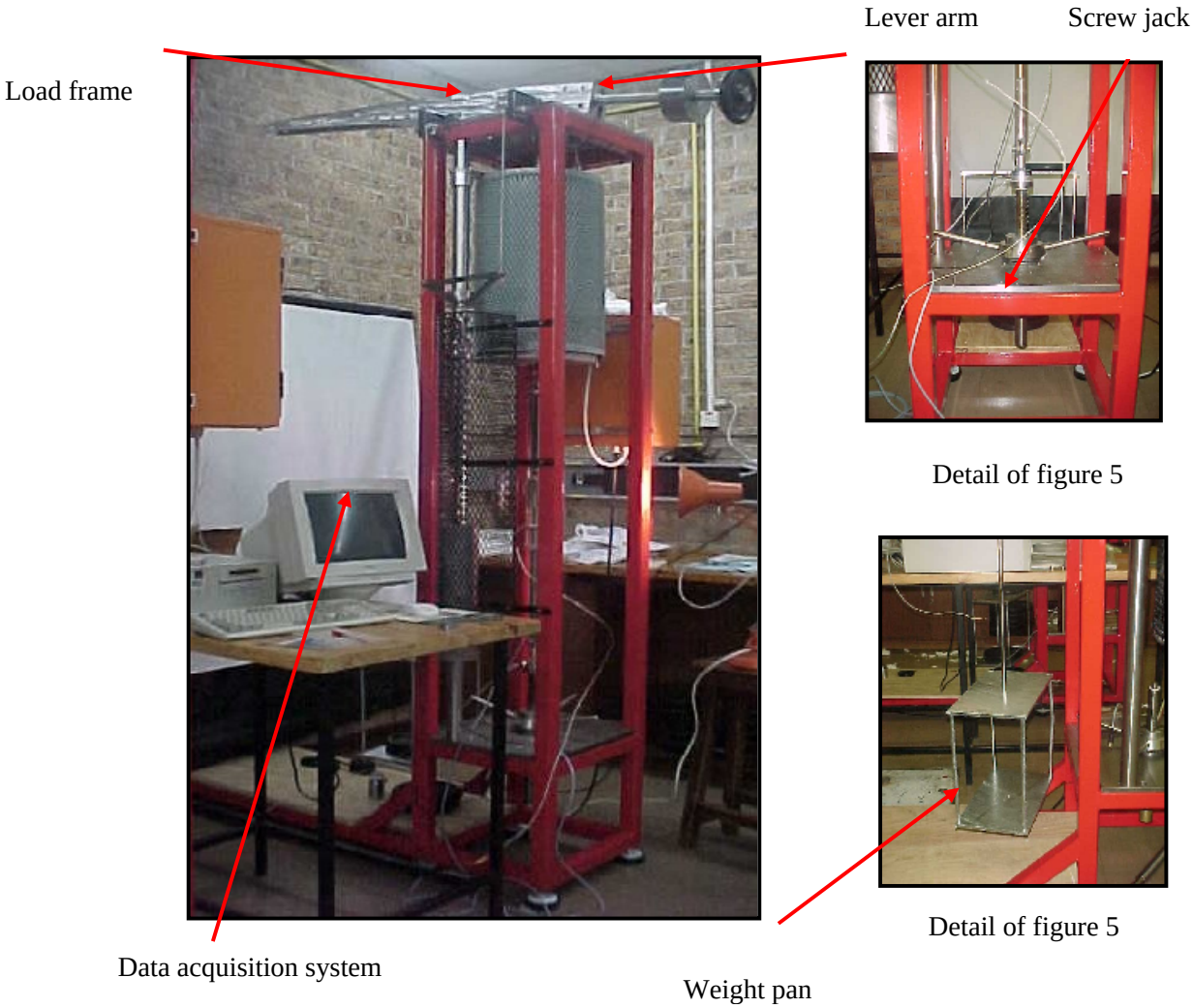

Figure 5: Constant load creep test rig

3.3.1.1. Sensors

The details of the sensors used for capturing the necessary data consist of the following:

SENSOR	DESCRIPTION	TYPE
Load cell (x 1 per rig)	Installed in the upper base plate of the rig, which is above the furnace. Installed here to allow, firstly, continuous load monitoring, and secondly, to avoid the complication of the load train if installed below the furnace.	Gefran: TU KIC, 100 kg
Thermocouple (x 2 per rig)	It must be noted that it is vital that when the thermocouples are attached, they are attached somewhere that will not influence the specimen being able to extend freely. There are two thermocouples per rig. This is owing to the length of the gauge (as per ASTM E139-00).	Unitemp: Type K (length = 450 mm, diameter = 2 mm)
LVDT ; linear variable differential transducer (x 1 per rig)	The relative displacement of the rods is measured outside the furnace by an LVDT.	Solartron: (± 25 mm stroke)

Calibration of the sensors should be done on a regular basis to ensure that they have not drifted.

3.3.1.2. Cooling system

A cooling system was installed on the creep rigs in order to keep the load cells cool. The original cooling system that was in place involved a large amount of water wastage. As a result a system was designed to allow the water to be re-circulated.

The cooling water is pumped through coils attached just under the load cells (around the upper pull rods). It is then pumped through a chiller water blower coil unit and then into a 50 litre tank from which it is pumped through to the coils again. The system allows for the water to maintain a constant temperature of between 19 and 21 °C.

3.3.2. Test approach

Before a test is performed, the measurement sensors should be calibrated (refer to appendix A for instructions on calibration methods).

The constant load creep test rigs have proved to be sensitive. It is therefore essential that tests are set up exercising caution and that components of the rigs are handled with care. The creep test set-up procedure (appendix B) and the end procedure (appendix C) should consequently be followed closely.

3.3.3. Specimens

Specimens were machined with the tensile axis parallel to the rolling direction; the rolling direction is as seen in figure 6. Notches along the gauge length are necessary for attachment of the extensometer.

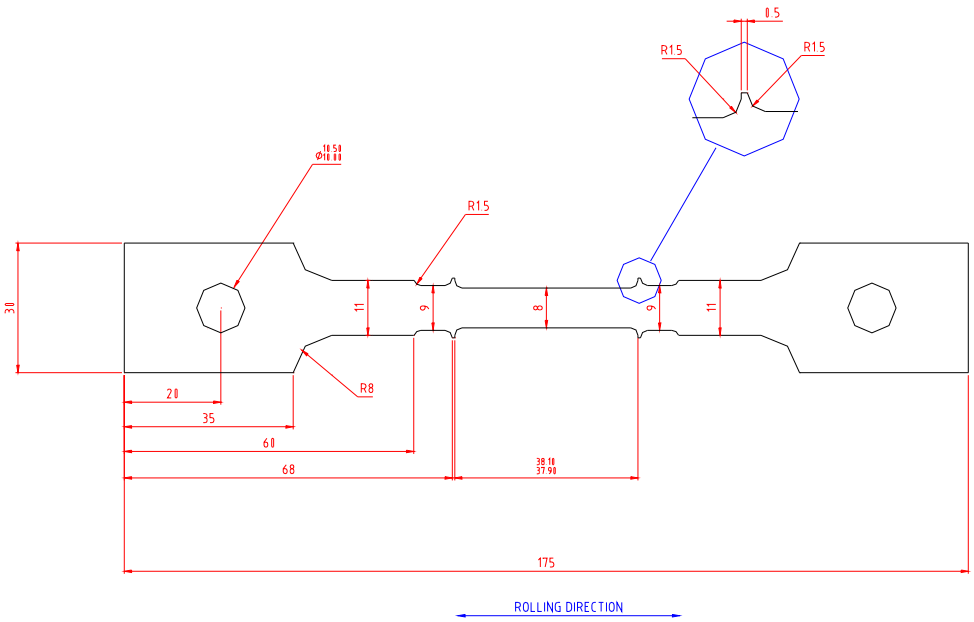

Figure 6: Creep test specimen

3.3.4. Testing procedure

All creep testing was performed using purpose built creep test rigs as described in 3.3.1, in accordance with ASTM E139-00 [68]. Once the test is set up and the set temperature of the furnaces has been reached, a one hour period is given in order to allow the system to attain thermal equilibrium. All creep tests were performed at a temperature of 850 °C. The temperature is kept constant during a test.

The majority of tests were run until fracture, although some were not due to time constraints. In the event of a test not being run to fracture it was necessary to run the test for at least long enough in order to gain the necessary data from the test prior to stopping the test.

Creep tests for this research were run at relatively low stresses. Two values of stress levels were investigated; this was in order to rank the creep behaviour accordingly. Table 4 shows the stress values that the specimens were creep tested at; this table also includes the specimen's thermo- processing history.

Table 4: Alloy thermo- processing history and stress to which alloy is exposed to

Alloy	Recrystallisation temp (°C)	Time at recrystallisation temp (mins)	Ageing temp (°C)	Time at ageing temp (hrs)	Solution temp (°C)	Time at solution temp (secs)	Stress during creep testing (MPa)
A	1050	30	700	2			10
	1050	30	700	20			10
	1050	30	700	2 hours	950	200	10; 15
	1050	30	700	2 hours	1000	200	10; 15
	1050	30	700	2 hours	1050	200	10; 15
B	1100	30	700	2 hours	950	200	10; 15
	1100	30	700	2 hours	1000	200	10; 15
	1100	30	700	2 hours	1050	200	10; 15

From this point, samples will be referenced according to their alloys designation and prior thermo- processing history. An example of which is shown in table 5:

Table 5: Referencing system of samples

Nomenclature	Alloy	Recrystallisation temp (°C)	Ageing temp (°C)	Solution temp (°C)
A 1050-700-950	A	1050	700	950

3.3.5. Creep curves

In analysing data produced from a creep curve, creep data can be represented in various ways, as discussed in chapter 2 (2.6). For this work it was most important to show the differences in creep resistance between two alloys and various heat treatment parameters. Curves therefore showing creep strain (%) were plotted against time. These curves clearly show a difference between time to fracture (or time to reach a certain strain value) between the different alloys, which is useful in determining the most creep resistant alloy or the heat treatment that produced the most creep resistant condition at the two different stress levels.

3.4. Exposure of samples to 850 ºC investigation

This section of the work was necessary in order to show the effect of prolonged time at service temperature of samples. Samples equivalent to certain test specimens were exposed to 850 °C for different time periods. This was so as to independently monitor the microstructural changes that occur during the prolonged creep testing period. The samples and the times of exposure (soaking) are seen in table 6.

Table 6: Samples to be exposed at temperature for prolonged times.

Sample	Time in hrs at 850 °C					
A 1050-700-950	10	20	40	100	200	400
A 1050-700-1050	10	20	40	100	200	400
B 1100-700-950	10	20	40	100	200	400
B 1100-700-1050	10	20	40	100	200	400

Note: Samples are labelled according to table 5 and have therefore undergone step 1, 2 and 3 of the heat treatment practise

The exposed samples were observed for changes in precipitation i.e. coarsening or an increase in volume fraction of the particles. It was also necessary to confirm whether or not there was a significant increase in grain size after various exposure times.

4. Chapter 4: Experimental results and discussion

Creep test results are presented in this chapter; this is to distinguish the difference in the creep resistance of the two alloys studied and also the difference in creep resistance between the various solution treatments and ageing times. Particular reference is made to the results that reveal which alloy had the highest creep resistance. Consequently some of the reasons for this are discussed, which range from debate around grain size values and the study of micrographs revealing grains and also changes in volume fraction of precipitation, which has in one case been manipulated by a longer ageing time. The identification of certain precipitates is also revealed and debated as to their influence on the creep resistance of the material.

4.1. Grain size investigation

4.1.1. Initial grain size match

This testing was a continuation of a previous study as discussed in chapter 2 (2.10.1). This testing was deemed necessary in order to better understand what role Nb in solution and precipitation morphology had in aiding the material's creep resistance. An earlier study showed that alloy A is superior to alloy B with regards to creep resistance[5]. This was unexpected as alloy B has a higher Nb content which generally leads to an increase in creep resistance[6]. Although on average alloy A had a larger grain size. Therefore the question that was raised was, "Can the creep resistance of alloy B be improved if the grain size is increased?"

Focus was therefore on increasing the grain size of alloy B to match that of the grain size of alloy A at its superior creep resistance (i.e. to match the grain size of alloy B to that of alloy A at 1050 °C which is in the region of 55 µm). In order to increase the grain size of alloy B a trial and error approach was utilised. Samples of alloy B were heat treated in the vicinity of 950 °C to 1150 °C and grain size changes were monitored carefully throughout this process.

4.1.1.1. Microscopy

At each heat treatment interval samples were studied using optical microscopy. Figure 1 shows the progression of grain size increase of alloy B (a-f); each one of these micrographs is

compared to figure 2 which shows a micrograph of alloy A, in the optimum creep resistant condition. Take note that the micrographs in figure 1 and 2 are labelled in accordance with the recrystallisation treatment temperature. Each one of these samples was heat treated for 30 minutes.

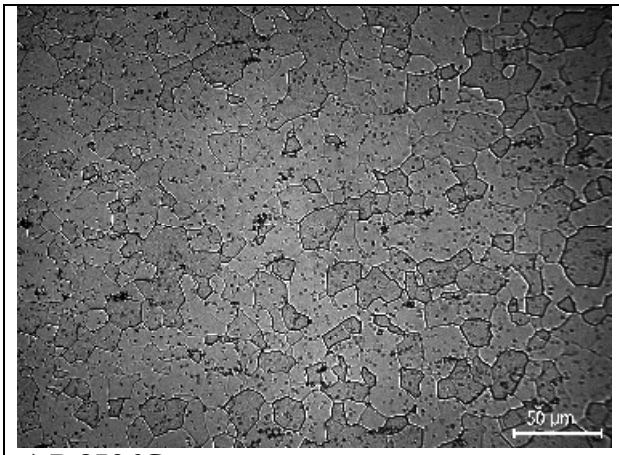

a) B 950 ºC

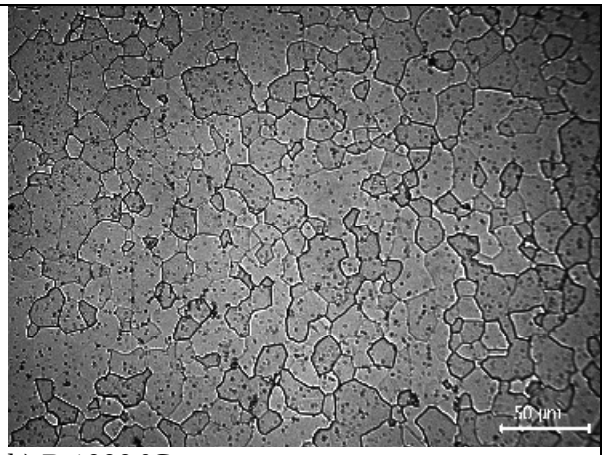

b) B 1000 ºC

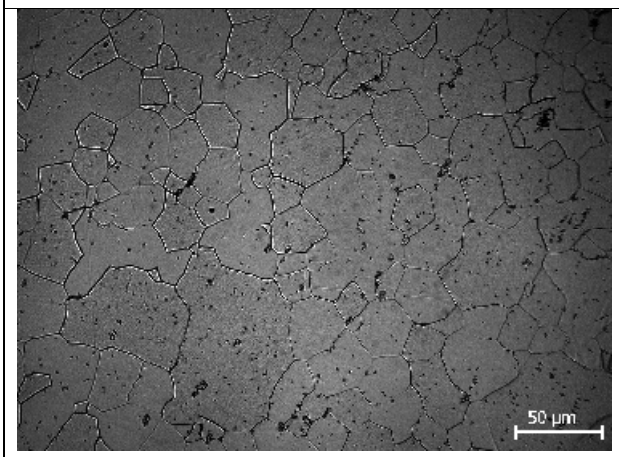

c) B 1050 °C

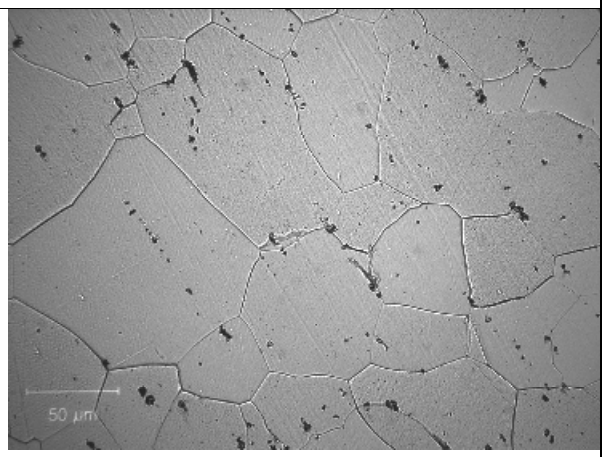

d) B 1080 ºC

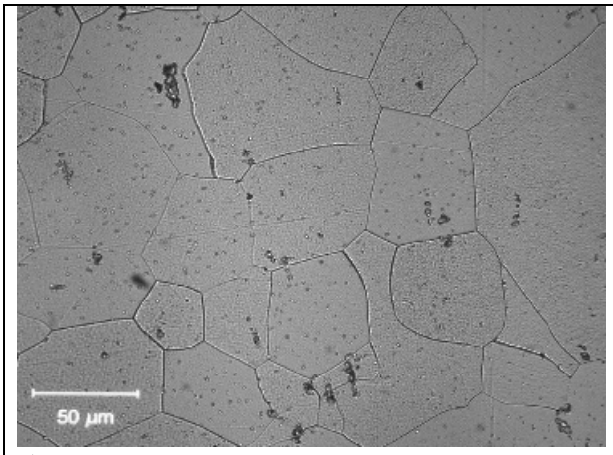

e) B 1100 °C

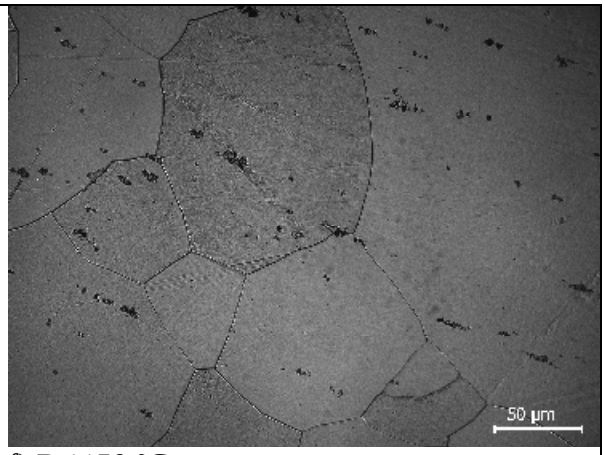

f) B 1150 °C

Figure1: Micrographs of alloy B showing a change in grain size after a different recrystallisation treatment temperature. Micron marker = 50 µm

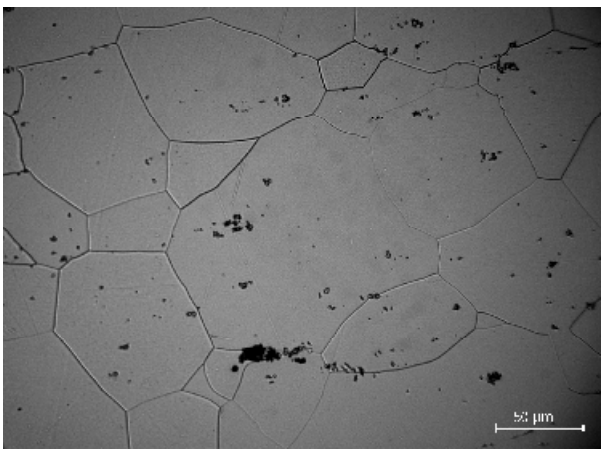

Figure 2: Micrograph of alloy A after a recrystallisation treatment temperature of 1050 °C. Micron marker = 50 µm

The micrographs of samples of alloy B (figure 1) indicate the steady increase in grain size with an increase in treatment temperature. Visually it appears that the grain size of alloy B is similar to that of alloy A at 1080 °C and 1100 °C (comparing figure 1 d and e to figure 2).

The relevant grain size for each sample was obtained using the mean linear intercept method; the results of which are presented in table 1.

Table 1: Average grain sizes of alloy B as compared to alloy A

Heat treatment temperature (°C)	**Average grain size**	
	Alloy A (µm)	**Alloy B (µm)**
950 °C		19.6 ± 0.5
1000 °C		24.2 ± 2.2
1050 °C	66.2 ± 7.6	31.2 ± 3.8
1080 °C		53.2 ± 2.8
1100 °C		71.9 ± 4.6
1150 °C		107.9 ± 6.9

Note: Time at temperature = 30 mins

4.1.1.2. EBSD

Due to the fact that it was indicated that the grain size of alloy B is the same as that of alloy A within the region of 1080 °C and 1100 °C, it was decided to confirm these grain size values. Samples that were investigated for confirmation were alloy A at 1050 °C and alloy B at 1100 °C.

For confirmation of grain size values electron backscattered diffraction was utilised. This confirmation was a necessary measure as errors in grain size measurement can lead to quite different experimental results under supposedly identical conditions[69]. As discussed in chapter 3 (3.2.3.2) a combination of maps and line scans were made use of in order to determine average grain size using EBSD. Figure 3 shows the maps produced for the two alloys.

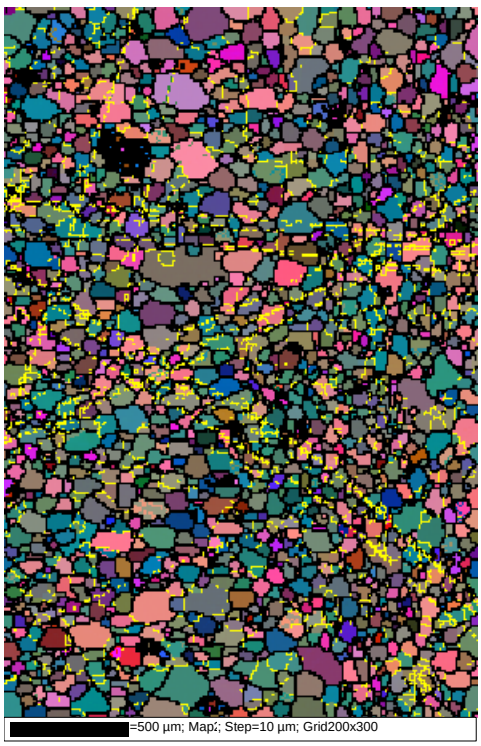

a) A 1050 (map 1)

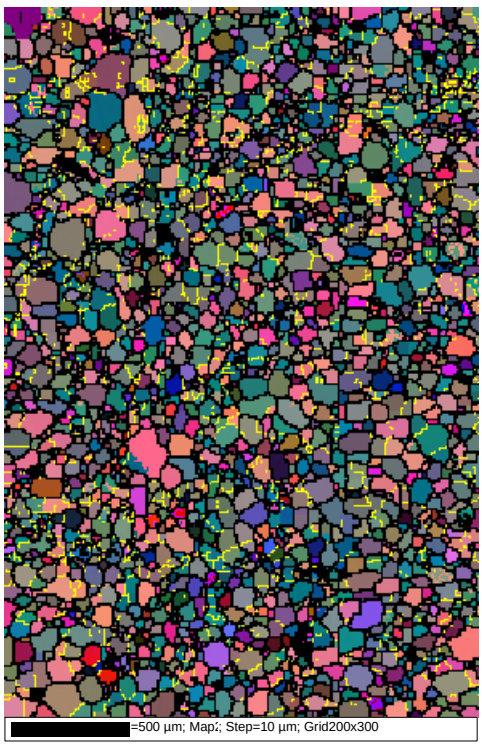

b) A 1050 (map 2)

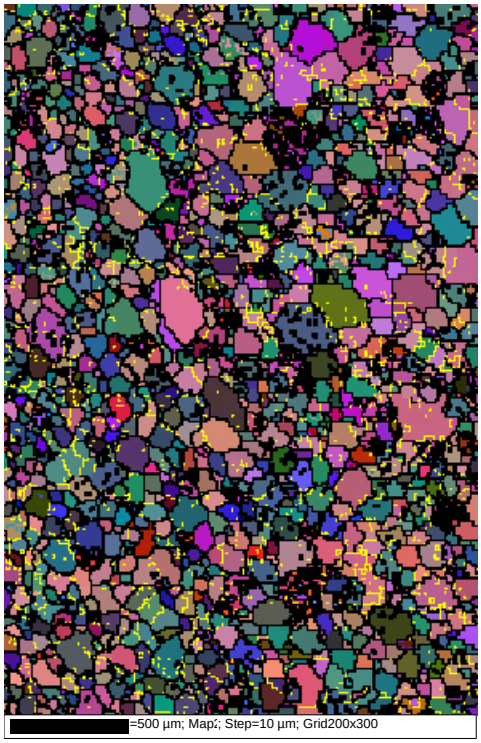

c) B 1100 (map 1)

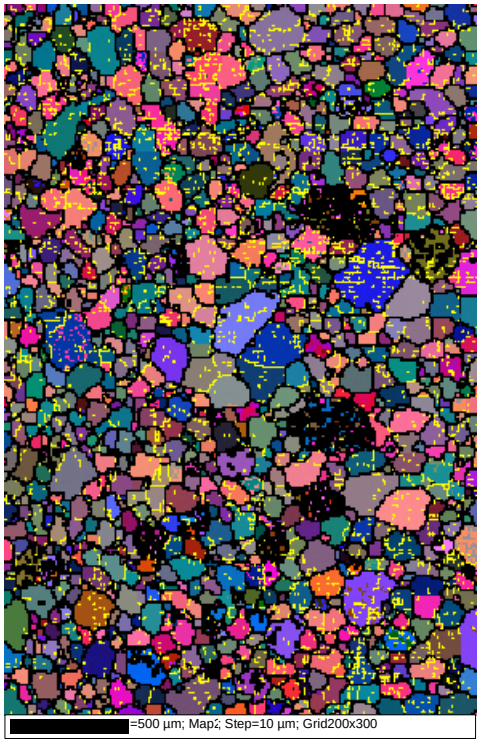

d) B 1100 (map 2)

Figure 3: EBSD maps of alloy A (a and b) and alloy B (c and d) after a 30 minute recrystallisation treatment. Note that the maps are labelled in accordance with their recrystallisation treatment temperature.

High angle boundaries (>10°) are indicated as black lines in figure 3. Some low angle boundaries (<2°) are also detected and are indicated by white lines.

After careful deduction of the results that the maps and line scans yielded with regards to grain size, a bar chart, as seen in figure 4, was produced which shows the results of a combination of maps and line scans that were performed on alloy A (after a treatment at 1050 ºC for 30 minutes) and on alloy B (after a treatment of 1100 ºC for 30 minutes).

Using EBSD to produce either a map or a line scan to yield grain sizes produced similar results, although line scans were more time effective as discussed in chapter 3 (3.2.3.2).

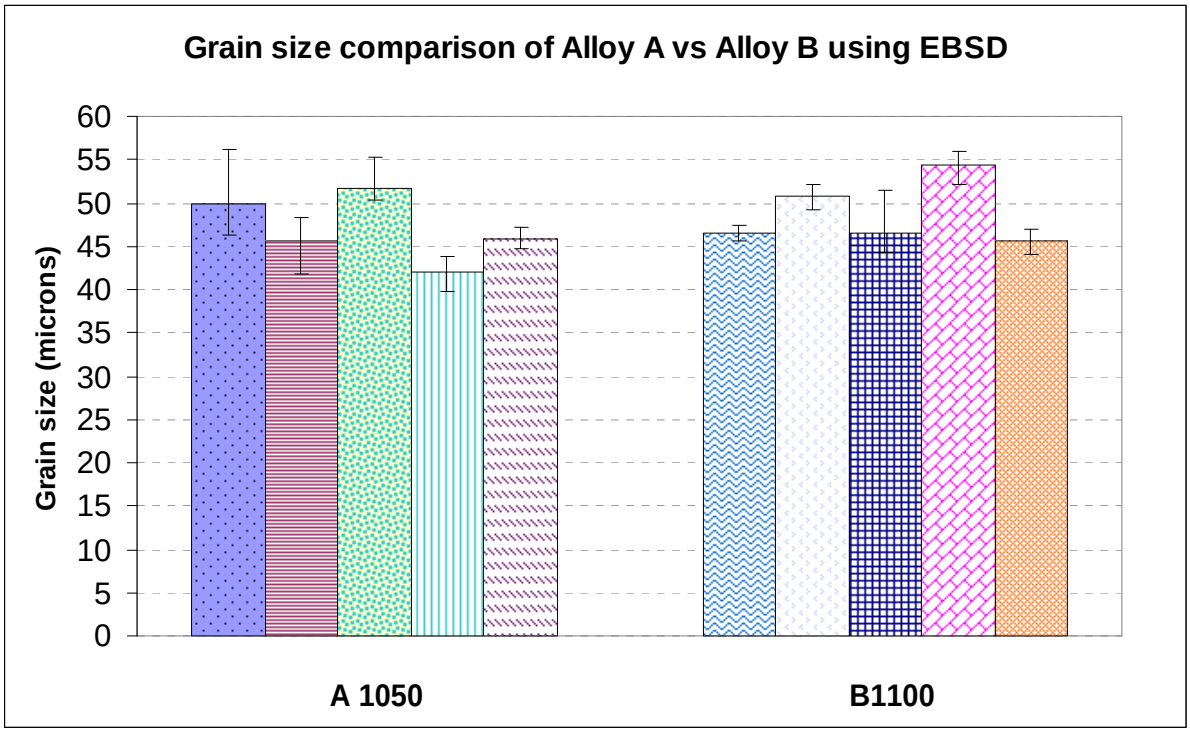

Figure 4: Grain sizes of alloy A versus alloy B (as produced by EBSD). Note each bar for each alloy shows a different field of view of the same sample.

Using EBSD alloy A produced an average grain size of 47,0 µm, with a standard deviation of 3,9 and alloy B produced an average grains size of 47,3 µm with a standard deviation of 3,7.

Figures 5 and 6 show the two alloys to have similar grain size distributions.

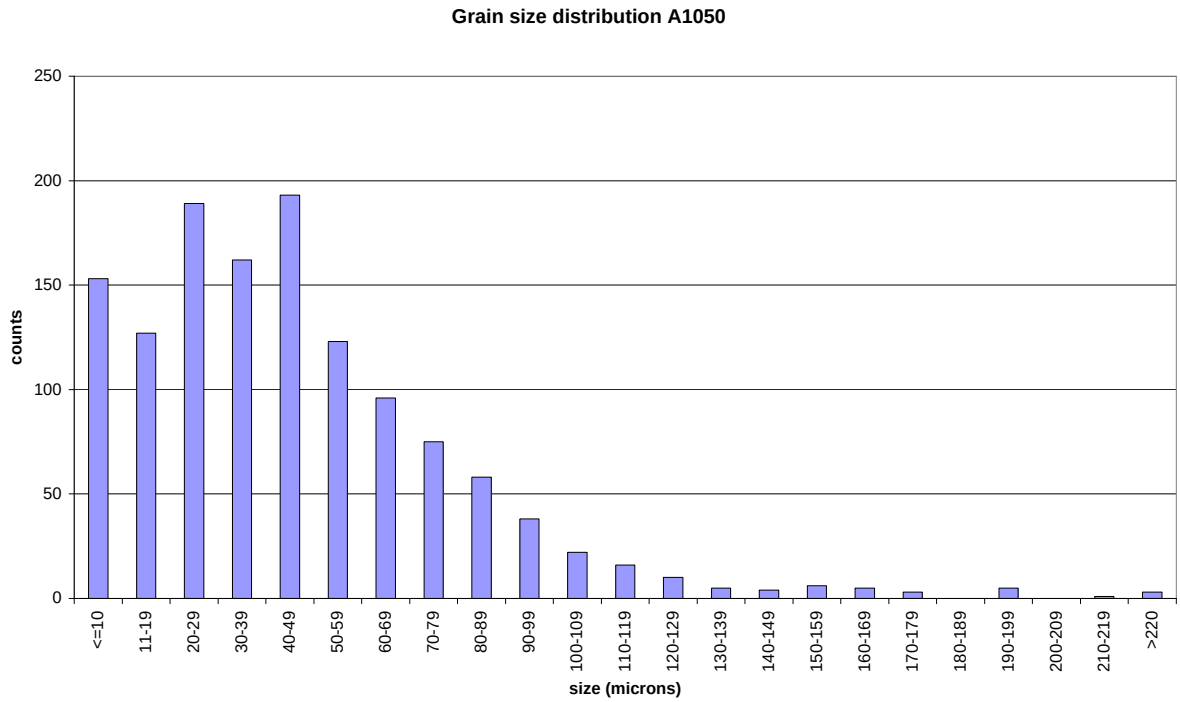

Figure 5: Bar chart showing grain size distribution for alloy A treated at 1050 °C

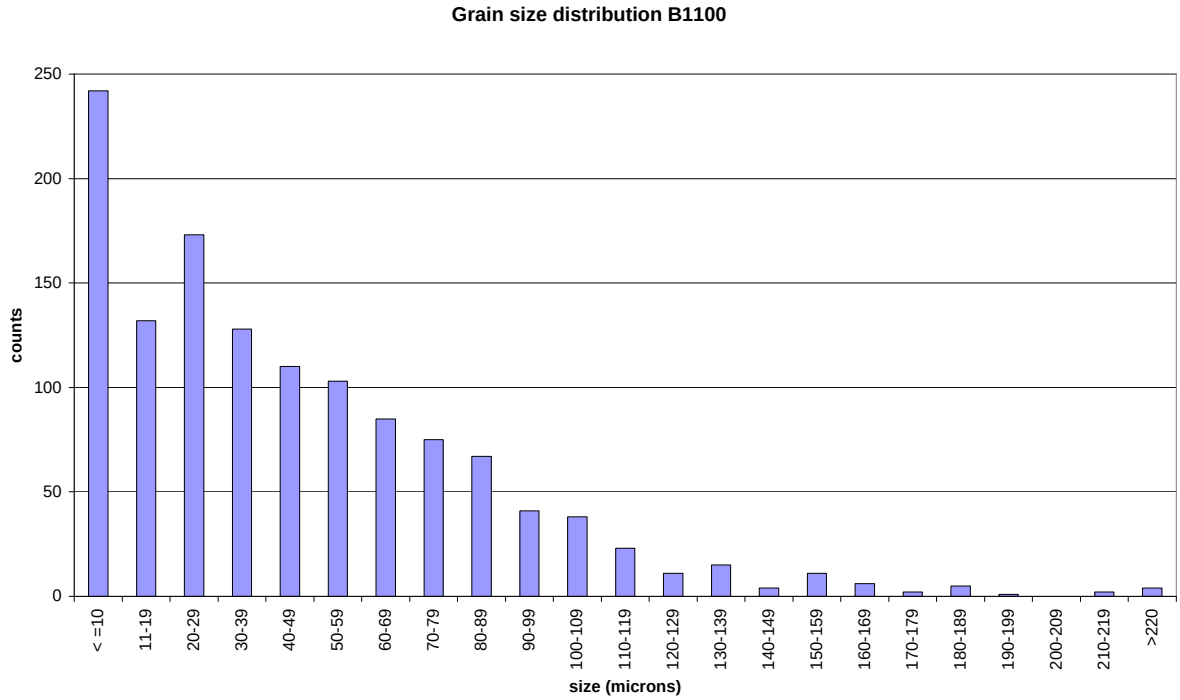

Figure 6: Bar chart showing grain size distribution for alloy B treated at 1100 °C

Although it is expected that an average larger grain size should ensue using EBSD[65], the reason that the opposite happened here can be explained. With reference to figure 7 it is clear that not all high angle grain boundaries etched sufficiently well and hence could not be reliably detected using light microscopy. This could imply that during grain size measurement these boundaries could be overlooked, which would influence the overall average grain size.

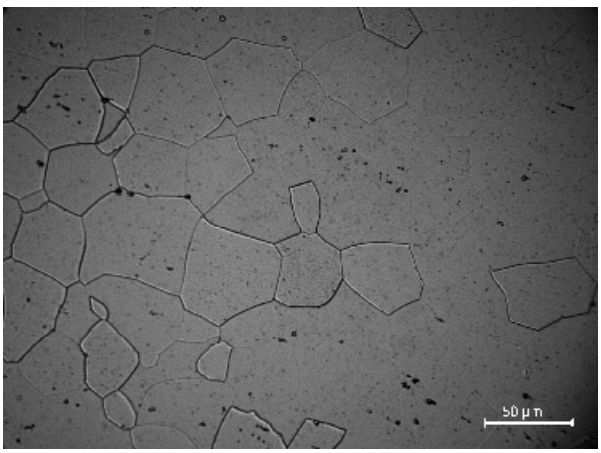

Figure 7: Micrograph of alloy A after heat treatment, showing defined and undefined grain boundaries

Based on the argument discussed it was therefore concluded that the grain size that alloy B would produce at a treatment temperature of 1100 °C would be the same as that of alloy A at a treatment temperature of 1050 °C (after each was soaked at the relevant temperature for 30 minutes).

4.1.2. Final grain size match

As discussed in chapter 3 (3.2.1) the prior thermo-processing consisted of three steps. So far in this chapter just the first step (i.e. the recrystallisation step) has been discussed. Due to the fact that two more steps followed this one, it was deemed necessary to confirm the final grain size of samples prior to creep testing (after the final heat treatment, including all three steps). Although it was not anticipated that the grain size for either alloy would grow significantly by the ensuing heat treatments (steps 2 and 3). Table 2 shows the heat treatment steps in tabular form.

Table 2: Heat treatment parameters for alloy A and alloy B

Treatment	Purpose	Time	Alloy A	Alloy B
Recrystallisation	Equivalent grain size	30 minutes	1050 °C	1100 °C
Ageing	Remove Nb solute	2 hours	700 °C	
Solution	Control Nb solution	200 seconds	950 °C	
Solution	Control Nb solution	200 seconds	1000 °C	
Solution	Control Nb solution	200 seconds	1050 °C	

4.1.2.1. Light Microscopy

For confirmation purposes the grain sizes were checked using the mean linear intercept method. Light micrographs (figure 8) are shown to substantiate the similarities in grain sizes. It was expected that minimal grain growth would occur during the course of step 2 and 3 heat treatments due to the pinning effect of Nb precipitates[48]. It is important to note that the grain sizes listed in table 3 are again similar to the results presented in table 1 and thus it may be concluded that step 2 (ageing) and step 3 (solution) treatments did not significantly alter the grain size that was formed during step 1 (recrystallisation) treatment.

Note: Samples are labelled for the remainder of the thesis as shown in table 5 (chapter 3).

Table 3: Average grain sizes of Alloy B as compared to alloy A (after final heat treatment)

Prior heat treatment	**Average grain size (µm)**
Alloy A	
1050-700-950	66.4 ± 4.6
1050-700-1050	70.3 ± 5.5
Alloy B	
1100-700-950	71.8 ± 8.4
1100-700-1050	70.2 ± 3.9

Note: Grain sizes were measured from light micrographs.

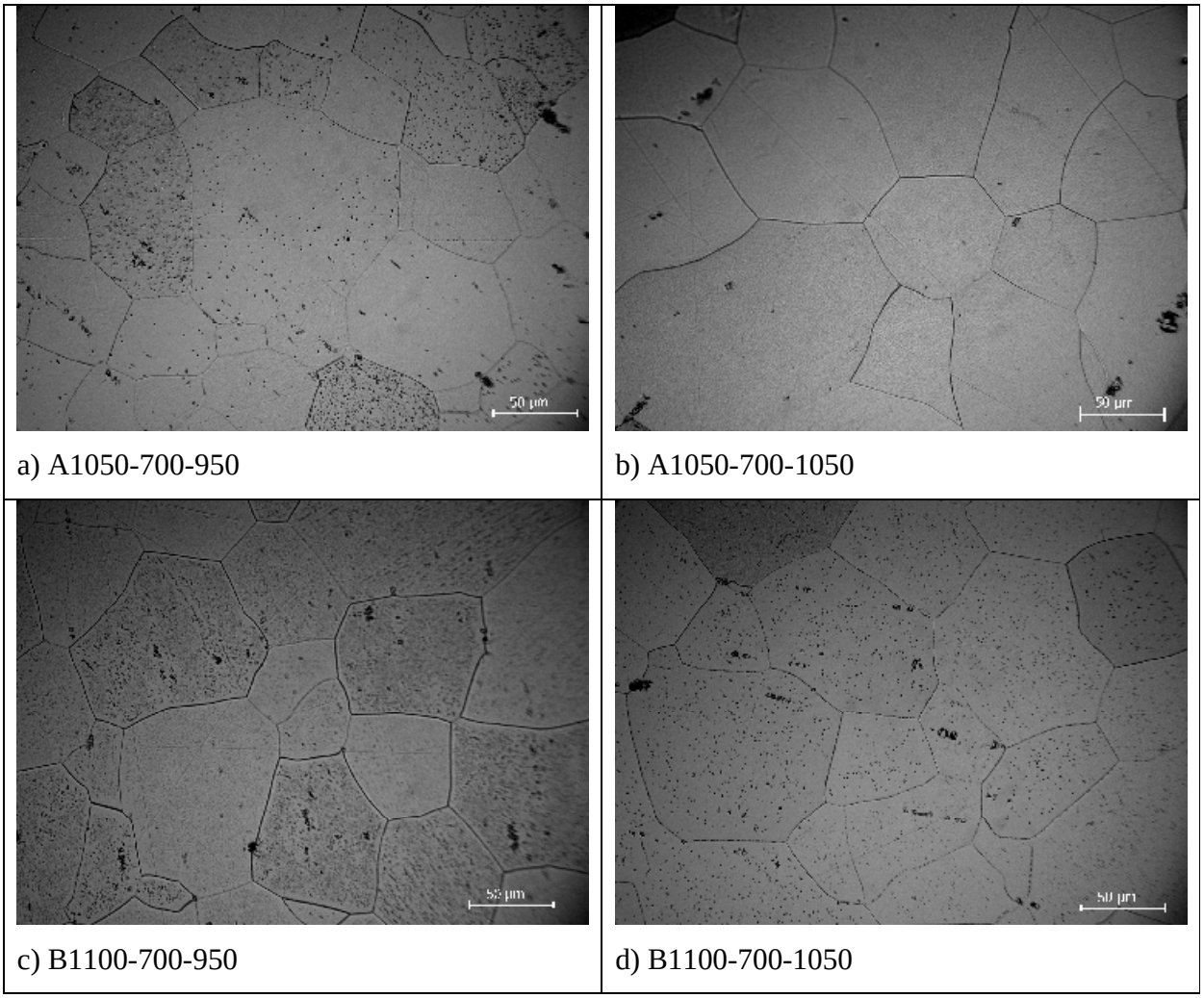

a) A1050-700-950

b) A1050-700-1050

c) B1100-700-950

d) B1100-700-1050

Figure 8: Micrographs of alloy A and Alloy B after the final solution heat treatment (step 3).

4.2. Precipitation studies

The images in figure 9 (a-j) reflect the differences between the two alloys at a particular heat treatment step. The micrographs displayed were produced in the SEM using the backscattered electron detector in order to improve contrast for grain boundary and precipitate detection. The backscattered detector also allows observations of grain boundaries on unetched samples. Each micrograph is labelled according to its prior thermo-processing route.

4.2.1. SEM observations

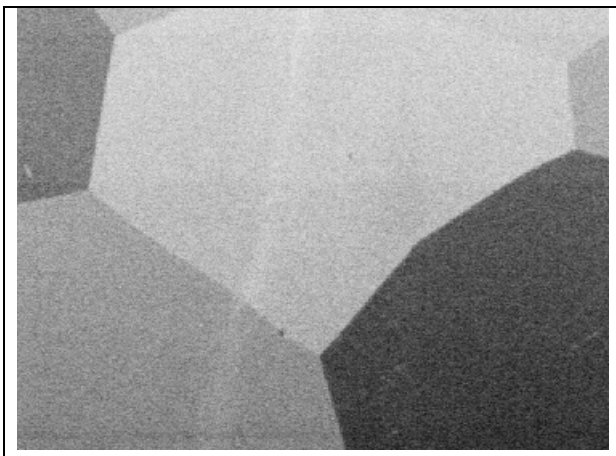

a) A 1050 (30 minutes) 10 µm

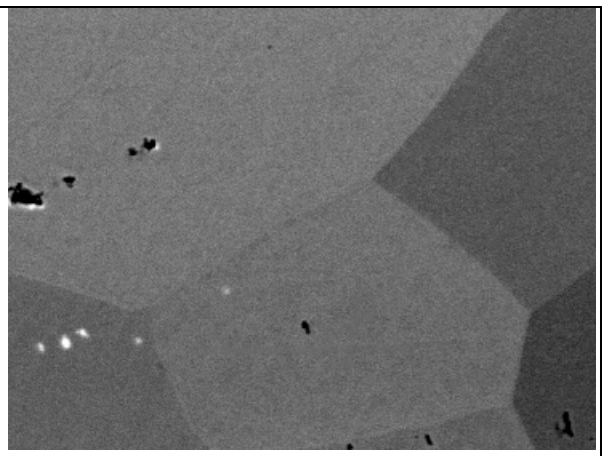

b) B 1100 (30 minutes) 10 µm

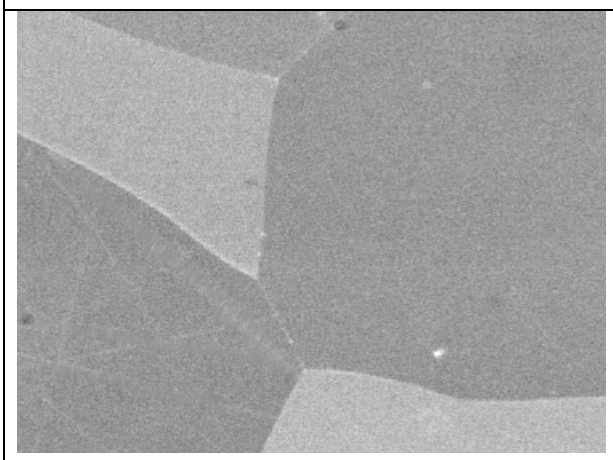

c) A 1050-700 (2 hours) 10 µm

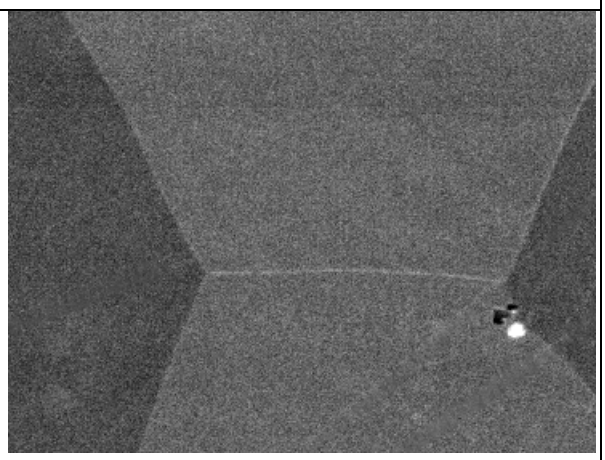

d) B 1100-700 (2 hours) 10 µm

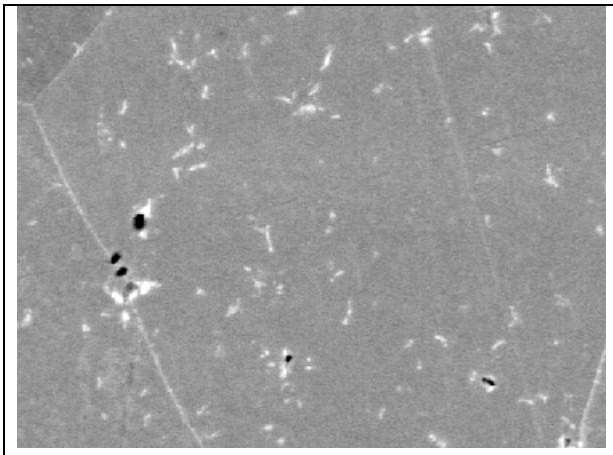

e) A 1050-700 (20 hours) 10 µm

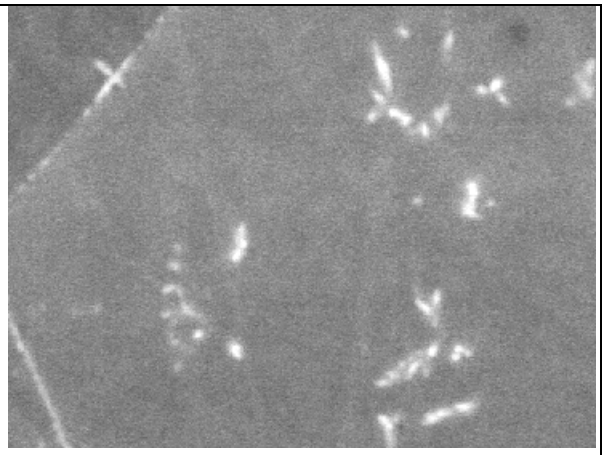

f) A 1050-700 (20 hours). At higher magnification. 3 µm

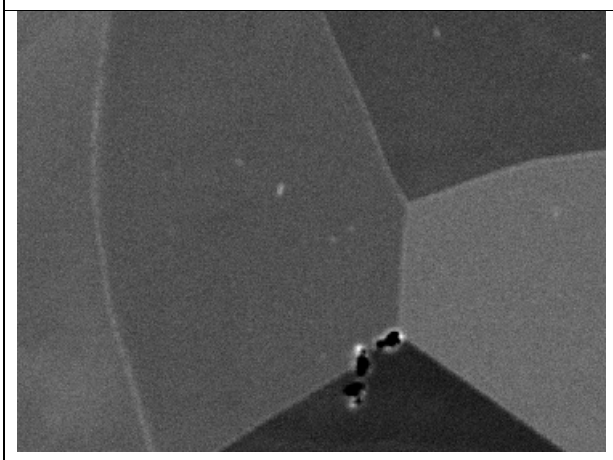

g) A 1050-700-950 10 µm

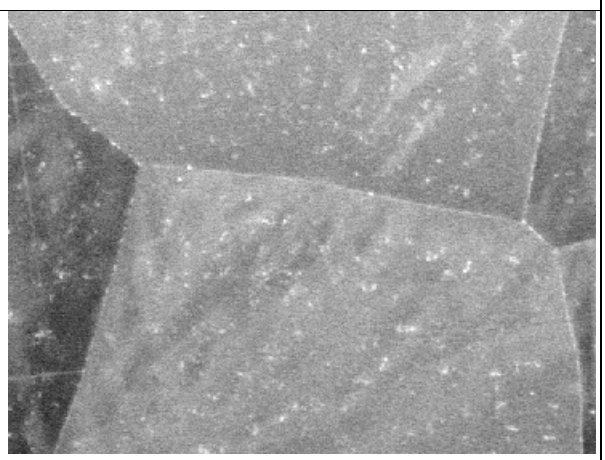

h) B 1100-700-950 10 µm

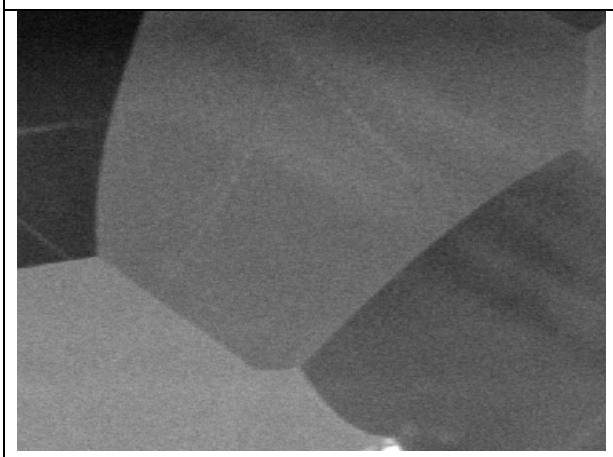

i) A 1050-700-1050 10 µm

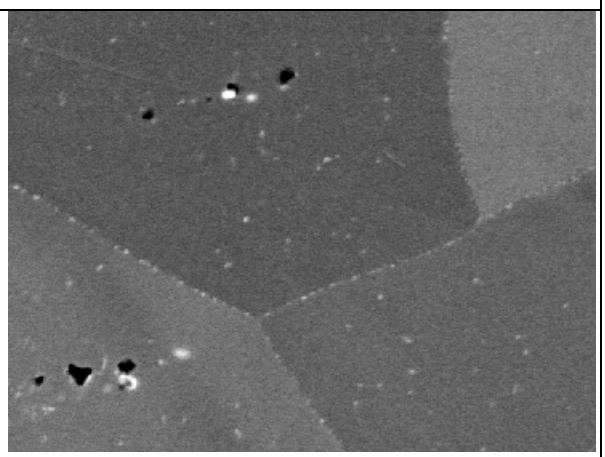

j) B 1100-700-1050 10 µm

Figure 9: SEM micrographs of alloy A and alloy B after heat treatments as specified on the individual figure captions.

The grain boundaries are visible in all of the micrographs. Most of the micrographs show fairly large particles that are generally black or dark grey in the core with a thin line/protrusion of white around this core. These particles are present throughout the processing stages for alloy A and alloy B and there appears to be the same percentage of them for both alloys. They occur randomly within the matrix and are spread out throughout it. These particles are probably TiN[57], which explain the darker contrast provided by the lower average atomic number compared to the matrix. Also the particles appear yellow in colour in the light microscope, which according to research done by Gordon and van Bennekom signifies that the composition is about 10 % TiC and 90 % TiN[46]. The outer part is likely to be rich in Nb (the white areas).

Micrographs (a) and (b) show no trace of the presence of precipitate phases, although the presence of some phase starts to become evident in (c) and (d) where the grain boundaries appear to have 'thickened' slightly. The latter was after both alloys had undergone an ageing treatment at 700 °C for 2 hours.

.

After ageing alloy A at 700 °C for 20 hours not only has the precipitate formation at the grain boundaries increased slightly, but intragranular precipitates have appeared as well. The shape of the latter precipitates is generally 'rod-like'. This is clearly visible in micrographs (e) and (f).

The initial precipitation population formed in alloy A after ageing at 700 °C for 2 hours (c) is still present after the 950 °C solution treatment (g), but this precipitation seems to disappear when solution treated at 1050 °C (i). On the other hand for alloy B the intragranular precipitate population increases when solution treated at 950 °C (h) and 1050 °C (j) from that at 700 °C for 2 hours (d). The precipitation is clearly visible along the grain boundaries and is finely dispersed intragranularly. It is in the form of small particles that are in the region of 0.5

µm in size. There does, however, appear to be a higher percentage volume fraction of precipitation after the 950 °C solution treatment than after the 1050 °C solution treatment.

The purpose of the solution treatment for alloy A seems to have been successful showing no evidence of precipitation after the 1050 °C treatment. For alloy B, however, the opposite seems to have happened with the solution treatment appearing to promote the precipitation of a second phase instead of placing the phase back into solution. Consequently, it is expected that precipitates might play a greater role in the creep deformation of alloy B.

4.2.2. Volume fraction of precipitates

The volume fraction of precipitates was determined using a simple procedure which entails surveying the microstructure and estimating the area fraction of the precipitate constituent. This estimation is guided by the use of comparing the microstructure to a standard chart to promote accuracy and standardisation (refer to 3.2.4.1, figure 4)[67]. The results from table 4 are given with reference to figure 9. Note that careful attention was exercised to ensure that the fields of view were representative of the general sample in each case.

Table 4: Estimation of volume fraction, as per standard chart[67]

Sample	**Percent by area of light constituent**
a) A 1050	0 %
b) B 1100	0 %
c) A 1050-700 (2 hours)	1 %
d) B1100-700	1 %
e & f) A 1050-700 (20 hours)	10 %
g) A 1050-700-950	1 %
h) B 1100-700-950	15 %
i) A 1050-700-1050	0 %
j) B 1100-700-1050	10 %

From table 4 it is quite clear that the most amount of precipitation occurs in micrographs (h) and (j). Nevertheless (e & f) also has a large percentage of the precipitates. However, this precipitation appears quite different to that in (h) and (j) in that the particles appear more 'rod-like' and coarser.

4.2.3. Electron dispersive spectroscopy (EDS)

In order to identify the type of precipitation that is evident in figure 9 (e, f, h and j) EDS was performed.

Each one of these samples also had the bulk material analysed for Fe, Cr, Nb and Ti. It is likely for the bulk that the highest constituents would be Fe and Cr, with small amounts of Nb and Ti.

The large blocky particles that appear randomly in the samples were also analysed to confirm their composition and the likelihood of them being TiN surrounded by a Nb rich outer area.

4.2.3.1. Alloy B

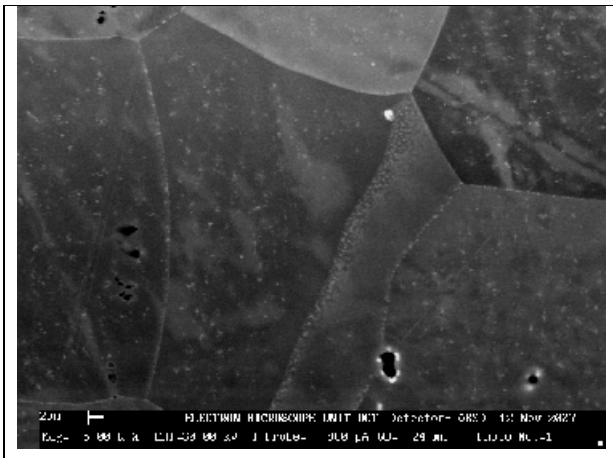

a) B1100-700-950

b) B1100-700-1050

Figure 10: Micrographs of alloy B showing a clear level of precipitation after a solution treatment

In figure 10 (a and b) the presence of precipitation is clear. This precipitation is evident on grain boundaries and within the bulk of the samples. Table 5 shows the results of the EDS analysis on these samples.

Table 5: EDS analysis of bulk and precipitation for alloy B

Alloy	**Fe (%)**	**Cr (%)**	**Nb (%)**	**Ti (%)**
Bulk: B1100-700-950	80.7	18.1	1.1	0.1
Bulk: B1100-700-1050	80.4	18.3	1.2	0.1
Precipitation: B1100-700-950	50.8	12.9	36.2	0.1
Precipitation: B1100-700-1050	60.9	15	24	0.1

With reference to table 5 it is clear for the analysis of the bulk of the samples that the main constituent is Fe and Cr, which is to expected. The Nb level is higher than expected and reflects the limited accuracy of standardless EDS analysis.

Nevertheless, the analysis of the precipitates is quite different to that of the bulk. Table 5 shows high Nb percentages for the precipitates as compared to the other elements. The other constituents that are revealed could be from the surrounding matrix, due to the spread of the electron beam interaction volume.

This could indicate this phase to be the Nb rich intermetallic Laves phase (Fe_2Nb), which is supported by other researchers such as Johnson[4]. Johnson's work covered determining the influence of Nb on the creep properties of ferritic stainless steel. In this case re-annealing was performed on samples in order to dissolve any precipitation that had formed, although after creep testing for a period of 100 hours precipitates had re-formed both at grain boundaries and within the grains. An analysis of these precipitates, extracted from creep test specimens, were identified as Laves phase (Fe_2Nb). The analysis gave results within the region of: Fe, 50%, Cr 7%, Nb 21 %, Mo 17% plus a small amount of Ti and Si. The Nb percentage supports the above EDS analysis (table 5).

This also collaborates with research done by Barteri and Mecozzi who also observed similar precipitation in a comparable composition of a ferritic stainless steel, noting that these small precipitates were Nb rich and either appeared isolated within the matrix or attached to the larger particles (TiN)[57].

It must, however, be borne in mind that this phase is difficult to analyse using EDS due to its small size, as the EDS interaction volume is probably greater than the precipitate itself (i.e. the beam could be analysing more of the matrix material instead of the precipitate itself). Thus the present analysis is not accurate, but sufficient information exists to infer that the Nb rich precipitates are indeed Laves phase.

4.2.3.2. Alloy A

With reference to figure 9, the initial precipitation population formed in alloy A after ageing at 700 °C for 2 hours (c) is still present after the 950 °C solution treatment (g), but is no longer present after the solution treatment at 1050 °C (i).

After ageing alloy A at 700 °C for 20 hours (e and f) precipitation is present with a 10 % volume fraction. This is the same volume fraction as seen in alloy B after a solution treatment of 1050 °C (j). However, at these stages the precipitation for alloy A appears quite different to that of alloy B, it is more 'rod-like' and appears coarser (figure 11). This change in particle shape and size could be related to the longer ageing time, as it appears that a longer ageing time promotes this change. On analysing these coarser precipitates they were found to be rich in Nb (53.90 %).

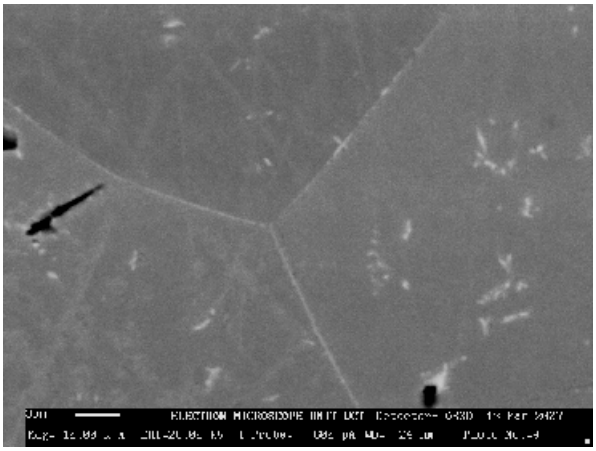

Figure 11: Micrograph of alloy A showing coarse precipitates formed after a prolonged ageing treatment.

4.2.3.3. Primary particles

The larger particles visible in the micrographs could be TiN; they appear as black shapes often surrounded by a thin white section. These would have formed at a high temperature possibly in the liquid or during solidification[57]. They are typical particles found in these steels and occur in alloys A and B. A magnified example of a cluster of these particles is seen in figure 12.

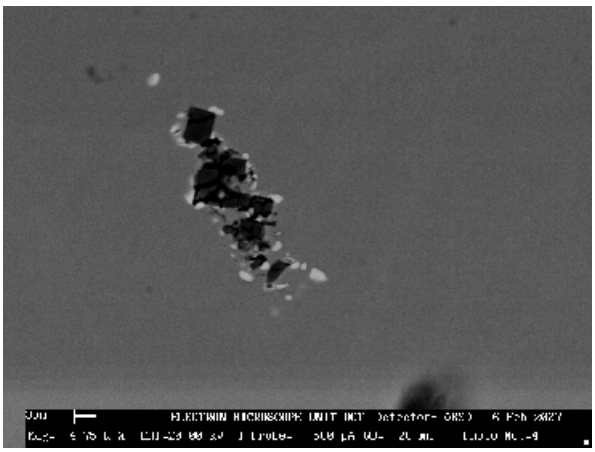

Figure 12: Cluster of primary particles

An EDS analysis produced the following results for the core of the particle Fe 15.3 %; Cr 5.6 %, Nb 5.4 %, Ti 73.8 %, which shows the core to be Ti rich. For the outside protrusions the

analysis looked quite different, Fe 41.2 %; Cr 11.6 %, Nb 42.1 %, Ti 5.1 %; which shows the protusion to be Nb rich. This analysis shows clearly the difference in Nb and Ti content within the different regions of the particle. This substantiates the claim that these particles are likely to be TiN surrounded by Nb (C, N). The spectra for the analysis's can be seen in figure 13.

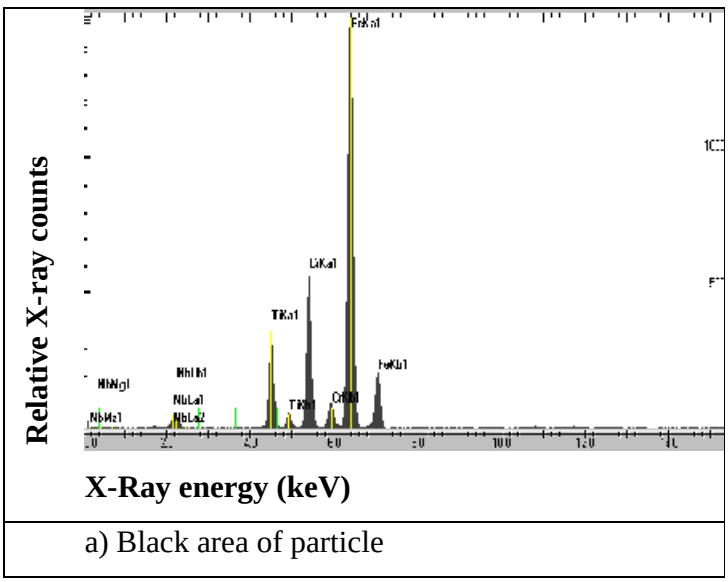

a) Black area of particle

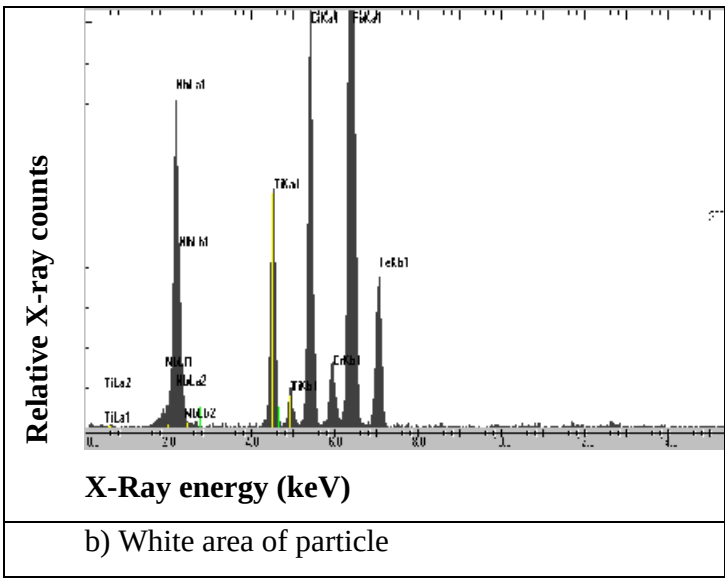

b) White area of particle

Figure 13: Analysis of a primary particle

The brighter areas of the particles are Nb where the darker areas are Ti, which relates to the atomic number of these elements. A higher BSE signal is produced from the higher atomic number volume (Nb: 41; Ti: 22).

4.3. Creep test results

The creep test results of the two alloys are presented in this section. In each graph take note of the legend which indicates the materials prior heat treatment parameters as discussed in chapter 3 (3.2.1).

The results have been categorised firstly according to the stress at which the test was run at, this is to show the difference between the creep resistance of alloy A and B after the solution treatment (i.e. after heat treatment step 3). Secondly the results of alloy A and B have been investigated solely in order to determine the effect of the solution treatment. These results also include the specimens of alloy A that were not treated to a solution treatment and those that were aged for a longer period of time.

Two curves are shown per run; this was to show the repeatability of the testing rigs and the testing procedure. Some of the results did not prove repeatable therefore they were repeated up to four times to promote more confidence with regards to reproducibility. It is, however, evident from the creep test results that the specimens of the same alloy and same prior thermo-processing route have produced a scatter in results. This is not uncommon, as even for materials of exactly the same composition; differences in creep properties may be introduced. These differences are generally attributed to minor variations in microstructure produced by what may be seen to be exactly the same heat treatment. An example of where this is common is in the case of chemical and electricity generating plants where steel components are generally manufactured from ingots, ranging in weight and size. The large size of these ingots would imply that all parts of a particularly large component cannot then receive exactly the same thermo-mechanical processing, which would result in definite variations in microstructure and subsequently material properties[35]. Also testing was performed on two rigs and there could be minor differences in the rigs themselves, although this is unlikely as rigorous monitoring was constantly performed.

4.3.1. Alloy A versus Alloy B

Creep tests in this category were performed at two different stress levels namely 10 MPa and 15 MPa.

The plots produced for the analysis between the two alloys did not exhibit an 'ideal' creep curve. There appears to be no primary creep region or steady state region; in fact the tertiary creep region dominates the creep curve altogether. This is predominantly evident of creep data in the case of high temperatures and low stresses[70] and could be characterised by a slow, albeit increasing strain rate with time i.e. the creep rate is increasing gradually from the start of each test. These curves are similar to that produced by Borneman[33] who, using a similar alloy, observed little evidence of the first or second stage. Borneman's creep curves on the other hand shows creep life in hours to 1 % and 2 % elongation instead of to failure or to a pre-determined time. A direct comparison of the results produced for this work could not be made to Bornemans work, however, as the parameters were quite different as discussed in chapter 2 (2.10).

4.3.1.1. Stress level at 10 MPa

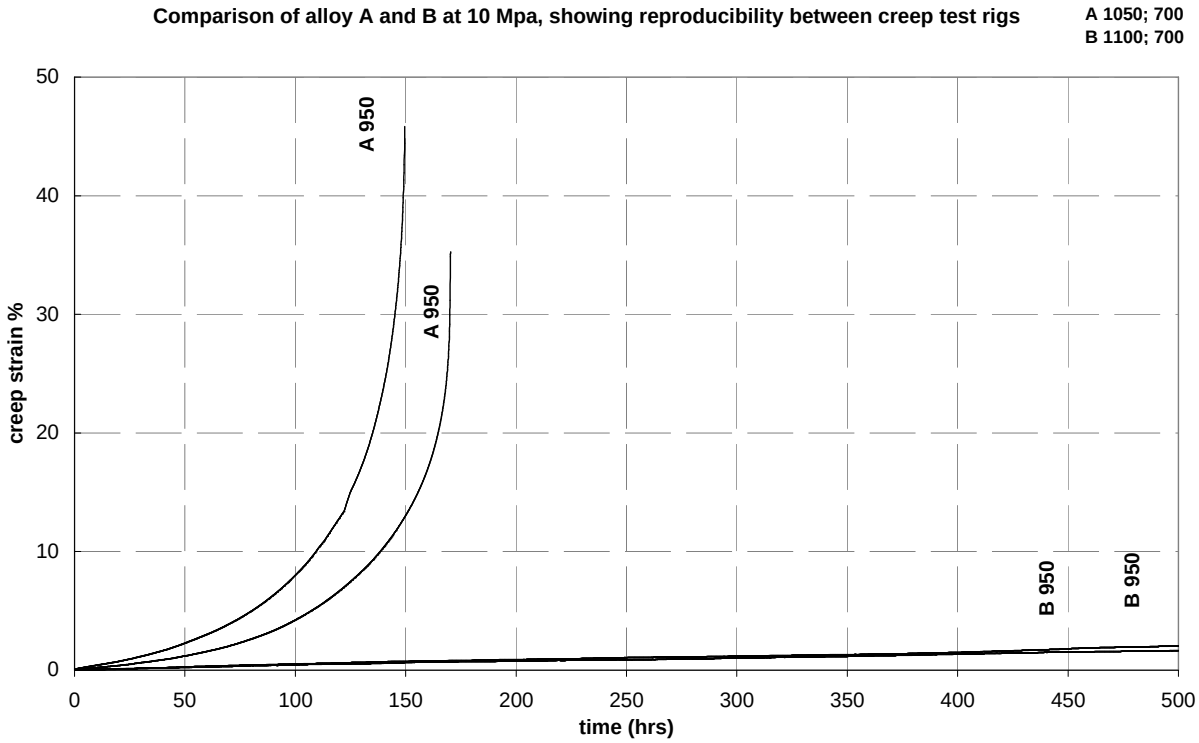

Figure 14: Creep test results for alloy A and alloy B after a final solution treatment of 950 °C at 10 MPa. Note the legend which indicates prior heat treatment procedure.

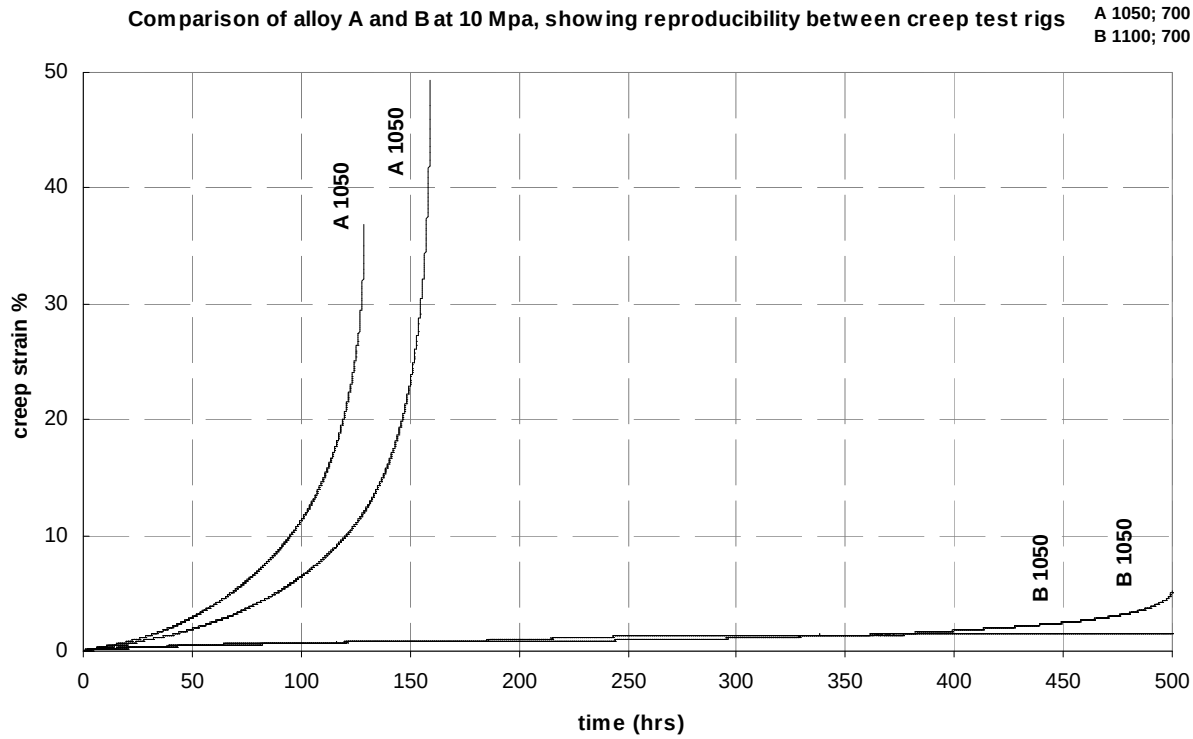

Figure 15: Creep test results for alloy A and alloy B after final solution treatment of 1050 °C at 10 MPa. Note the legend which indicates prior heat treatment procedure.

Figures 14 and 15 illustrate the difference in creep resistance for two different solution treatment temperatures (950 °C and 1050 °C) of alloy A and B at 10 MPa. It is clear that the creep resistance of alloy B has been altered by the growing of the grain size, this is in comparison to the earlier study as described in chapter 2 (2.10.1)[5], in fact it is noticeable that alloy B is now superior to alloy A with regards to creep resistance.

Tests for alloy A were all run to fracture; with all of the specimens fracturing before 200 hours, regardless of the final solution treatment temperature. Conversely tests for alloy B were not run to fracture due to time constraints. Alloy B specimens were run up to 1000 hours (except for one alloy of B, 1100-700-1050 which fractured just before 700 hours), although the results are only shown up to 500 hours. This was simply to allow creep test results for both alloys to be shown on the same set of axes. It was also felt that it was unnecessary to continue with tests for alloy B after 1000 hours as by this time it was quite clear that alloy B was superior to alloy A with regards to creep resistance, a fact which was already evident at

200 hours. Even so at 1000 hours alloy B specimens that had a final solution treatment of 950 °C had still not fractured and had only reached a creep strain of just over 3 %. In the interests of being able to perform a reasonable number of tests over the broad range of test variables, it was decided to limit the test time to less than 1000 hours and only repeat tests more than twice that were absolutely essential to allow reliable presentation of data.

4.3.1.2. Stress level at 15 MPa

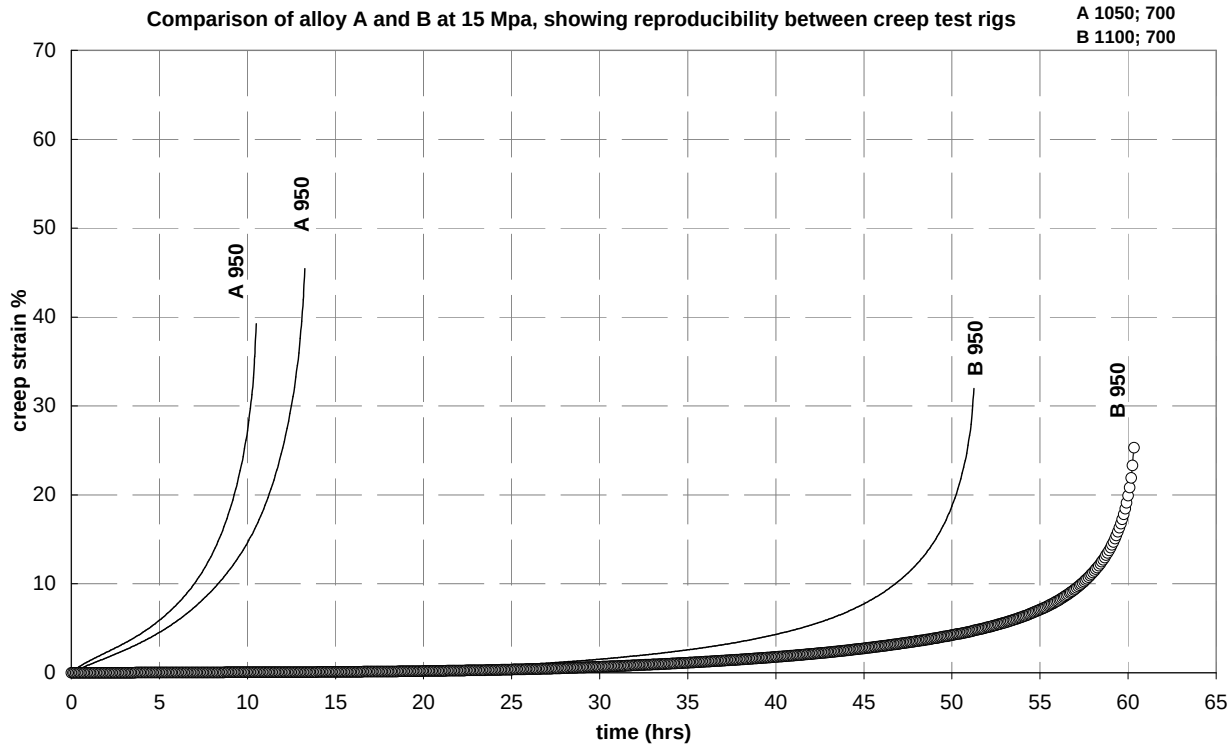

Figure 16: Creep test results for alloy A and alloy B after final solution treatment of 950 °C at 15 MPa. Note the legend which indicates prior heat treatment procedure.

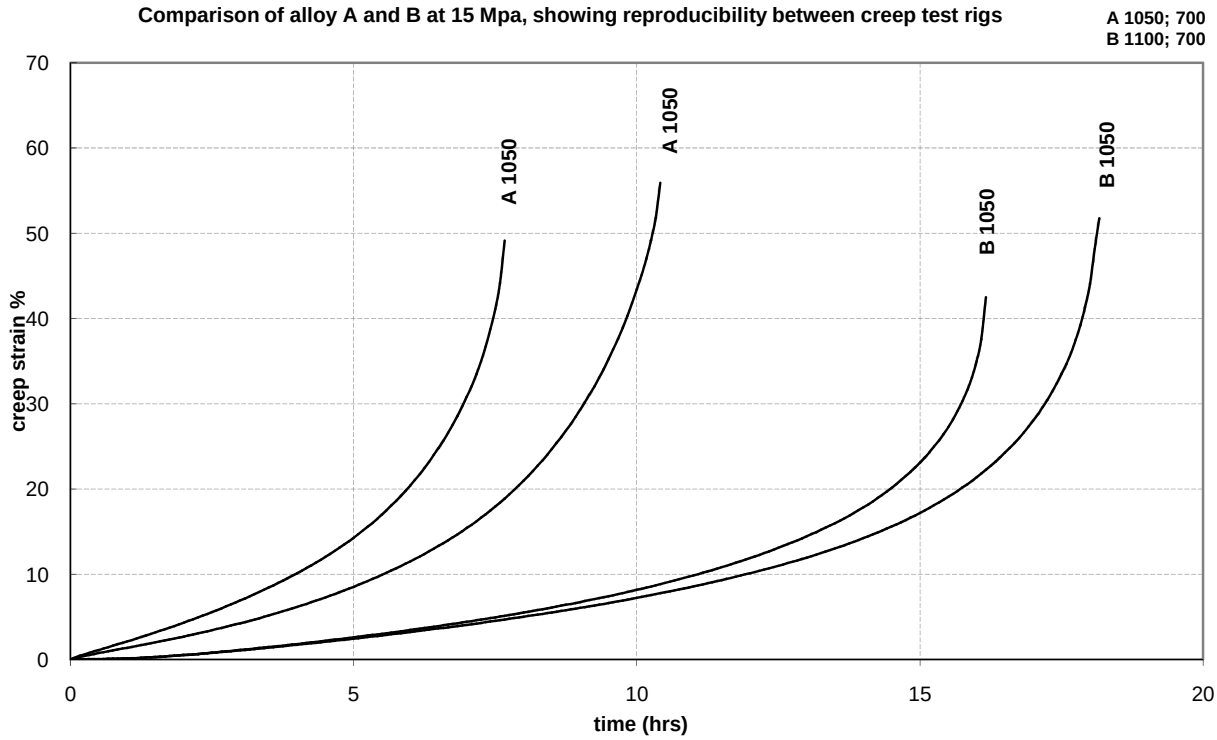

Figure 17: Creep test results for alloy A and alloy B after final solution treatment of 1050 °C at 15 MPa. Note the legend which indicates prior heat treatment procedure.

Figures 16 and 17 illustrate the difference in creep resistance for two different solution treatment temperatures (950 °C and 1050 °C) of alloy A and B at 15 MPa. As expected from the results at 10 MPa it is still clear that alloy B is superior to A with regards to creep resistance.

Tests for alloy A were all run to fracture; with the specimens fracturing before 15 hours, regardless of the final solution treatment temperature. Tests for alloy B were also run to fracture at this higher stress value, with specimens fracturing before 65 hours. The anomaly that appears to stand out at this stress value is the fact that alloy B at a solution temperature of 1050 °C did not perform particularly well (related to the 950 °C solution temperature). The reasons for this are further investigated in 4.3.2.1 (page 82).

In order to decipher the reasons for alloy B being superior to alloy A regarding creep resistance it was necessary to refer to the microstructures. On comparing the creep results of alloy A and B at a final solution temperature of 950 °C and 1050 °C for both stress values, the final grain size prior to creep testing is the same (as seen in table 3). As the greater creep resistance for alloy B cannot be explained by grain size differences, it seems that the factors affecting this superior creep resistance must be related to either the amount of Nb in solution or the consequence of some precipitation strengthening mechanism.

Intermetallic phases can affect the mechanical properties of a material, in particular by increasing the strength and decreasing the elongation of the steel[50]. This would indicate that the creep resistant superiority of alloy B could be related to the precipitation of the finely dispersed phase, which is likely to be the Nb rich Laves phase, as a large amount of precipitation of Laves phase is known to increase strength[50, 54]. This strength is related to the Laves phase particles obstructing the flow of vacancies along the grain boundaries during creep.

With reference to the fracture elongation of the steel it was noted that during creep specimens of alloy A produced on average a greater fracture elongation than alloy B; this is particularly evident in figure 16. This once again could be attributed to the Laves phase precipitation in alloy B, as a drop in elongation is due to the precipitation of the Laves phase in a great amount[50].

4.3.2. Influence of solution treatment

This section of the creep testing focused on the effect a variation of the heat treatment parameters would have on the creep resistance of the alloys; the variations that were investigated were:

- solution treatment temperature (investigated for alloy A and B)
- ageing time without solution treatment (investigated only for alloy A)

4.3.2.1. Solution treatment temperature

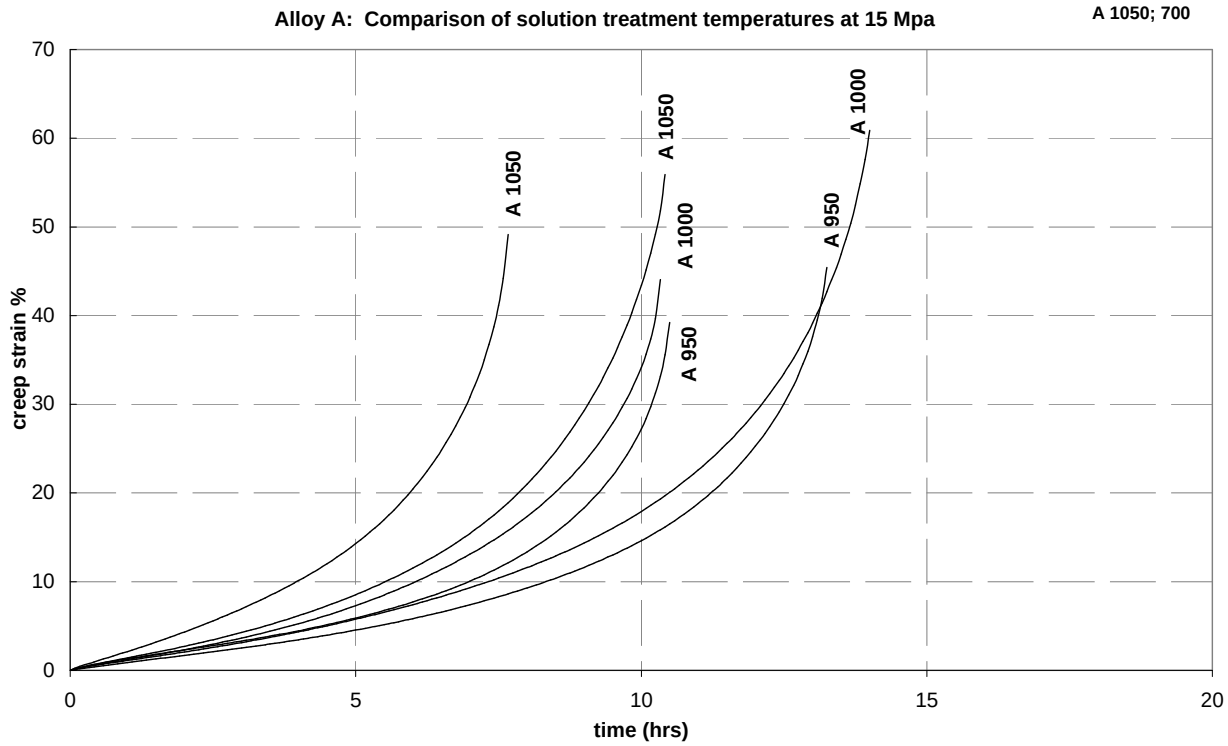

Figure 18: Creep test results of alloy A showing an indistinguishable difference in final solution treatment temperatures at 15 MPa. Note the legend which indicates prior heat treatment procedure.

From the creep curve seen in figure 18 a clear distinction between the effects of the three final solution treatment temperatures on the creep resistance of alloy A cannot be established. Even at a lower stress of 10 MPa (figure 19) the majority of fracture times occurred between 130 and 200 hours regardless of solution treatment temperature.

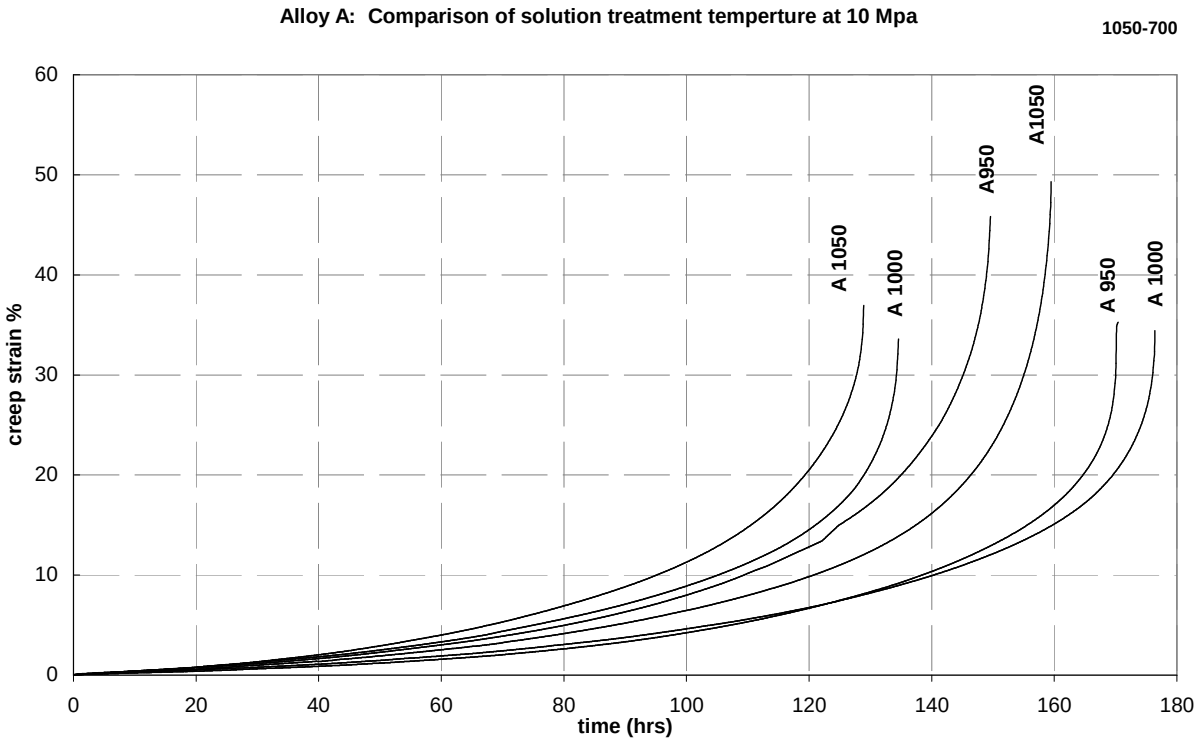

Figure 19: Creep test results of alloy A showing an indistinguishable difference in final solution treatment temperatures at 10 MPa. Note the legend which indicates prior heat treatment procedure.

In an attempt to identify these differences creep tests for alloy A were run at even lower stress values of 5 MPa and 7.5 MPa, and still a difference could not be asserted. These results can be seen in figure 20.

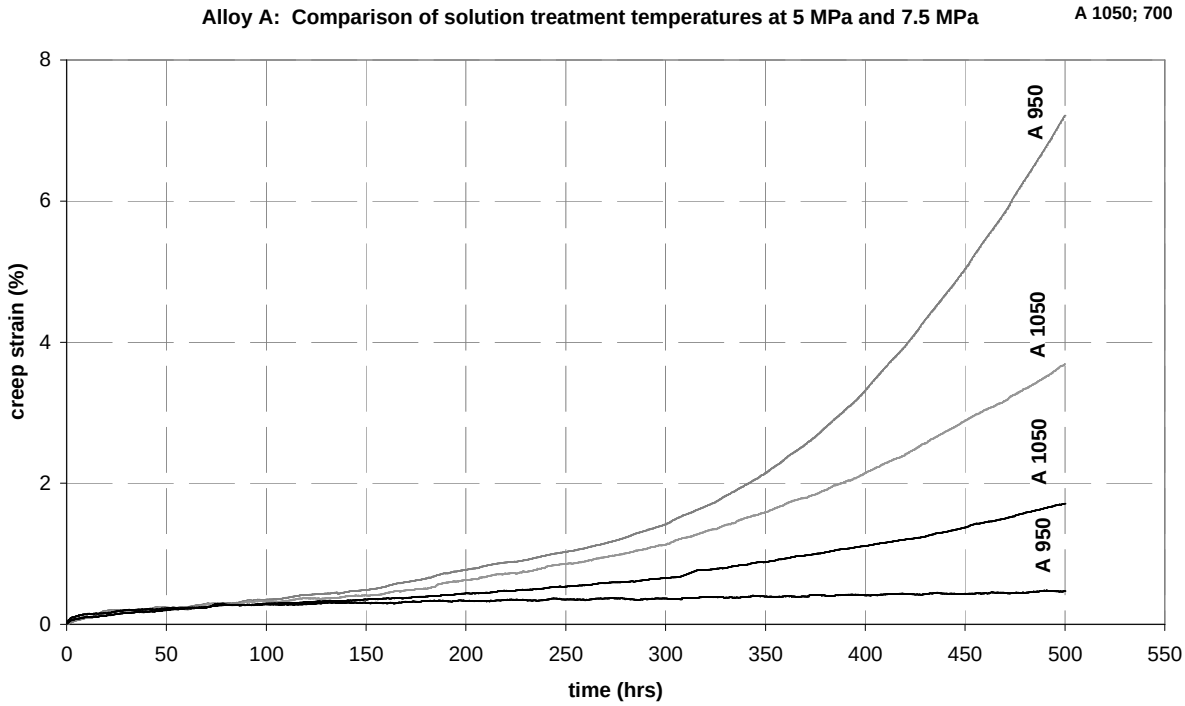

Figure 20: Creep test results for alloy A showing an indistinguishable difference in solution treatment temperature of 950 °C and 1050 °C at stresses of 5 MPa and 7.5 MPa. The grey curves show tests at 7.5 MPa, whilst the black curves show tests at 5 MPa. Note the legend which indicates prior heat treatment procedure.

These results indicate that the solution treatment temperature within a range of 950 °C to 1050 °C does not appear to affect the creep resistance of alloy A with any degree of certainty.

The results for alloy B, however, appear quite different. The difference between the different solution treatment temperatures is more pronounced, this can be seen in figure 21.

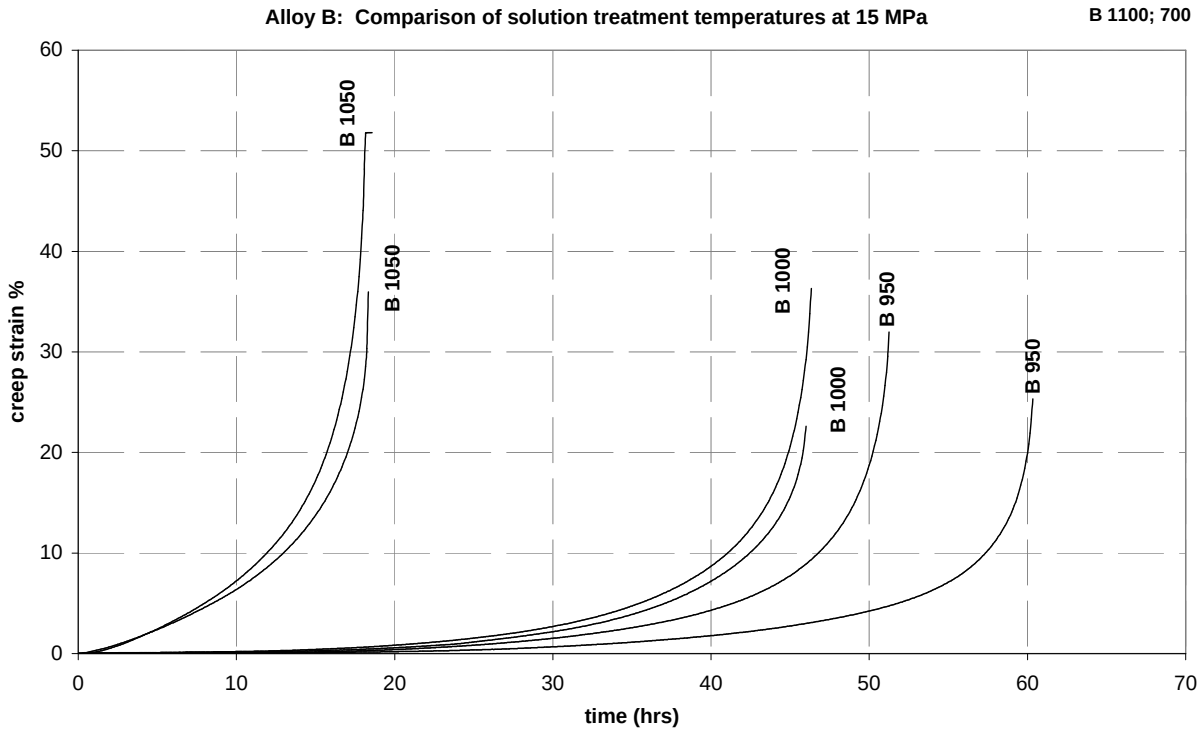

Figure 21: Creep test results for alloy B showing the difference in solution treatment temperatures at 15 MPa. Note the legend which indicates prior heat treatment procedure.

It is clear from the creep curve in figure 21 that alloy B produces the least creep resistant specimens after a solution treatment of 1050 °C. This test was repeated beyond the two tests in order to confirm these results and each time produced similar values. In order to better understand this result two specimens of alloy B that had a heat treatment of 1100-700-1000 (i.e. final solution treatment of 1000 °C) were run at 15 MPa to determine whether or not these specimens would have better creep resistance as compared to the specimens that had undergone a solution treatment of 1050 °C. Results for this test show that these specimens fractured in the region of 46 hours which shows that they have an improved creep resistance relative to the final solution treatment of 1050 °C, but not as good as the 950 °C treatment. The superiority of creep resistance with regards to the different solution treatment temperature for alloy B could possibly be explained by the microstructure. The volume fraction of precipitation for alloy B after a solution treatment of 950 °C is higher than that after a solution treatment of 1050 °C; this is noted in table 4 and can be seen in the micrographs in the preceding paragraphs. Figure 22 (a and b) shows a micrograph of B1100-700-950 and one of

B1100-700-1050 at a higher magnification, which shows the difference in percentage volume fraction of precipitation between these two samples more clearly.

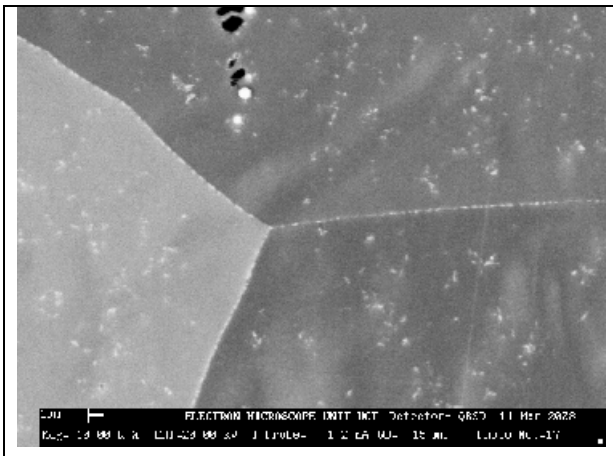

a) B 1100-700-950

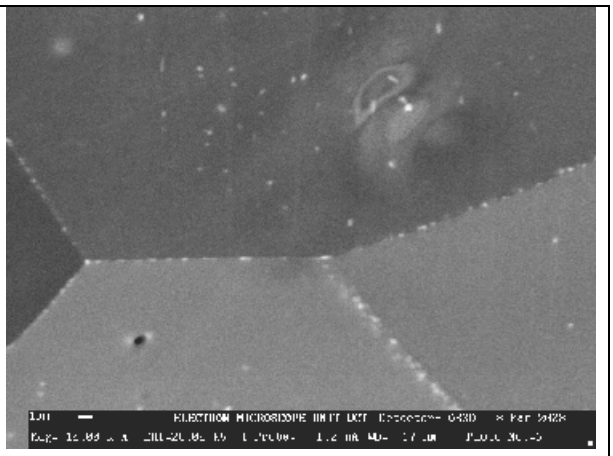

b) B 1100-700-1050

Figure 22: Micrographs showing the sample B 1100-700-950 (a) to have more percentage volume fraction precipitation than the sample B 1100-700-1050 (b)

4.3.2.2. Influence of ageing time

The creep curves presented in this section show the creep resistance of specimens of alloy A that have had no final solution treatment. Instead the effect of a prolonged ageing time at 700 °C is presented. Therefore the results show the difference in creep resistance between the two ageing treatment times of 2 hours and 20 hours. These results are presented in figure 23.

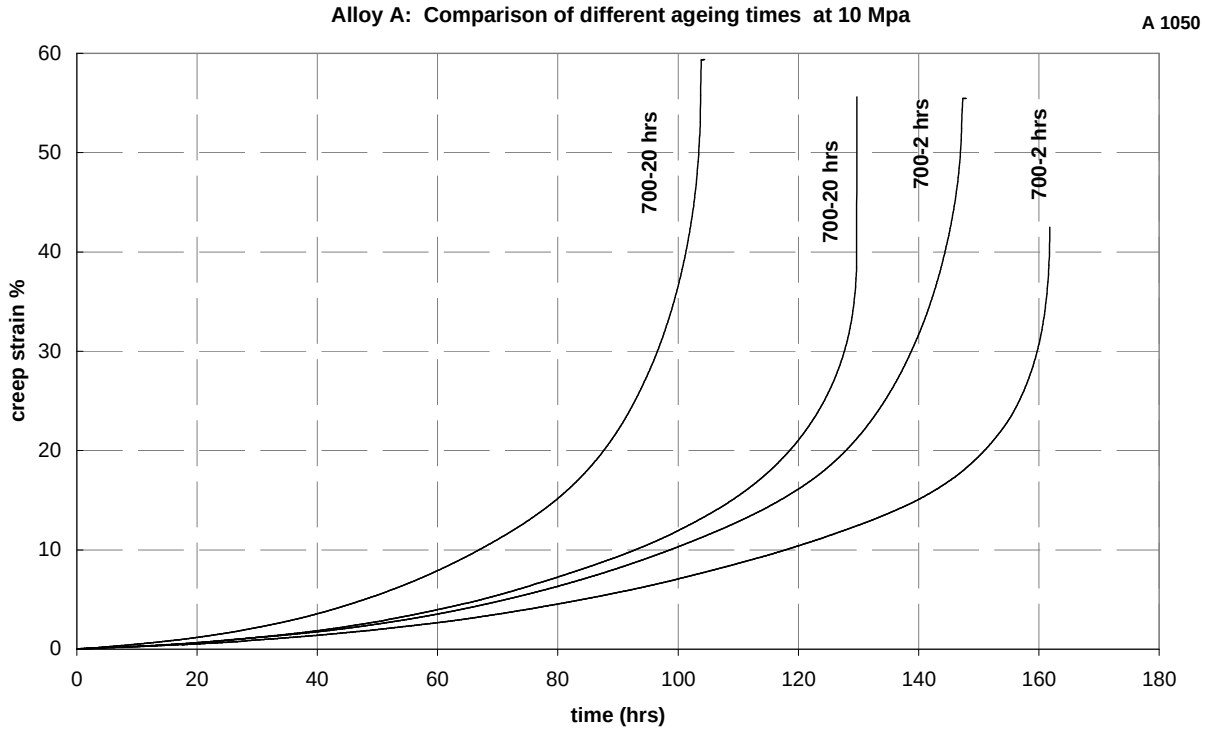

Figure 23: Creep test results of alloy A showing the difference between an ageing time of 2 hours and 20 hours at 10 MPa. Note the legend which indicates prior heat treatment procedure.

From the creep curve in figure 23 it can be seen that despite the scatter in time to fracture the specimens aged for 20 hours show a shorter time to fracture than the treatment for 2 hours at 700 °C. With reference to figure 9 (c) and (e), alloy A after ageing for 2 hours showed little signs of precipitation (except for the thickened grain boundaries) whereas after ageing for 20 hours alloy A showed profuse precipitation. This implies that the presence of the Nb rich phase almost hindered the creep resistance, this is in contrast to the effect this phase seemed to have on alloy B. On the other hand, as previously discussed, after an ageing time of alloy A at 700 °C for 20 hours the phase did appear coarser as opposed to that of alloy B (after the solution treatments). This implies that this coarsening effect of the phase has negatively affected the creep resistance.

After an ageing treatment of 700 °C for 2 hours (after cold rolling and annealing between 900 °C and 1000 °C) Miyakazi et al concluded that the precipitates that were visible in Nb bearing

ferritic stainless steel were Laves phase (Fe_2Nb) and attributed an increased proof strength of the material to this phase[12]. Work done by Sim et al[48] showed that for Nb containing ferritic stainless steels the yield strength at 700 °C decreased as the ageing time increased. They also noted that after an ageing time of 30 minutes the Fe_2Nb particles were quite fine, although with increased ageing time these particles rapidly coarsened into a more rod-like shape. In summary, this work concluded that the coarse rod shaped Fe_2Nb formed during ageing was disadvantageous to the high temperature strength in Nb containing steels. This supports the findings in this section; hence this reduction in creep resistance of the 20 hour ageing treatment as opposed to the 2 hour ageing treatment appears to be related to the coarsening of the Laves particles.

Creep test results of specimens that were heat treated to three different solution treatment temperatures and specimens that were creep tested were no solution treatment was performed can be directly compared in figure 23 and 19, as all specimens were exposed to the same stress level. These results indicate that the solution treatment does not significantly improve the creep resistance of alloy A.

4.4. Investigation of microstructural evolution during creep testing

The investigation of the microstructural evolution during creep testing was performed by simulating the test temperature condition in a muffle furnace. Consequently isothermal treatments were performed at 850 °C for soak times ranging from 10 hours to 400 hours. These treatments were performed for both alloys.

The effect of soaking at various times is presented in the following section. Note that each alloy is presented separately.

4.4.1. Alloy A

Figure 24 and 25 (a-f) show micrographs of alloy A after particular soaking times. Each one of these samples had undergone a prior heat treatment process (as seen in table 2) and are labelled in the figure according to this.

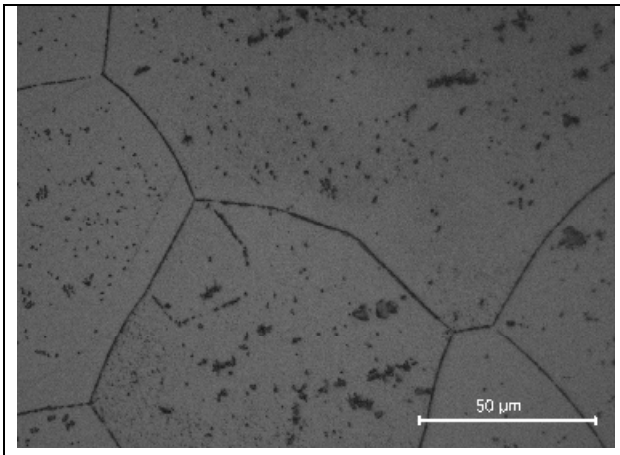

a) After 10 hours

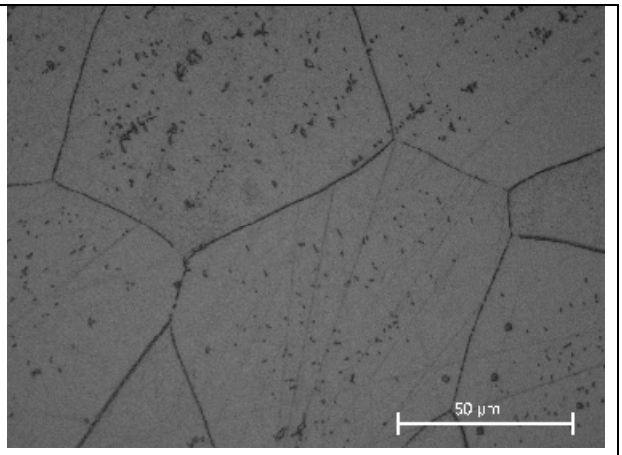

b) After 20 hours

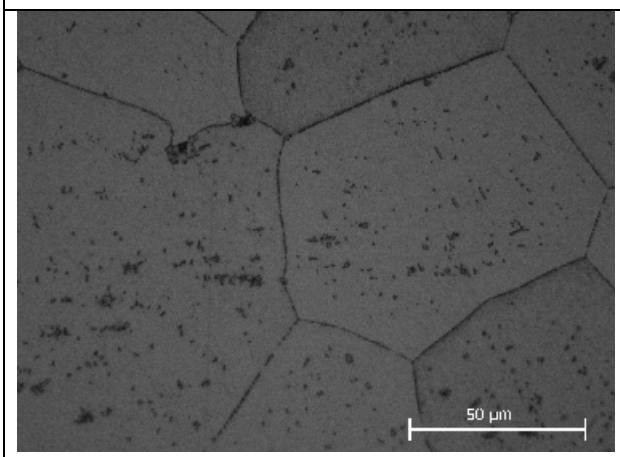

c) After 40 hours

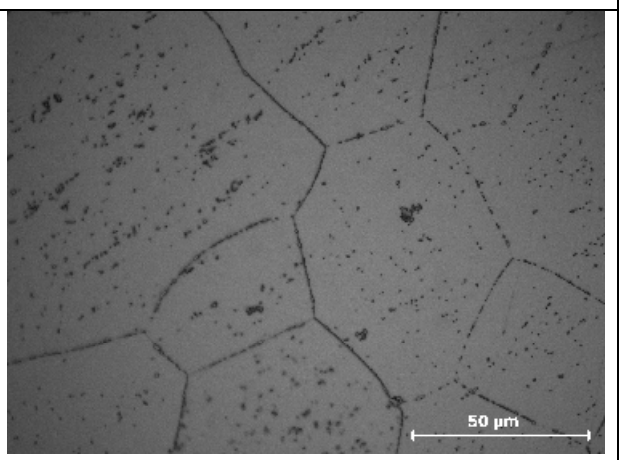

d) After 100 hours

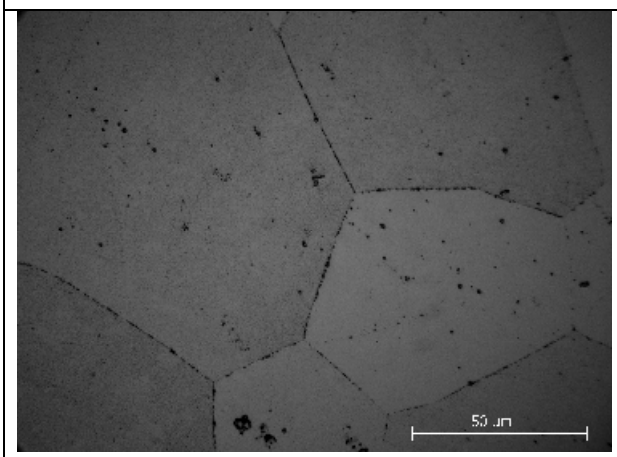

e) After 200 hours

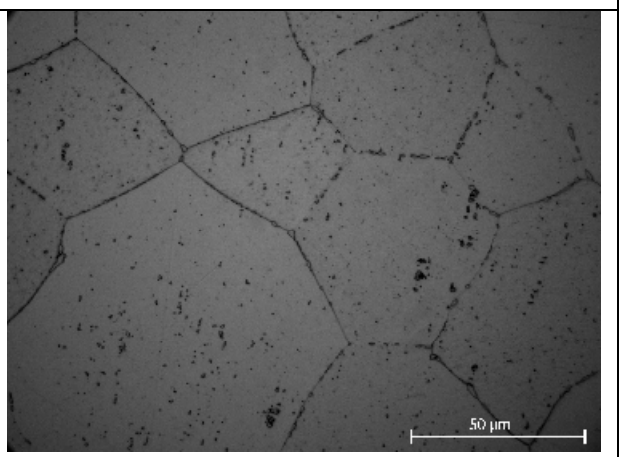

f) After 400 hours

Figure 24: Alloy A: A1050-700-950

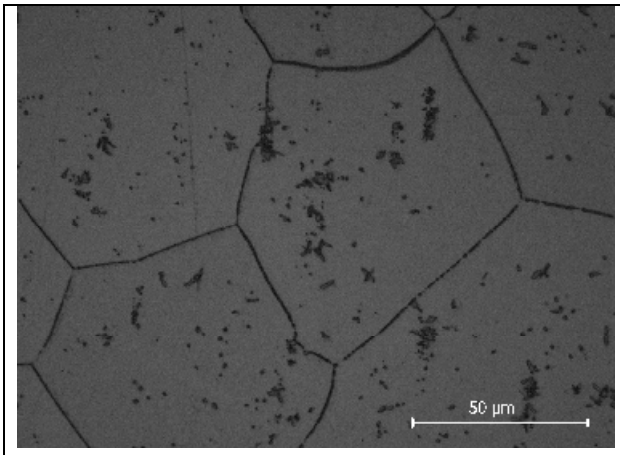

a) After 10 hours

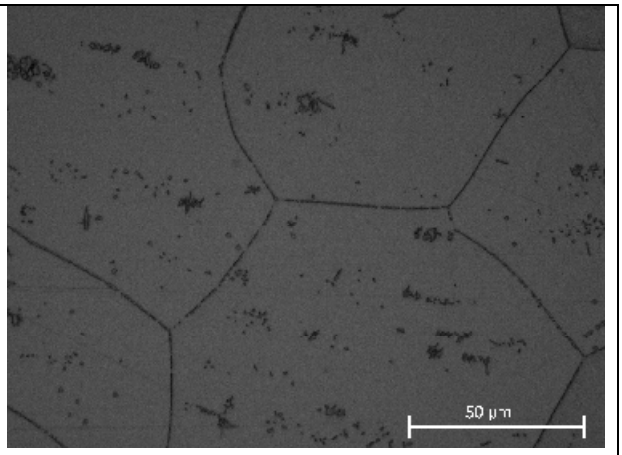

b) After 20 hours

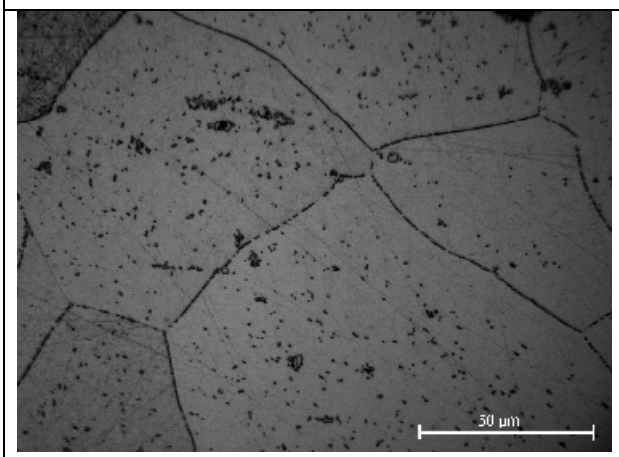

c) After 40 hours

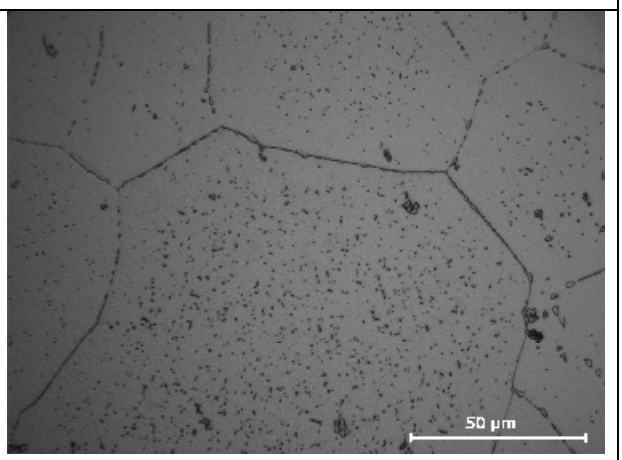

d) After 100 hours

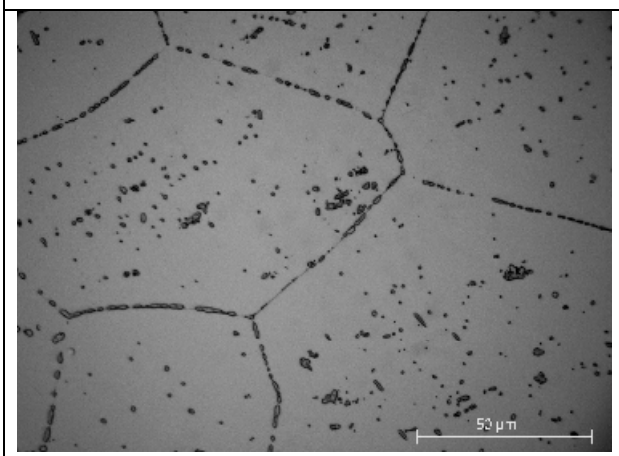

e) After 200 hours

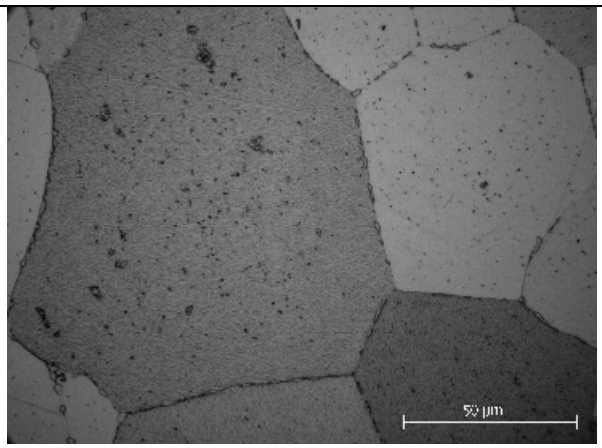

f) After 400 hours

Figure 25: Alloy A: A 1050-700-1050

For alloy A similar precipitation patterns occur for the 950 °C and the 1050 °C solution treatment conditions, across the soaking time range. However, the micrographs in figure 25 (e and f) show slightly larger precipitates at grain boundaries than the equivalent time (200 hours and 400 hours) for the 950 °C solution treatment condition as seen in figure 24 (e and f). The formation of these coarser precipitates on the grain boundaries possibly indicate that more Nb was in solution at the start of the test, therefore with more Nb in solution at the start of the test, there is more Nb available to diffuse and grow the grain boundary precipitates. Not withstanding this difference in microstructure, there is little evidence in the creep data to suggest that any difference in the microstructures has caused different creep behaviour. This is evident in the creep curve in figure 19, where it can be seen that the solution treatment temperature within a range of 950 °C to 1050 °C does not significantly affect the creep resistance of alloy A.

The grain size remains constant regardless of the soaking time.

4.4.2. Alloy B

Figure 26 and 27 (a-f) show micrographs of alloy B after particular soaking times. Each one of these samples had undergone a prior heat treatment process (as seen in table 2) and are labelled in the figure according to this.

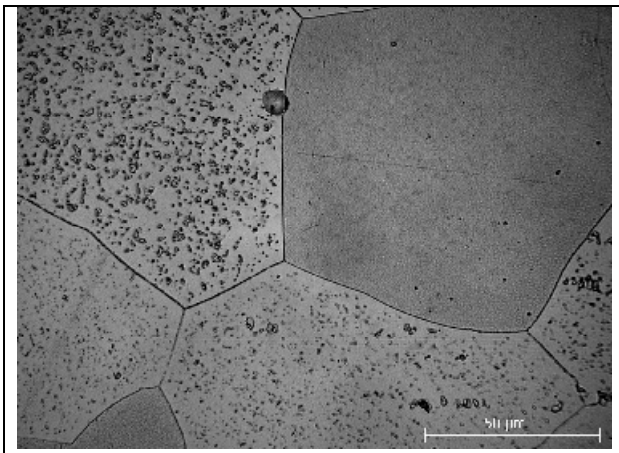

a) After 10 hours

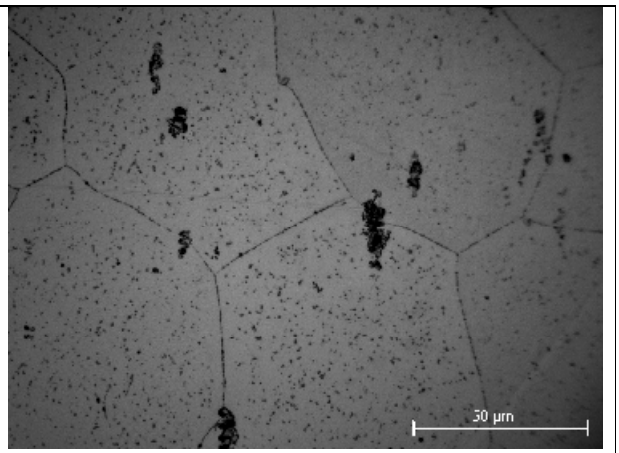

b) After 20 hours

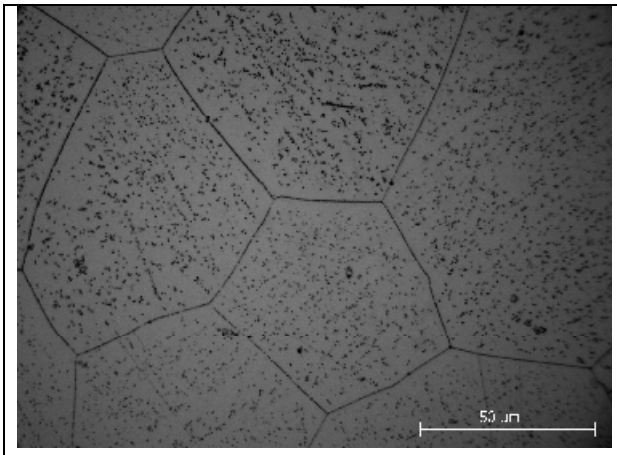

c) After 40 hours

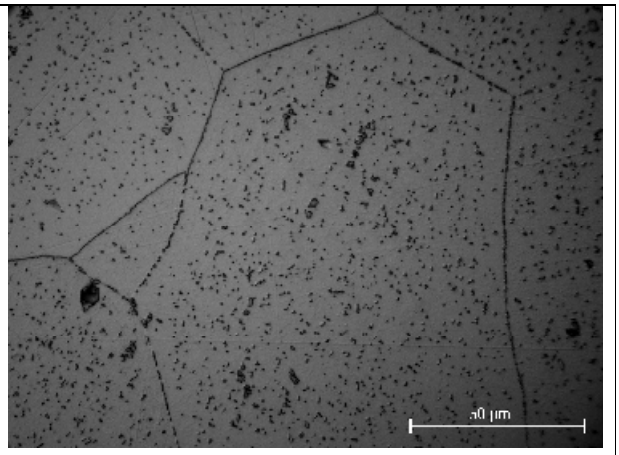

d) After 100 hours

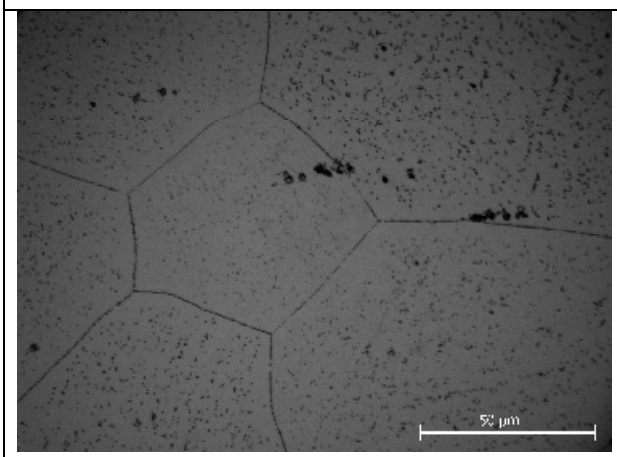

e) After 200 hours

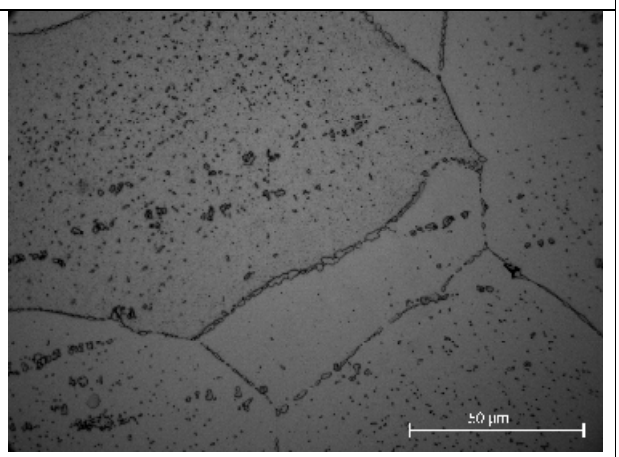

f) After 400 hours

Figure 26: Alloy B: B 1100-700-950

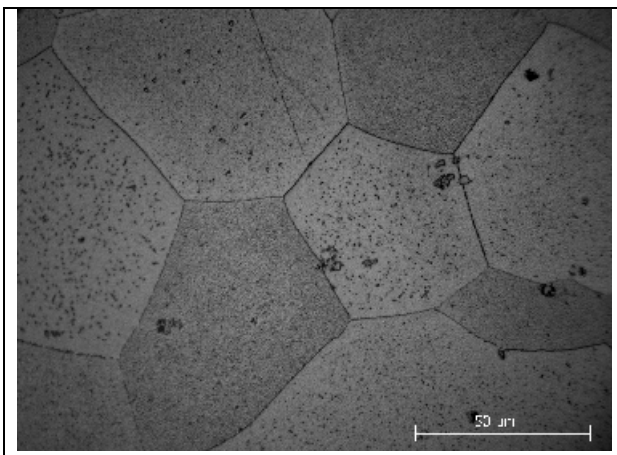

a) After 10 hours

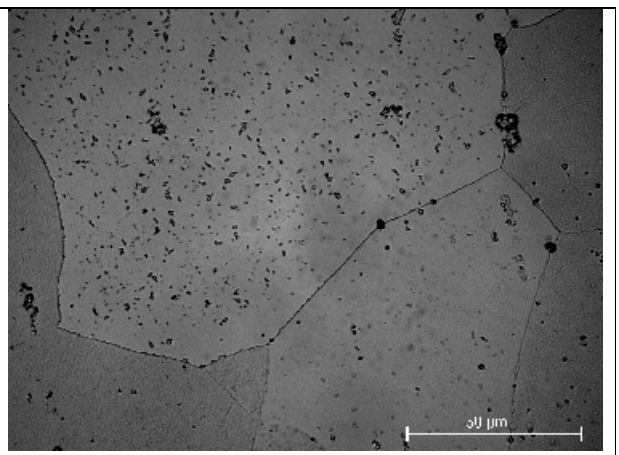

b) After 20 hours

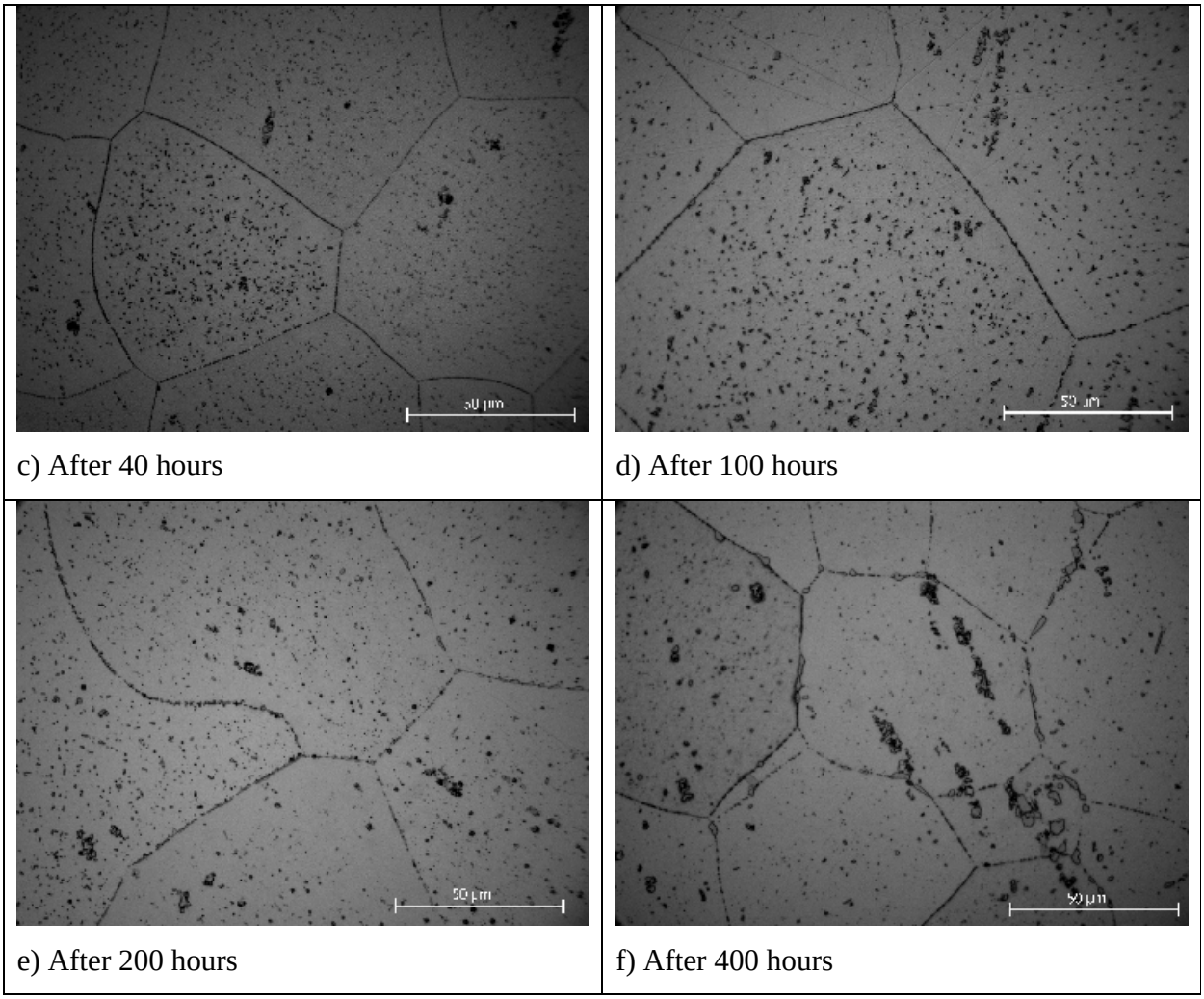

c) After 40 hours

d) After 100 hours

e) After 200 hours

f) After 400 hours

Figure 27: Alloy B: B 1100-700-1050

For alloy B similar precipitation patterns were also seen to occur for the 950 °C and the 1050 °C solution treatment conditions, across the soaking time range. For alloy B, however, there does appear to be more volume fraction of precipitation than is seen in alloy A. This increase in precipitation is predominantly evident within the grains.

The micrographs in figure 26 and 27 (f) show visible precipitation at grain boundaries. There does though appear to be more of it for B 1100-700-950, as seen in figure 26 (f), where the precipitation is profuse and dense along the grain boundaries. This could be evident of the Laves phase precipitating out over time at service temperatures, as the grain boundaries of fully stabilised ferritic stainless steels are strengthened by the precipitation of a Nb rich

intermetallic phase. This increased grain boundary precipitation could therefore corroborate the reason for the increased creep resistance of alloy B after a solution treatment at 950 °C as compared to the other solution treatment temperatures. This would also insinuate that there is easier grain boundary sliding during testing for samples that had undergone a 1050 °C solution treatment temperature due to the fact that there is less grain boundary precipitation in these samples.

The grain size remains constant regardless of the soaking time.

4.4.3. Alloy A versus alloy B

The most noticeable difference between the micrographs for both alloys appears to be after a soaking time of 400 hours where the grain boundaries are now more delineated with precipitation. It must, however, be noted that the length of the tests between the two alloys is quite different. At stress levels of 10 MPa the test duration for alloy A is always less than 200 hours regardless of prior heat treatment procedure. Whereas for alloy B the test time is much greater than 500 hours at the same stress level. Therefore for this study, the larger precipitates on the grain boundaries are only significant for alloy B.

Grain sizes remain constant between the two alloys.

The TiN particles are present and seem to remain stable for both alloys throughout the soaking times.

5. Chapter 5: Summary and conclusions

The overall study was concerned with the effect that a different level of Nb content would have on the creep resistance of type 441 ferritic stainless steel. Two different alloys were investigated that had differing Nb contents. A previous study monitored the effect of different solution treatment temperatures on the creep resistance of both alloys. The solution treatment was performed in order to promote recrystallisation and grain growth; both alloys were solution treated in the temperature range of 950 °C-1050 °C. This study revealed that the alloy with the least Nb content (alloy A) had a better creep resistance compared to that of the alloy with the high Nb content (alloy B) regardless of the solution treatment temperature. Light microscopy revealed that after each solution treatment alloy A had on average a larger grain size to that of alloy B. This study concluded that the increase in creep resistance was attributed to an increase in grain size as a function of solution treatment temperature and that grain size had a greater influence than Nb level on creep resistance.

The present study investigated how a solution treatment temperature and level of Nb content would influence creep resistance if the grain size was fixed (i.e. if the grain size of both alloys was the same). To do this the grain size of alloy B was grown to match that of alloy A at its optimum creep resistance (with reference to the previous study).

Once the grain size of the alloys was equalised samples of both alloys were aged in order to promote precipitation of Nb; finally samples were solution treated in order to control the level of Nb in solution of the sample at the start of the creep test. The solution treatment temperatures were 950 °C, 1000 °C and 1050 °C for both alloys. Samples of both alloys were then creep tested at different stress levels.

Creep test results revealed that the creep resistance of alloy B was now superior to that of alloy A. This was contrary to the previous study.

For samples of alloy B it was found that the different solution treatment temperatures had a noticeable affect on the creep resistance. In fact results showed that there is a significant difference within the range of 950 °C to 1050 °C, with the samples that were solution treated at 950 °C having the greater creep resistance. It was suggested that the reason for this greater resistance was due to the increased volume fraction of precipitation at this solution treatment temperature as compared to the other temperatures. This indicated that there was more Nb out of solution in the form of precipitation, leading to some form of precipitation strengthening mechanism. The precipitation was in the form of finely dispersed particles, that were dispersed both intragranularly and also on grain boundaries. An EDS analysis confirmed these particles to be rich in Nb, leading to the theory that this phase was likely to be Laves phase (Fe_2Nb).

On the contrary creep test results revealed that the solution treatment temperature within a range of 950 °C to 1050 °C does not seem to affect the creep resistance of alloy A i.e. whether the specimen was solution treated at 1050 °C or 950 °C seemed irrelevant. Microstructural analysis of these samples showed no (or very little) signs of precipitation after a solution treatment at 950 °C and 1050 °C. This indicated that there was no change in Nb in solution throughout the heat treatment stages, as it would be expected that the level of Nb whether in solution or out of solution in the form of precipitation would contribute to the overall creep resistance of the alloy.

Even samples of alloy A that did not undergo a solution treatment (and were only aged) showed little change in creep resistance as compared to those samples that had been treated to three different solution treatment temperatures. These results suggest that the solution treatment does not significantly improve the creep resistance of alloy A.

On the other hand it was argued that samples of alloy A that were aged for a longer time (with no solution treatment) appeared to have even less creep resistance. Microstructural analysis of these samples revealed a noticeable volume fraction of precipitation. The appearance of this precipitation however was quite different to that of the precipitation seen in samples of alloy B (after a solution treatment) in that the precipitation appeared more ‘rod-like’ and coarser in

alloy A. Although EDS analysis revealed this precipitation to be rich in Nb it was concluded that the reason for this precipitation not improving the creep resistance, but, instead proving to be detrimental to it was due to this coarsening effect.

To simulate the microstructural evolution during creep testing, samples were exposed to the creep test temperature for different soaking times, which ranged from 10 hours to 400 hours. For alloy A similar precipitation patterns were seen to occur for the 950 °C and the 1050 °C solution treatment conditions, across the soaking time range. But, there was evidence of slightly larger precipitates at grain boundaries after 200 hours and 400 hours for the 1050 °C condition as compared to the same soaking times at the 950 °C condition. It was, however, concluded that this larger precipitation would not be considered, as the majority of creep tests of alloy A had ran for less than 200 hours anyway. Besides this, there was no evidence in the creep data to suggest that any difference in the microstructures had caused different creep behaviour. This was clear in the creep curves that had compared the effect of solution treatment temperature.

For alloy B similar precipitation patterns were also seen to occur for the 950 °C and the 1050 °C solution treatment conditions, across the soaking time range. For alloy B, after a solution treatment at 950 °C, however, the precipitation at the grain boundaries was found to be more profuse and dense along the grain boundaries as compared to the other solution treatment temperatures. This was explained as the Laves phase, which had precipitated out over time at service temperatures, resulting in an improved creep resistance. This profuse grain boundary precipitation could therefore corroborate the reason for the increased creep resistance of alloy B after a solution treatment at 950 °C as compared to the other solution treatment temperatures.

The grain sizes were found to remain constant between the two alloys, across the range of soaking times and the TiN particles were present for both alloys and also remained stable throughout the exposure times.

This summary leads to the following conclusions:

- It has been established that when both alloys have the same grain size (within the region of 70 μm), alloy B is significantly more creep resistant than alloy A.
- Alloy B has the higher Nb content and the creep resistance was found to increase with Nb level for fixed grain size. The greater creep resistance of alloy B is likely to be related to a combination of Nb solid solution strengthening and Nb rich precipitation.
- The influence of a finely dispersed intermetallic phase as a precipitation strengthening method on the creep resistance of the material is apparent. Prior to creep testing (post thermo-processing) micrographs clearly show the abundance of precipitation in samples of alloy B and the lack of this precipitation in alloy A. The Nb rich phase that is present in alloy B at the final heat treatment stage (prior to creep testing), is dispersed both intragranularly and also on grain boundaries. The effect of the coarsening of these particles can, however, lead to a decrease in creep resistance. This was evident in alloy A after a prolonged ageing time of 20 hours.
- For alloy B the solution treatment does influence creep resistance for a fixed grain size, in particular the temperature at which the solution treatment is performed has an effect on the creep resistance. This appears to be linked to the Nb rich precipitation that was induced by the solution treatment. In contrast the solution treatment temperature does not seem to significantly influence the creep resistance of alloy A; this in turn is related to the fact that samples after a solution treatment showed no (or very little) signs of precipitation. The creep test results of alloy A therefore show that there is a poor correlation between solution treatment and creep resistance.
- From the present results certain creep characteristics can be recognized. Diffusion is playing a role in the creep behaviour, this is characteristic of the strong dependence of creep rate on the grain size and the high temperature which the tests are run at indicate diffusion would play a role regardless. Diffusional creep is also known to be prevalent at high temperature and low stresses. Samples that had less grain boundary precipitation may also be subjected to grain boundary sliding. But, to prove this post creep micrographs focusing within the area of deformation of the specimens would have to be investigated.

6. Chapter 6: Recommendations

6.1. Alloy A versus alloy B

To confirm the effect of the Laves phase precipitation on the shorter fracture elongation of samples of alloy B, both alloys could be checked for hardness values. It is nonetheless likely that alloy B would be harder than alloy A due to the higher percentage volume fraction of precipitation in this alloy.

It is apparent that a more detailed study of the microstructures of both alloys is now required to better understand the creep behaviour and the parameters that are influencing creep such as precipitation morphology, Nb level in solution and the relevant creep mechanism. This study could be particularly useful for alloy B, as a function of prior solution treatment temperature.

6.2. Alloy A

Samples of alloy A that had undergone ageing for 20 hours instead of 2 hours appeared to produce inferior creep resistant qualities. This was explained by the coarsening of the Nb rich precipitation. To verify this effect, samples of alloy A could be aged for more than 20 hours in order to promote additional coarsening of the precipitation. Creep testing of these longer aged samples could then assist in confirming the effect of the coarsened precipitation on the creep resistance of alloy A.

6.3. Alloy B

Creep tests for alloy B under a stress of 10 MPa were run up to 1000 hours, these tests could be repeated and run until fracture of the specimens occurred. This would then give a more accurate assessment of how much more superior alloy B is to alloy A. Alternatively the possibility of using a form of accelerated creep testing could be made use of. This is done by using an extrapolation procedure, which allows the long-term performance of a material to be estimated from short term data.

6.4. Operative creep mechanism

In terms of determining the operative creep mechanism, it would be helpful to establish the steady state strain rate at various levels of stress and then to calculate the stress exponent, n. The resulting stress exponents can then be interpreted in terms of different creep mechanisms.

It would be recommended that other methods also be used in conjunction with this, such as, microstructural observation after creep testing (within the area of deformation of the specimen). This would assist in determining any changes in grain characteristics, such as, grain elongation and therefore denote the presence of Lifshitz sliding or Rachinger sliding (grain boundary sliding).

6.5. Constant load creep test rigs

Due to the fact that creep tests can and generally do run for extended time periods it is recommended that a stand-by power source is allocated to the rigs. This would allow creep testing then not to be affected by an unscheduled power outage. An uninterrupted power supply should also be utilised for the data logger in conjunction with the stand-by power source.

7. Chapter 7: References

1. Lagier, J., Rombeaux, P., Ragot, J and Vaugeois, P. 1993. Ferritic stainless steels in exhaust systems. Innovation stainless steel. Florence, 11-14 October. Italy: 159-164

2. Douthett, J. A. 1981. Oxidation Resistant 12 % Cr Automotive Stainless Steel. *Proceedings of International Congress and Exposition, Society of Automotive Engineers, Inc*. Cobo Hall, Detroit, Michigan, 23-27 February 1981: 810036

3. Columbus Stainless Steel. *Ferritic products*. http://www.columbus.co.za/products/productsmain.htm [12 February 2008]

4. Johnson, J.N. 1981. An influence of Columbium on 870°C creep properties of 18% chromium ferritic stainless steels. *Proceedings of International Congress and Exposition, Society of Automotive Engineers, Inc.* Cobo Hall, Detroit, Michigan, 23-27 February 1981:810035.

5. Cain, V. 2005. High temperature creep behaviour of Niobium bearing ferritic stainless steels. Unpublished M-Tech thesis, Cape Technikon, Cape Town.

6. Fujita, N., Ohmura, K., Kikuchi, M., Suzuki T., Funaki, S., Hiroshige, I. 1996. Effect of Nb on high temperature properties for ferritic stainless steels. *Scripta Materialia*, 35 (6): 705-710, March.

7. SASSDA (South African Stainless Steel Development Association). *Info on Stainless*. http://www.sassda.co.za [November 2006]

8. Davies, J. R. (eds). 1994. *Stainless Steels. ASM speciality handbook.* Materials Park OH: ASM International.

9. Columbus Stainless Steel (PTY) Ltd. Technical data sheet, 1.4509. February 2007.

10. Lacombe, P., Baroux, B., Beranger, G. 1993. *Stainless Steels*. France: Les Editions de Physique Les Ulis.

11. AK steel product data bulletin. 2000. 441 Stainless Steel.

12. Miyakazi, A., Takao, K., Furukumi, O. 2002. Effect of Nb on the proof strength of ferritic stainless steels at elevated temperatures. *ISIJ International*. 42 (8): 916-920, May.

13. Cavazos, J.L. 2006. Characterisation of precipitates formed in a ferritic stainless steel stabilized with Zr and Ti additions. *Materials Characterization*. 56: 96-101, May.

14. Hua, M, Garcia, CI, DeArdo, AJ. 1997. Dual stabilized ferritic stainless steels for demanding applications such as automotive exhaust systems. *Iron and Steelmaker*: 41-44, April.

15. Keown, S.R & Pickering, F.B. 1984. Niobium in Stainless Steels. *Niobium international symposium*. San Francisco, CA, USA. 8-11 November: 1113-1141.

16. De Ardo, A.J. 2003. Niobium in modern steels. *International Materials Review*, 48 (6): 371-402, December.

17. Fujita, T. 1986. Advanced high-chromium ferritic steels for high temperatures. *Metal Progress*: 33-40, August.

18. Schmitt, J. H. 2002. Some examples of stainless steel use in the automotive industry. *Key Engineering Materials*, 230-232: 17-22.

19. Nirosta and Thermax data sheet. 2002. Stainless steels for automotive exhaust systems.

20. Hill, J. B. 1993. Meeting North American demands for stainless steels for automotive exhaust systems. *Steel Times International*. 35-38. July.

21. Edsall, W. D. 1988. Stainless steel for automotive exhaust systems. *Chromium Review*. No 9: 1-4, December.

22. Atmosphere, climate and environment. *Catalytic converters*. http://www.ace.mmu.ac.uk/eae/Air_Quality/Older/Catalytic_Converters.html[January 2007]

23. Manufacturers of emission controls association. *Clean air facts: The catalytic converter, technology for clean air*. http://www.meca.org [December 2007]

24. Anon. 2006. Exhaust export could create jobs. *Business Link (Automotive industry development centre)*: 12 July.

25. Joe Armstrong (Chairman of the catalytic converter interest group). 2006. PE catalytic converter industry growing global market share in face of intense competition. *The Herald*: 20 December.

26. SASSDA (South African Stainless Steel Development Association). *Sectors-Catcon*. http://www.sassda.co.za/sectors/catcon.htm [December 2006]

27. Tyrer, L. 2006. Catalytic converter growth to boost pipe and tube industry. *Engineering News*: 18 December.

28. Virginia Tech. *Classes*. http://www.sv.vt.edu/classes/MSE2094_NoteBook/97ClassProj/exper/bailey/www/bailey.Html [October 2005]

29. Dowling, N. E. 1999. *Mechanical behaviour of materials 2nd ed.* New Jersey: Prentice Hall International.

30. Baillie, C. & Vanasupa, L. 2003. *Navigating the materials world*. London: Academic Press

31.Cartage.Themes http://www.cartage.org.lb/en/themes/Sciences/Physics/SolidStatePhysics/AtomicBonding/CrystalStructure/Crystalline/Crystalline.htm [January 2007]

32. Evans R. W. & Wilshire, B. 1993. *Introduction to creep*. London: The institute of materials.

33. Borneman, P. R. 1982. Alloying effects of reactive elements in ferritic stainless steels. *Proceedings of International Conference on Recent Developments in Speciality Steels and Hard Materials*. Pretoria, South Africa. 8-12 November: 307-314.

34. Zhu, S. M., Tjong, S., Lai, J.K.L. 1997. Creep behaviour of a ß(NiAl) precipitation strengthened ferritic Fe-Cr-Ni-Al alloy. *Acta Metallurgica*, 46(9): 2969-2976, December.

35. Evans, R. W. & Wilshire, B. 1985. *Creep of metals and alloys*. London: The institute of metals.

36. Chandler, H. 1998. *Metallurgy for the non-metallurgist*. Ohio: Materials Park.

37. Nabarro, F. R. N. 2002. Creep at very low rates. *Metallurgical and Materials Transactions*, 33A: 213-218, February.

38. Coble, R. L. 1963. A model for boundary diffusion controlled creep in polycrystalline materials. *Journal of Applied Physics*, 34 (6): 1679-1682, June.

39. Langdon, T. G. 2002. Creep at low stresses: An evaluation of diffusion creep and Harper-Dorn creep as viable creep mechanisms. *Metallurgical and Materials Transactions*. 33A: 249-259, February.

40. Nabarro, F. R. N. 2000. Harper-Dorn creep-A legend attenuated. *Physica Status Solidi* (a) 182: 627-629, September.

41. Harper, J & Dorn, J. E. 1957. Viscous creep of Aluminium near its melting temperature. *Acta Metallurgica*, 5 (11): 654-665, November.

42. Nabarro, F. R. N. 1989. The mechanism of Harper-Dorn creep. *Acta Metallurgica*, 37 (8): 2217-2222, December.

43. Greenfield, P. 1972. *Creep of metals at high temperatures*. Great Britain: Mills and Boon Limited.

44. Honeycombe, R. W. K. 1984. *The plastic deformation of metals. 2nd ed*. London: Edward Arnold Publishers Ltd.

45. Bhandarkar, M.D., Shanthidas Bhat, M., Zackay, V. F. 1975. Structure and elevated temperature properties of Carbon-Free Ferritic alloys strengthened by a Laves phase. *Metallurgical Transactions*, 6A: 1281-1289, June.

46. Gordon, W & van Bennekom, A. 1996. Review of stabilization of ferritic stainless steels. *Materials Science and Technology*. 12: 126-131, February.

47. Fujita, N, Ohmura, K, Yamamoto, A. 2002. Changes of microstructure and high temperature properties during high temperature service of Nb added ferritic stainless steels. *Materials Science and Engineering*. A351: 272-281, October.

48. Sim, G.M., Ahn, J. C., Hong, S. C., Lee, K. J., Lee, K. S. 2005. Effect of Nb precipitate coarsening on the high temperature strength in Nb containing ferritic stainless steels. *Materials Science and Engineering*. A 396: 159-165, January.

49. Woodhead, J. H and Quarrel, A. G. 1965. Role of carbides in low-alloy creep resisting steels. *Journal of the Iron and Steel Institute*. 605-620, June.

50. Sawatani, T, Minamino, S, Morikawa, H. 1980. Effect of Laves phase on the properties of Ti and Nb stabilized low C, N-19%Cr, 2% Mo stainless steel sheets. *ISIJ International*, 22 (3): 172-180, December.

51. Yamamoto, K., Kimura, Y., Wei, F.G., Mishima, Y. 2002. Design of Laves phase strengthened ferritic heat resisting steels in the Fe-Cr-Nb (-Ni) system. *Materials Science and Engineering*. A 329-331: 249-254.

52. Murata, Y., Koyama, T., Morinaga, M., Miyakazi, T. 2002. Prediction of the Laves phase morphology in Fe-Cr-W-C. *ISIJ International*, 42 (12): 1423-1429, August.

53. Speich, G. R. 1962. Precipitation of Laves phase from Iron-Niobium (Columbium) and Iron-Titanium solid solutions. *Transactions of the Metallurgical Society of AIME*, 224: 850-858, August.

54. Cui, J, Kim, I.S, Kang, C. Y, Miyahara, K. 2001. Creep stress effect on the precipitation behaviour of Laves phase in Fe. *ISIJ International*, 41 (4): 368-371, January.

55. Kuzucu, V., Aksoy, M., Korkut, M. H., Yildirim, M.M. 1997. The effect of niobium on the microstructure of ferritic stainless steel. *Materials Science and Engineering*. A230: 75-80, December .

56. Morris, D.G., Munoz-Morris, M.A., Baudin, C. 2004. The high temperature strength of some Fe_3Al alloys. *Acta Materialia*. 52: 2827-2836, February.

57. Barteri, M., Mecozzi, M. G. 1999. Low cost weldable ferritic stainless steel for hot end of automotive exhaust gas systems. *Proceedings of the conference on stainless steel: Science and Market*. Sardinia, Italy. 6-9 June: 75-84.

58. Barteri, M, Fazio, F and Fortunati. 1999. Stainless steels in car exhaust gas systems. *La Metallurgica,* 5: 31-36, May.

59. Dollman, M. 2003. The influence of microstructure on the creep properties of 441 ferritic stainless steel. Unpublished MSc thesis, University of Cape Town, Cape Town.

60. Yamada, K., Igarashi, M., Muneki, S., Abe, F. 2002. Effect of heat treatment on precipitation kinetics in high Cr ferritic steels. *ISIJ International,* 42 (10): 779-784, June.

61. Houghton Durferrit. 2000. Cyanide-free annealing baths.

62. Bjerregaard, L., Geels, K., Ottesen, B., Ruckert, M. 2000. Struers Metalog Guide. Denmark.

63. ASTM E112-88. 1988. Standard Test Methods for Determining Average grain size. American Society for Testing Materials.

64. Humphreys, F. J. 2001. Review: Grain and subgrain characteristics by electron backscatter diffraction. *Journal of Materials Science,* 36: 3833-3854, December.

65. Humphreys, F. J. 2004. Characterisation of fine-scale microstructures by electron backscatter diffraction (EBSD). *Scripta Materialia,* 51: 771-776, May.

66. Day, A & Trimby, P. 2001. HKL Technology: Channel 5 manual.

67. Van de Voort, G. F. 1984. *Metallography: Principles and Practice*. USA: McGraw-Hill.

68. ASTM E139-00. 1990. Standard Practice for Conducting Creep, Creep Rupture and Stress Rupture Tests of Metallic Materials. American Society for Testing Materials

69. Phaniraj M.P., Prasad, M.J.N.V., Chokshi, A.H. 2006. Grain-size distribution effects in plastic flow and failure. *Materials Science and Engineering,* 463(1-2): 231-237, August.

70. Cadek, J. 1988. *Creep in metallic materials*. New York: Elsevier

Appendix A

Constant load creep test rig calibration procedure

Software

Running the software
From the desktop click on CreepRigNew to enter the data logging programme

The minimum sample rate in the software for the creep rigs is 2 seconds, although several minute rates can also be accommodated.

The number of samples (edit box) sets the effective test duration.

The displacement values (LVDT values) are autozeroed automatically on the start of logging the data. This feature can be disabled by clicking the AZ checkboxes to the off state before running the test. Also Rig 1 and /or Rig 2 may be disabled by clicking the enable checkboxes to the off state before running.

The last configuration may be loaded by clicking the 'Load config' button. The current configuration may be saved by clicking on the 'save config' button.

Before a test is performed, the measurement sensors must be calibrated. Each sensor should be calibrated.

Calibration:
It is firstly necessary to click on the 'calibrate' button to enter the calibration page. The calibration for each sensor is done in the following manner.

Thermocouples:
Click on the offset radio button and the TC row radio button. Calibrate the offset of the TC's by changing the 'offset value' in the edit box of the software. Note that about 40 µV equates to about 1 °C for a type K thermocouple. Click on the 'save' button to save the calibrations to memory.

LVDT'S:

Calibrate the LVDT's by fixing the initial mounting position of the LVDT. Click on the offset column radio button and the LVDT row radio button. Then depress the spring (not right to the bottom). Using a Vernier measure the distance that the LVDT has been allowed to displace, note this measurement (a value of about 33mm is sufficient). Make sure this displacement has been secured. This will then become the zero mm point. Then click on the 'execute current chan cal' button. The offset value is automatically calculated. Note that the offset value may be manually entered by changing the 'offset value' in the edit box of the software.

After offset calibration is performed, click on the 'scale' column radio button. Allow the LVDT to displace, using a Vernier measure the distance that the LVDT has displaced (53 mm for this particular LVDT is acceptable). Enter 53 in the 'scale cal val' edit box of the calibration page then click on the 'execute current chan cal' button. The scale value is automatically calculated. Click on the 'save' button to save the calibrations to memory.

Load cells:

Calibrate the load cells by removing all mass from the weight pan. Attach specimen into setup (technically there is now no load on the specimen) click on the 'offset' radio button and the 'load cell' radio button (of the load cell which is to be calibrated). Make sure that the counterweight on the lever is brought forward enough to allow the lever to rest firmly against the frame. Click on the 'execute current chan cal' button. The offset value is automatically calculated (which should be reading close to zero kg). Click on the 'save' button. Note that the offset value may be manually entered by changing the 'offset value' in the edit box of the software.

After offset calibration is performed, click on the 'scale' radio button. Attach a calibrated mass piece to the specimen (± 10 kg is acceptable). Enter the calibration mass value in the 'scale cal val' edit box. Then click on the 'execute current chan cal' button. The scale value is automatically calculated. Click on the 'save' button to save the calibrations to memory.

Remember that the load is accurate up to 100 grams, this is why the load cell reading may vary slightly.

To exit the calibration page click on the 'exit' button.

Appendix B

Constant load creep test rig set-up procedure

The basic procedure to follow in setting up a creep test using the rigs is as follows:

1. Ensure counter weight on lever is brought forward so as to bring the lever forward to touch the front end of the frame.
2. Insert sample into grips.

3. Ensure that the reading for the load cell is as close to zero as possible. If not satisfactory it may be necessary to recalibrate the load cell.

4. Attach extensometer clamps to sample gauge length. Ensure that the clamps are secure to prevent slippage during testing.

5. Attach lower pull rod and pin.

6. Adjust the counter weight on the lever until the lever is horizontal. A spirit level should be used to be certain the lever is horizontal. Allow the load cell to stabilise.

7. Adjust screw jack such that the lower pull rods are hanging completely free from the lower pull rod assembly.

8. Adjust lever to horizontal position.

9. Add the plates for LVDT placement.

10. Attach LVDT.

11. Attach monitoring thermocouples onto specimen; one as close to the top of the gauge length as possible and one as close to the bottom of the gauge length as possible. Ensure that the thermocouples are securely attached to the lower pull rod.

12. Adjust lever to horizontal.

13. Gently lower the furnace over the sample making sure that nothing clashes with the brittle furnace tube.

14. Check that the load train is hanging completely free from the furnace and other components.

15. Insert ceramic brick inserts into the top open end of the furnace.

16. Turn on tap for cooling water (for load cells, max operating temperature for load cells is 60 °C).

17. Switch on furnace and set all three zones of the furnace to the desired testing temperature.

18. When the set temperature has been reached on the furnace temperature controllers, check that the temperature distribution shown by the monitoring thermocouples is within acceptable limits. Allow the furnace to settle at the desired temperature for ± one hour.

19. Using the screw jack, slowly adjust the lower pull rod assembly downwards until the top brace of the lower pull rod assembly is just touching the pin through the lower hot pull rod.

20. Gently load the required weight onto the weight pan. Remember to take into account the correct lever ration when calculating the required weight pan load. Be certain to allow the load cell to stabilise.

21. Ensure all information entered into the data acquisition system is correct and start logging.

Appendix C

Constant load creep test end procedure

The basic procedure to follow when a creep test, using these rigs is finished, is as follows:

1. Ensure that the furnaces have reached room temperature before attempting to dismantle a test. If not the furnaces have not cooled down sufficiently, this could lead to burning or ruining the load cells from over exposure to heat.

2. Remove ceramic brick inserts from top open end of furnace.

3. Carefully remove weight from weight pan, it is recommended that the weight pan is held steady whilst doing this.

4. Push up furnace.

5. Move counter weight on lever forward so as to free pin from brace. Move forward enough so as to position lever securely against frame.

6. Remove LVDT.

7. Remove thermocouples.

8. Remove LVDT plates.

9. Remove lower pin.

10. Remove lower pull rod (watch out for movement of the lever).

11. Undo bolts on extensometer and remove from notches on specimen.

12. Let extensometer drop to upper brace (it may be necessary to remove bolts on both sides of top of extensometer).

13. Remove upper pin and specimen.

14. Using Windows Explorer search in CreepdataNew for logged data.

15. Open the file into Excel.